2006

Flow simulation for optimized performance of displacement pumps manufactured by engineered machined products

Jordan D. Bilyeu
Michigan Technological University

Flow Simulations for Optimized Performance of Displacement Pumps Manufactured by Engineered Machined Products

By

Jordan D. Bilyeu

A Thesis

Master of Science in Mechanical Engineering

Michigan Technological University

2006

This thesis, "Flow Simulations for Optimized Performance of Displacement Pumps Manufactured by Engineered Machined Products," is hereby approved in partial fulfillment of the requirements for the Degree of MASTER OF SCIENCE IN MECHANICAL ENGINEERING.

DEPARTMENT:
Mechanical Engineering – Engineering Mechanics
Michigan Technological University

Signatures:

Thesis Advisor: _____
Dr. Amitabh Narain
Professor

Department Chair: _____
Dr. William Predebon
Professor

Date: _____

Table of Contents

Acknowledgments

This research would not have been possible without the support of a number of people.

First and foremost, I would like to thank Engineered Machined Products (EMP) of Escanaba, MI. My experiences with them during my six month co-op and subsequent summer internship improved my engineering skills and increased my confidence. Their confidence in my abilities led to this research project. The support provided by Joel Clishe, Erik Alanko, Todd Stephens, and Jeremy Carlson allowed this project to survive and prosper. It is my hope that the results and processes developed in this project will benefit Michigan Tech and EMP.

I would also like to thank my faculty advisor, Dr. Amitabh Narain. His advice allowed the project to move in the correct direction at key times. Without his knowledge, my results and the project as a whole would not be as accurate and successful.

Thanks also to Drs. Jason Yang, Donna Michalek, and Barbara Bertram for graciously serving on my thesis committee. Their input on my thesis and defense helped clarify this document and make it much better than it would have been otherwise.

Finally, I'd like to thank my family – my father, Arnie; mother, Shirley; and brother, Kinsey – as well as my fiancée, Cassandra Nelson, and her family. Their emotional support during my graduate school experience helped me to complete the program successfully and with confidence.

Nomenclature Glossary

CFD	Computational Fluid Dynamics
EMP	Engineered Machined Products
FLUENT	Computer program for simulating fluid flows
GAMBIT	Computer program for creating CFD meshes
GPM	Gallons per minute
PSI	Pounds per square inch of pressure
RPM	Revolutions per minute

1. Introduction

1.1 Introduction and Research Objectives

The introduction of strict emission regulations and the increasing cost of fuel has driven engine manufacturers to develop more highly efficient engines and components. Engineered Machined Products (EMP) of Escanaba, MI is developing electrical oil and water pumps to help engine manufacturers reach their efficiency goals. By using electrical pumps, the mechanical losses from belt or gear driven pumps are eliminated. In addition, electrical pumps can run at any speed at any time, since there is no direct relationship between engine speed and pump speed. Thus, the pump can be programmed to run only as fast as necessary.

In order to develop the most efficient pump possible with the least cost (time and money), several pumps were simulated on the computer using the computational fluid dynamics (CFD) code FLUENT. By using the computer, various designs can be evaluated using numerical experiments, without the need to machine and assemble a physical pump.

The research completed at Michigan Technological University focused on four pumps, called the C14, C15, GN1, and Mock pumps. Simulations provided velocity and pressure fields for the flow inside each pump. The formulation of the equations used by FLUENT are shown in Section 2. In order to limit the objectives, this thesis focuses only on the prediction of mass flow rates through the outlet boundary and various gaps (see Section 1.4), as well as torque values on the inner and outer gerotor gears and any other rotating surfaces, both as a function of pump speed and pump pressure.

Although such predictions were made for each pump, a sample prediction is shown in Table 1-1. This table compares the outlet mass flow rates for the C14 pump using the hexahedral mesh (see Section 2.5) at a pump pressure of 20 PSI. The table shows the raw mass flow rates reported by FLUENT, the corrected mass flow rates (see Section 2.6.1), and how they compare with experimental data. Similar tables show how the computed torque values compare with the experimentally determined values.

Pump Pressure	Pump Speed	Experimental Mass Flow Rate	Raw Computational Mass Flow Rate	Raw Percent Difference	Corrected Computational Mass Flow Rate	Corrected Percent Difference
PSI	RPM	GPM	GPM	%	GPM	%
20	1000	0.743	0.7977	7.36%	0.7677	3.32%
	1500	1.126	1.2065	7.15%	1.1533	2.42%
	2000	1.510	1.6156	6.99%	1.5385	1.89%
	2500	1.896	2.0273	6.93%	1.9225	1.40%
	3000	2.285	2.4349	6.56%	2.3066	0.95%
	3500	2.676	2.8412	6.17%	2.6902	0.53%

Table 1-1: Example Result for the C14 Hexahedral Mesh Baseline

The mass flow rate and torque predictions were then used to show the impact of changing the dimensions of the top, bottom, and side gaps, as well as changing the inlet and outlet sizes and the angles at which they enter the pump (see Section 1.4 for a description of these gaps).

1.1.1 Optimization of the C14 Pump

The first pump to be modeled was called the C14 pump. This pump is an oil pump used for over-the-road vehicles. The simulations began by performing a baseline analysis of the pump. EMP had been using this pump for some time before this research began, so experimental data was available. The purpose of performing a baseline analysis was to see how well the computational results compared with the experimental results. Once accurate results were obtained from the model, various geometry changes were implemented in an attempt to find the optimum combination of geometry that would produce the most efficient pump.

1.1.2 Proof of Method Through Other Pumps

The C15, GN1, and Mock pumps served as a test of the method developed for simulating these type of pumps. Each pump has different characteristics and operating conditions, as described in Section 1.4. While EMP had experimental data for each of these pumps, it was not made available until the computational numbers were complete. In this way, EMP could ensure that the method used for calculating the flow through the pumps could not be manipulated to match the experimental data. When the computational and experimental numbers matched, EMP could be confident in the accuracy of the developed models for simulating new pumps.

1.2 Previous Work

Many engineers have analyzed gerotor and other types of positive displacement pumps analytically, but few have used CFD packages to simulate the flow within the pump. A kinematic analysis of gerotor pumps was performed by Fabiani *et al* [1]. Other engineers simulate gerotor pumps using analytical programs, such as the Advanced Modeling Environment for Simulation (AMESim) [2]. This simulation was able to accurately predict the oil flow rate through the pump at low pump speeds, but at high pump speeds (over 4000 RPM), the simulated flow differs from the experimental flow. This occurs because the effects of cavitation and aeration were not modeled.

Kluger *et al* studied the performance of several pumping systems by studying experimental results [3]. Pumps tested included positive displacement pumps (crescent type with involute gears, crescent type with hypocycloidal gears, gerotor, and Duocentric pumps) and a variable displacement (vane) pump. The experimental results showed that the Duocentric and hypocycloidal pumps had 5-10% greater overall efficiency over the other pumps. All results were normalized for displacement, as exact displacements could not be matched.

Jiang and Perng simulated vane and gear pumps using mixed tetrahedron, hexahedron, and polyhedron unstructured meshes [4]. They specified atmospheric pressure at the inlet of the pump and the pump rise (50-100 PSI) at the outlet. Pumps were simulated at speeds ranging from 500 to 6000 RPM. A sliding interface was used to combine the moving and deforming mesh of the pumps with the stationary mesh in other parts of the pump. They were able to match the volumetric efficiency with experimental results. The computational torque values were under-predicted at low speeds (below 2200 RPM) and over-predicted at high speeds (above 2200 RPM). The authors concluded that the cavitation seen in experimental results caused the differences in torque values. Other studies used hexahedral mesh elements and the standard k-ϵ turbulence model to simulate vane and gerotor oil pumps in automatic transmissions [5].

1.3 Gerotor Pump Operation

The pumps simulated in this research use gerotors to pump the fluid. A gerotor is a set of two gears, where the inner gear is driven by a motor and the outer gear is driven by the motion of the inner gear. The inner gear may have anywhere from four to more than ten gear teeth of generated geometry. The outer gear always has one more tooth than the inner gear, and rotates about a point that is a constant distance away from the rotation point of the inner gear.

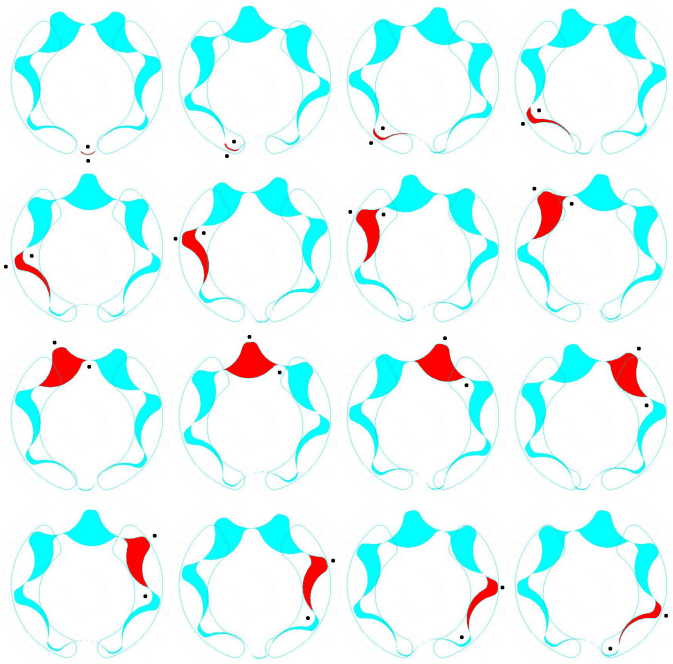

Figure 1-1: Gerotor Pump Operation

Figure 1-1 shows a gerotor in varying stages of operation [6]. As the gerotor turns in a clockwise direction, the gear teeth on the left side of the gerotor separate. This results in an increasing volume between the inner and outer gears. This increasing volume decreases the pressure in the volume, which allows atmospheric pressure to push the fluid into the pump. On the right side of the pump, the gear teeth are meshing together, which creates a decreasing volume between the gears. This decreasing volume increases the pressure, subsequently squeezing the fluid out of the pump. The fluid on the high-pressure side of the pump is separated from the low-pressure side of the pump by the seal created at the tip of the inner gear tooth, which experiences rolling friction with the outer gear tooth. The inlet is the kidney-shaped opening on the left side of the gerotor, where the fluid enters perpendicular to the top face of the gerotor gears. The outlet is the kidney-shaped opening on the right side of the pump.

1.4 Gerotor Pump Model Description

1.4.1 C14 Pump

The C14 pump is an oil pump for over-the-road vehicles. It uses the 8030 gerotor from Nichols-Portland, which means that the inner gear of the gerotor has 8 teeth (thus the outer gear has 9 teeth), and the theoretical displacement of the gerotor is 0.30 in^3/rev/inch. The gerotor is 0.625 inches thick, resulting in a theoretical displacement of 0.1875 in^3/rev. This pump was simulated with 15w40 engine oil at 100°C at speeds of 1000-3500 RPM at 20-80 PSI. At maximum pump speed, the pump can theoretically flow 2.84 GPM.

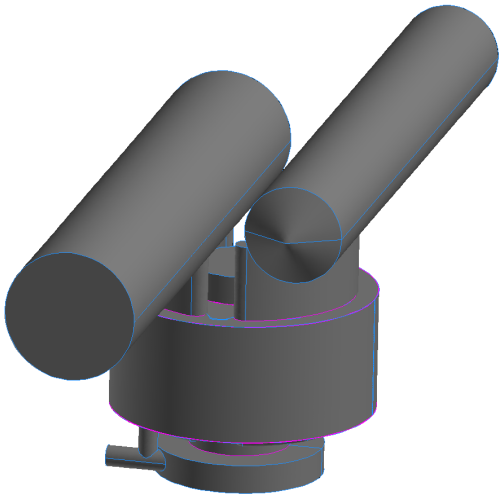

Figure 1-2: C14 Pump

1.4.2 C15 Pump

The C15 pump is another oil pump for over-the-road vehicles. It uses the 6022 gerotor from Nichols-Portland, with 6 teeth on the inner gear and a theoretical displacement of 0.22 in^3/rev/inch. This gerotor was 0.1875 inches thick, resulting in a theoretical displacement of 0.04125 in^3/rev. This pump was also simulated with 15w40 engine oil at 100°C at speeds of 1000-6000 RPM at 20-80 PSI. The main reason for simulating this pump was to determine whether the model would work correctly with a different number of gerotor teeth. At maximum pump speed, the pump can theoretically flow 1.07 GPM.

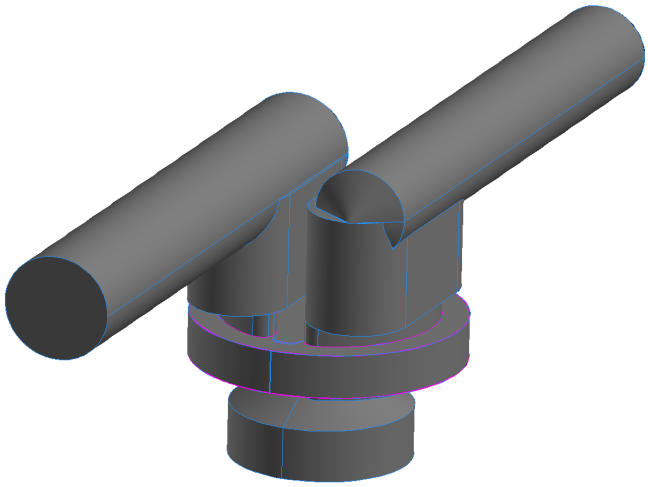

Figure 1-3: C15 Pump

1.4.3 GN1 Pump

The GN1 pump is a diesel fuel pump for over-the-road vehicles. It uses the same 8030 gerotor as the C14 pump, but is only 0.2 inches thick, resulting in a theoretical displacement of 0.06 in^3/rev. This pump was simulated with VISCOR Diesel Calibration Fluid at 24°C at speeds of 1000-3500 RPM at 300 PSI. This pump was tested to determine if the model could handle a different fluid at high pressure. At maximum pump speed, the pump can theoretically flow 0.91 GPM.

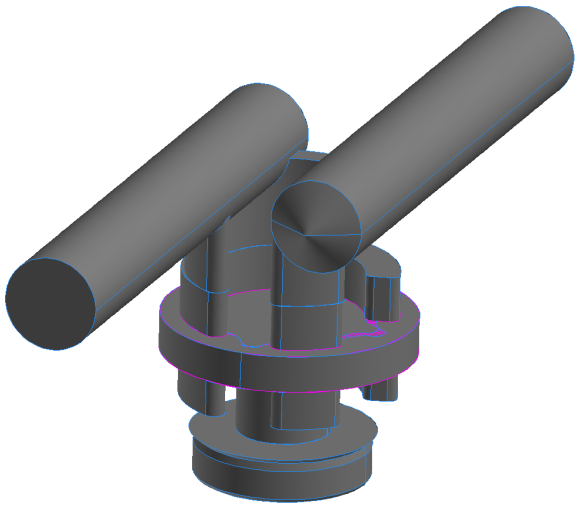

Figure 1-4: GN1 Pump

1.4.4 Mock Pump

The Mock pump is a large capacity oil pump for over-the-road vehicles. It uses the 6250 gerotor from Nichols-Portland, with 6 teeth on the inner gear and a theoretical displacement of 2.50 in^3/rev/inch. This gerotor is 1.47375 inches thick, for a theoretical displacement of 3.684 in^3/rev. This pump was simulated using both 15w40 and SAE30 motor oils at 200°F at speeds of 1250-3750 RPM. This pump was modeled because of its increased pumping capacity and the fact that different pump designs could be machined and assembled easily. At maximum pump speed, the pump can theoretically flow 60.5 GPM.

Two different geometries were simulated for the Mock pump. The original geometry is called Revision A. It has similar geometry to the other pumps, but experimental data indicates that significant cavitation is present at high pump speeds. Therefore, Revision B of the Mock pump was developed. This revision includes geometry changes that have shown experimentally to greatly reduce the cavitation present in Revision A. Figure 1-5 shows the differences between the two geometries.

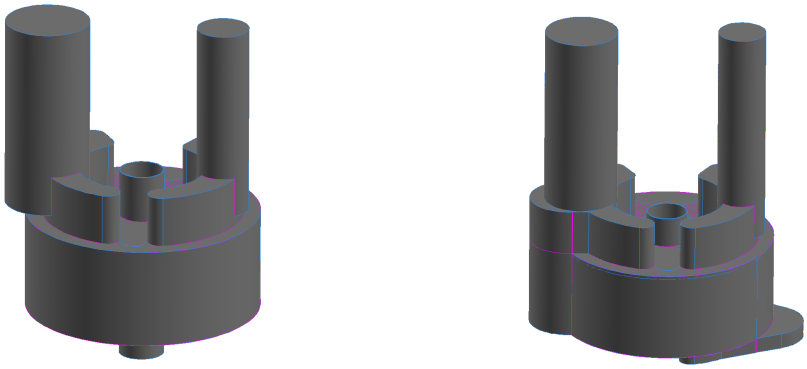

Revision A **Revision B**

Figure 1-5: Mock Pump

1.5 Computational Model Description

The computational model of each pump was split into many smaller fluid volumes using GAMBIT [7]. This section describes the names of each volume and where they are located within the pump.

The heart of the model is called the "gerotor fluid volume". This volume is bounded by the inner and outer gear faces and is exactly the height of the physical gerotor gears. Note that it was unnecessary to model the gerotor gears, as heat transfer was not significant. Figure 1-6 shows the gerotor fluid volume for the Mock Pump – Revision A simulation.

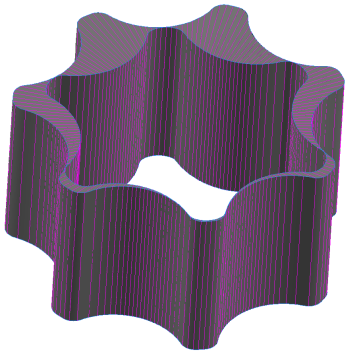

Figure 1-6: The Gerotor Fluid Volume

The top and bottom gaps are located above and below the gerotor fluid volume. The axial clearance of the pump is measured when the pump is not operating, with the bottom faces of the gerotor gears resting on the housing surfaces. During pump operation, these faces are not touching. Thus, the top and bottom gaps are each half as thick as the axial clearance of the pump. Figure 1-7 shows the top and bottom gaps added to Figure 1-6.

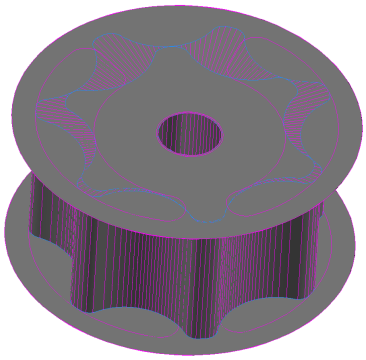

Figure 1-7: Top and Bottom Gaps

The side gap is bounded by the outer cylindrical face of the outer gear and the pump housing. This gap is a hollow cylinder with a thickness of half the diametral clearance of the pump, for similar reasons as the top and bottom gaps. Figure 1-8 shows adds the side gap to Figure 1-7.

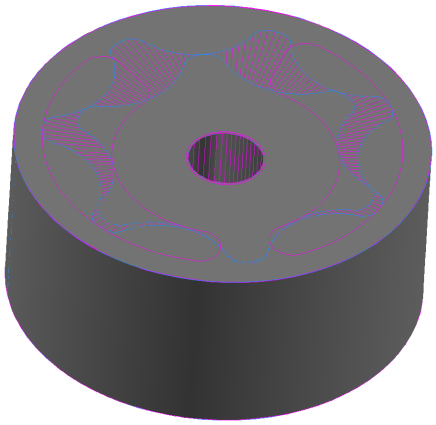

Figure 1-8: Side Gap

The kidney shaped faces on the top gap are the shared faces with the inlet and outlet ports. The inlet port is on the left side of the pump, where the clockwise rotation of the pump creates an increasing volume in the gerotor fluid volume. The outlet port is on the right side of the pump, where the gerotor fluid volume decreases in volume. The inlet and outlet ports (with cutouts) are added to the current image in Figure 1-9.

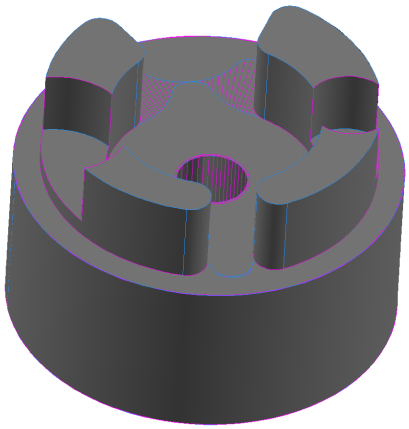

Figure 1-9: Inlet and Outlet Ports

The hole in the top gap models where the motor shaft enters the inner gerotor gear. A volume called the "shaft side upper" volume is bounded by the rotating shaft and the pump housing. A similar gap is also located on the bottom of the pump. Both the "shaft side upper" and "shaft side lower" gaps are added to the model in Figure 1-10.

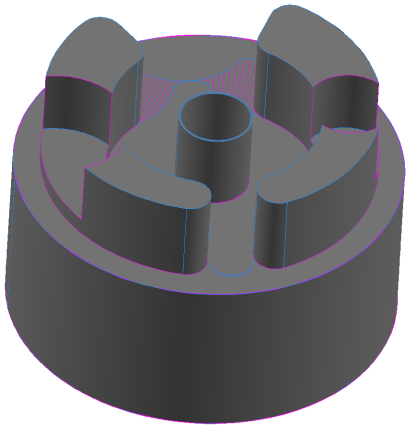

Figure 1-10: Shaft Side Upper and Shaft Side Lower Gaps

The cutouts in the inlet and outlet ports are where the inlet and outlet tubes connect. These tubes simulate the connections of the physical pump as well as a short length of the hoses that are connected to the pump. This is done so that any fluctuations in the flow variables are sufficiently low at the inlet and outlet boundaries, which are located on the top of these two volumes, respectively. The inlet and outlet tubes are added in Figure 1-11.

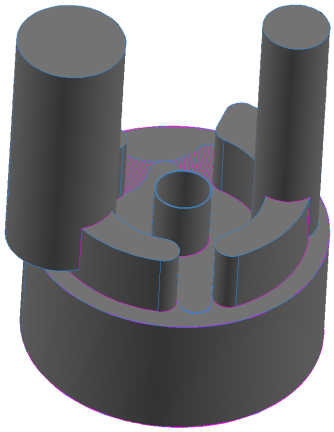

Figure 1-11: Inlet and Outlet Tubes

If the pump is rotated such that the bottom gap is visible, the user would notice kidney-shaped faces similar to those seen on the top gap. These faces are shared with the inlet and outlet shadow ports. Shadow ports are machined into the pump housing to help balance the pressure forces on the gerotor gears axially and to reduce viscous losses. The pump is rotated and the shadow ports are added in Figure 1-12. Note that on this particular pump they are very shallow. Deeper ports are present on the C14 and C15 pumps.

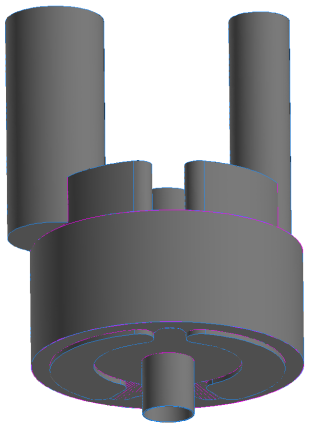

Figure 1-12: Inlet and Outlet Shadow Ports

The geometry presented in Figures 1-6 through 1-12 are typical for all the pumps modeled in this project. The differences between the pumps can be seen in Section 1.4 above.

2. Mathematical Formulation

2.1 Governing Equations

FLUENT, the computational fluid dynamics code used in this research, uses the conservation of mass, momentum, and energy equations to solve any fluid flow problem. This section summarizes these equations and the turbulence model used in the gerotor pump simulations [7-11].

2.1.1 Mass Balance

If a three-dimensional domain is defined using Cartesian coordinates (where the spatial coordinate system is denoted x, y, and z), the differential form of the continuity (mass balance) equation can be written as follows:

$$\frac{\partial \rho}{\partial t}+\frac{\partial}{\partial x}(\rho u)+\frac{\partial}{\partial y}(\rho v)+\frac{\partial}{\partial z}(\rho w)=0 \qquad \textit{Eq. 2.1}$$

Equation 2.1 consists of a time-dependent unsteady term $(\partial/\partial t)$ and three velocity-dependent convective terms $(\partial u/\partial x, \partial v/\partial y, \partial w/\partial z)$, where u, v, and w represent the fluid velocity components in the x, y, and z directions and ρ is the density of the fluid.

In steady-state or constant density systems, the unsteady term does not play a role and it automatically gets neglected, leaving the three convective terms. *Equation 2.1* can be simplified by using indicial notation, where the fluid velocities u, v, and w and the spatial coordinates x, y, and z can be written as v_i and x_i, respectively, where i = 1, 2, and 3, corresponding to the three Cartesian coordinate directions to obtain:

$$\frac{\partial \rho}{\partial t}+\frac{\partial}{\partial x_i}(\rho v_i)=0 \quad ; \qquad \text{where } i = 1, 2, \text{ and } 3 \qquad \textit{Eq. 2.2}$$

2.1.2 Momentum Balance

The Navier-Stokes (momentum balance) equations can be described most easily by using Newton's second law, which states that a force is equal to a mass multiplied by an acceleration. For fluid dynamics problems, it is convenient to use these terms on a per unit volume basis. Thus, the inertial fluid acceleration term multiplied by the fluid density is equal to the per-unit volume applied force on the fluid particle. The applied forces can be classified as either body forces (typically gravitational forces) which operate on the entire domain of fluid, or surface forces, which result from the

interactions of the fluid element with its environment (pressure forces and viscous stresses). The surface stresses are quantified by defining the stress tensor $\tau_{i,j}$ which describes the stresses in each of three Cartesian *j*-directions on faces normal to each of the three Cartesian *i*-directions.

$$\boldsymbol{f} = m\,\boldsymbol{a} \qquad \textit{Eq. 2.3}$$

$$\rho \frac{D\boldsymbol{V}}{Dt} = \boldsymbol{f}_{body} + \boldsymbol{f}_{surface} \qquad \textit{Eq. 2.4}$$

$$\boldsymbol{f}_{body} = \rho\,\boldsymbol{g} \qquad \textit{Eq. 2.5}$$

$$\boldsymbol{f}_{surface} = \vec{\nabla}\cdot\boldsymbol{\tau} = \frac{\partial \tau_{ij}}{\partial x_j} \;\text{; where } i, j = 1, 2,3, \quad \boldsymbol{\tau} = \left[\tau_{ij}\right] \text{ tensor} \qquad \textit{Eq. 2.6}$$

If the surface forces can be directly related to the velocity of the fluid element by the relationship shown in *Equation 2.7*, the fluid is said to be Newtonian.

$$\tau_{ij} = -p\,\delta_{ij} + \mu\left(\frac{\partial v_i}{\partial x_j} + \frac{\partial v_j}{\partial x_i}\right) + \delta_{ij}\lambda\vec{\nabla}\cdot\boldsymbol{V} \qquad \textit{Eq. 2.7}$$

In this equation, μ is the fluid viscosity, p is the hydrodynamic pressure, λ is the coefficient of bulk velocity, and δ_{ij} is the Kronecker delta function (equal to 0 when $i \neq j$ and equal to 1 when $i = j$). Using the Newtonian assumption, *Equation 2.6* can be simplified.

$$\boldsymbol{f}_{surface} = \vec{\nabla}\cdot\boldsymbol{\tau} = -\vec{\nabla}\,p + \frac{\partial}{\partial x_j}\left[\mu\left(\frac{\partial v_i}{\partial x_j} + \frac{\partial v_j}{\partial x_i}\right) + \delta_{ij}\lambda\vec{\nabla}\cdot\boldsymbol{V}\right] \qquad \textit{Eq, 2.8}$$

$$\textit{where } i, j = 1,2,3$$

Some additional assumptions can be made to further simplify the governing momentum balance equations. Because the fluids used in the simulations are incompressible, the fluid density may be treated as a constant. Consequently, the divergence of the fluid velocity vector is equal to zero. Finally, by assuming that the fluid viscosity is a constant independent of pressure, temperature and position, *Equation 2.8* can be simplified to become *Equation 2.9*.

$$\rho \frac{D\boldsymbol{V}}{Dt} = \rho\,\boldsymbol{g} - \vec{\nabla}\,p + \mu\nabla^2\boldsymbol{V} \qquad \textit{Eq. 2.9}$$

2.1.3 Turbulence Model

The turbulence model used in all simulations was the k-ϵ model. This is a semi-empirical model base on model transport equations for the turbulence kinetic energy (k) and its dissipation rate (ϵ). These values are obtained from the following transport equations:

$$\frac{\partial}{\partial t}(\rho k)+\frac{\partial}{\partial x_i}(\rho k u_i)=\frac{\partial}{\partial x_j}\left[\left(\mu+\frac{\mu_t}{\sigma_k}\right)\frac{\partial k}{\partial x_j}\right]+G_k+G_b-\rho\epsilon-Y_M+S_k \qquad \textit{Eq. 2.10}$$

and

$$\frac{\partial}{\partial t}(\rho \epsilon)+\frac{\partial}{\partial x_i}(\rho \epsilon u_i)=\frac{\partial}{\partial x_j}\left[\left(\mu+\frac{\mu_t}{\sigma_\epsilon}\right)\frac{\partial \epsilon}{\partial x_j}\right] +C_{1\epsilon}\frac{\epsilon}{k}(G_k+C_{3\epsilon}G_b)-C_{2\epsilon}\rho\frac{\epsilon^2}{k}+S_\epsilon \qquad \textit{Eq. 2.11}$$

where G_k represents the generation of turbulence kinetic energy due to mean velocity gradients, and G_b is the generation of turbulence kinetic energy due to buoyancy. Y_M represents the contribution of the fluctuating dilation in compressible turbulence to the overall dissipation rate. The relation of G_k, G_b, and Y_M to the mean velocity components μ_i as well as the definitions of k and ϵ are well known and given in the FLUENT manual (see Appendix F) and standard textbooks. $C_{1\epsilon}$, $C_{2\epsilon}$, and $C_{3\epsilon}$ are constants. σ_k and σ_ϵ are the turbulent Prandtl numbers for k and ϵ, respectively. S_k and S_ϵ are source terms.

The turbulent (eddy) viscosity μ_t is computed using *Equation 2.12*.

$$\mu_t=\rho C_\mu\frac{k^2}{\epsilon} \qquad \textit{Eq. 2.12}$$

The values of the model constants were kept at their default values as per recommendations by a FLUENT support engineer, and are as follows:

$$C_{1\epsilon}=1.44,\ C_{2\epsilon}=1.92,\ C_\mu=0.09,\ \sigma_k=1.0,\ \sigma_\epsilon=1.3 \qquad \textit{Eq. 2.13}$$

2.2 Boundary Value Problems

In order to create a mesh for the gerotor pumps simulated in this project, the fluid passages needed to be split up into multiple fluid volumes. In this way, each fluid volume can have the most appropriate mesh applied. However, by creating multiple volumes, the number of boundary conditions increases, and care must be taken to define each surface correctly. Using GAMBIT, the geometry files provided by EMP for each pump model were imported so that a computational mesh could be created. After splitting the fluid passages into multiple fluid volumes, the continuum types (for the fluid volumes) and boundary types (for each surface on a fluid volume) were defined.

2.2.1 Domain or Continuum Types

GAMBIT is a powerful tool that can be used to create meshes for a number of different flow solvers. For FLUENT versions 5 and 6, the choices for continuum types are limited to "fluid" and "solid".

"Fluid" continuum types are used exclusively in this project. This continuum type instructs the flow solver to solve for all mass, momentum, and energy equations. The "solid" continuum type drops the mass and momentum equations, solving only the energy equation. The "solid" continuum type can be used to calculate heat transfer from one fluid to another that is separated by a solid wall, such as within a heat exchanger. Because of the way the gerotor pumps were modeled in GAMBIT, the "solid" continuum type was not necessary. Heat transfer within the pump was assumed to be negligible, since the inlet fluid temperature is held constant.

2.2.2 Boundary Types

The basic boundary type used in these simulations is the "wall". This surface defines where the fluid volume ends, such as the solid surfaces within the pump that the fluid cannot flow through. Most "wall" boundaries are static (not moving) with a no-slip wall condition, meaning that the fluid velocity at the wall is equal to the speed of the wall. In some cases, the speed of the wall is not equal to zero, as is the case where the wall describes a shaft or the rotating surfaces of the gerotor gears. These surfaces are called "moving walls", with prescribed translations, rotations, or both.

The method used while creating the geometry of the pump within GAMBIT has a large impact on how the boundary conditions of each fluid volume should be defined. One of the best ways to make the geometry and subsequent mesh as clean and small as possible is to make two or more fluid volumes connected, such that one or more faces are shared. Figure 2-1 shows the Mock Pump – Revision A geometry of the top gap and the inlet and outlet ports. Notice that the bottom edges of the inlet and outlet ports are magenta in color, which indicates that they are connected to the top gap volume. Because of this connection, any mesh that is applied to the top gap is also applied to the connected faces on the inlet and outlet ports. When done correctly, this reduces the overall size of the mesh and makes excellent connections between fluid volumes. When this is done, an "interior" boundary condition is automatically applied to the magenta colored faces. "Interior" boundary conditions are surfaces that allow fluid to flow freely between two volumes.

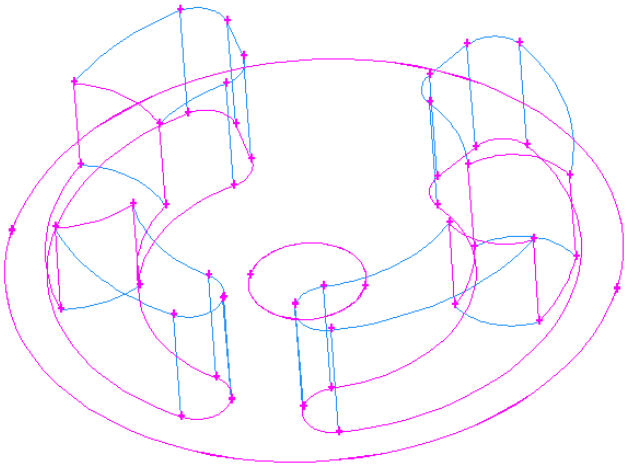

Figure 2-1: Mock Pump Top Gap, Inlet and Outlet Port Geometry

Sometimes connecting two fluid volumes is not possible. Connecting two volumes may make creating a wedge or hexahedral mesh impossible for one volume. Sometimes two fluid volumes are physically connected, but need to be separate. The connection between the top (and bottom) gap with the gerotor fluid volume is one example. In this case, an "interface" zone needs to be applied to each corresponding surface. Since the gerotor fluid volume rotates and the top gap remains stationary, the mesh cannot be shared between both volumes. When the bottom surface of the top gap and the top surface of the gerotor fluid are defined as "interface" zones, fluid can flow freely between the two volumes. In areas where the two "interface" zones do not overlap, the "interface" zone is automatically changed to a standard "wall" boundary. In this way, the fluid will flow between two volumes only where the "interface" zones overlap. Note that "interface" zones need to be created in pairs and the pairs explicitly related within FLUENT.

The inlet boundary of the pump is defined as the circular surface at the end of the inlet tube. The boundary is defined as a "pressure inlet", with an inlet pressure of 0 PSI at the temperature specified by the experimental data. The outlet boundary is defined in the same manner as the inlet boundary, except it is defined as a "pressure outlet" with the pressure set as the pressure rise of the pump (80 PSI, for example). In this way, the total pressure rise through the pump is explicitly defined, and the mass flow rates are calculated by FLUENT.

The inner and outer gear faces of the gerotor fluid volume are defined as stationary walls within GAMBIT, and their motion is defined by a user defined function (UDF) within FLUENT. More detail on this procedure is given in Section 2.4.

2.3 Solution Methodology

For incompressible flow problems such as those described in this document, the implicit segregated solver in FLUENT is very robust and highly effective. The segregated solver solves the three governing equations (mass, momentum, and energy) separately. The other choice within FLUENT is to use the coupled solver, which solves the governing equations simultaneously. The coupled solver requires a great deal more computer memory than the segregated solver, but is able to reach a converged solution with a smaller number of iterations. Because of the limitations of computer memory available when running these simulations, the segregated solver was used.

The segregated solver works by first updating the fluid properties based on the previous iteration (or solution initialization, if the simulation has just begun), then solves the *u*, *v*, and *w* momentum equations (using pressures and face mass fluxes) to obtain an updated velocity field. A pressure correction equation is then used to adjust the pressure and velocity fields and the face mass fluxes until the continuity equation has been satisfied. Next, the energy and turbulence equations are solved using the current values of pressure, density, and velocity. Finally, a check is made to determine whether the current values have satisfied the convergence criteria. If so, the iterations stop, and, in the case of the gerotor pumps, the mesh is deformed and time increased to the next time step, and iterations restarted. If the solution is not converged, the fluid properties are updated and the process is repeated.

2.4 Convergence Issues

2.4.1 Mesh Density

The accuracy and speed of the computer simulations is highly dependent on the three-dimensional mesh used to discretize the flow domain. Both the type and coarseness of the mesh are important factors in generating an acceptable, converged solution.

In the models of the gerotor pumps simulated in this project, hexahedral meshes were used whenever possible. Hexahedral meshes allow for larger grid sizes than tetrahedral meshes with the same accuracy. Many fluid volumes within the models were able to use hexahedral meshes, such as the side gap, some shadow ports, and later, the gerotor fluid volume. Other areas of the model used wedge meshes, which are five-sided extrusions of a triangular face mesh. Volumes that used these meshes include the inlet and outlet tubes and early versions of the gerotor fluid volume (see Section 2.5). Finally, in areas of irregular geometry, tetrahedral meshes were used. Figure 2-2 shows an example of each type of element.

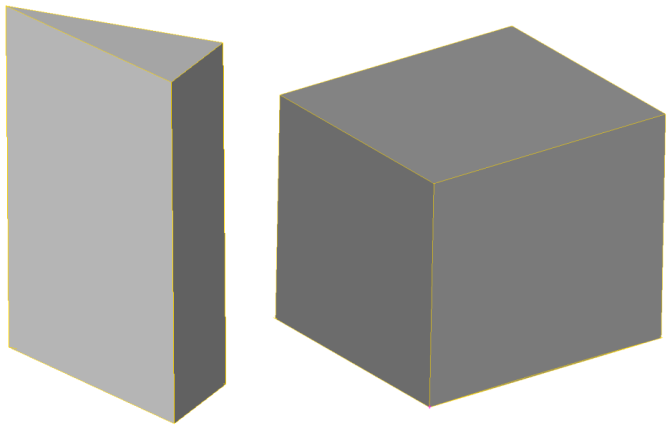

Wedge Element **Hexahedral Element**

Figure 2-2: Wedge and Hexahedral Mesh Elements

In most cases the mesh of each individual fluid volume within the model was directly connected to adjacent fluid volumes, such that both volumes shared a common face, and thus shared the mesh on that face. As discussed in Section 2.2.2, volumes that are physically connected but cannot be made to share a common face are connected using "interface" boundary conditions, which allow non-conformal meshes to be successfully simulated.

Some of the volumes in the models are very thin, such as the top, bottom, and side gaps. These gaps used hexahedral or wedge elements with at least three elements along the shortest edge, as recommended by FLUENT. Most edge meshes used interval sizes of 0.02 inches, while some of the more complex geometries using tetrahedral meshes used interval sizes of 0.01 inches. Care was taken to change mesh densities gradually, as large changes in grid density can lead to convergence issues.

A grid dependency study was performed to determine the above edge mesh dimensions. Figure 2-3 shows the outlet mass flow rates for four different grid densities for the C14 wedge mesh baseline simulation at 3500 RPM and 80 PSI. The four grid densities studied were 301,727, 472,324, 648,966, and 976,234 elements. As the figure shows, the outlet mass flow rates and torque values increase drastically with an increase in the mesh density. The greatest mesh density values are nearly identical to the third largest grid size. Since the largest grid size required a significant increase in computational resources for little change in flow variables, the mesh size of 648,966 elements was used for the C14 pump. Similar grid density was used for the other pumps, although the total number of elements varied, mostly due to the thickness of the gerotor.

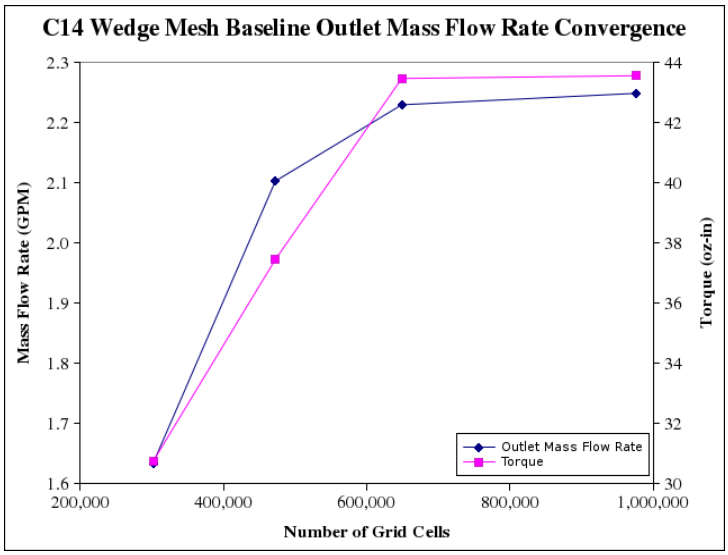

Figure 2-3: Grid Dependency Study

2.4.2 Flow Model Residuals

In order to obtain a flow solution for which the user has confidence, several scaled flow model residuals have to be monitored. For these simulations, seven residuals were monitored: one residual for the continuity equation, three residuals for the momentum equation (one each for the x-, y-, and z-velocities), one residual for the energy equation, and two residuals for the k-ϵ turbulence model equations.

FLUENT gives the engineer control over the convergence criterion for each residual monitored. For the continuity and momentum residuals, the default value of 0.001 was used, and the default value of 1e-6 used for the energy residual. However, for the k-ϵ residuals, the convergence criteria was changed to 0.002. This was done mostly to reduce the time required to solve each time step. Early simulations were run using the default criteria of 0.001, which resulted in each time step requiring about 25-30 iterations. When the criteria was reduced to 0.002, each time step only required about 10 iterations, drastically reducing the time required to solve a large number (typically 1000) of time steps. This reduction in convergence criteria was shown to have a negligible effect on the flow variables (outlet mass flow rate and torque values), and was thus deemed appropriate.

Figure 2-4 shows the residual history for the first 15 time steps for the Mock Pump – Revision B at 3793 RPM and 120 PSI. It shows that the first two time steps require 200 iterations (the maximum allowed per time step), then the residuals quickly fall into a repeating pattern as the time steps increase.

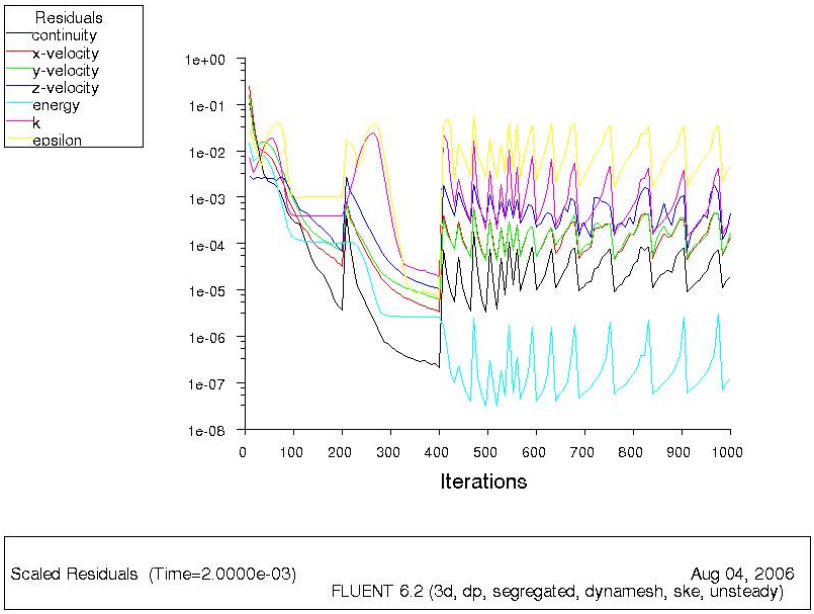

Figure 2-4: Typical Residuals History

2.5 *Mesh Motion Issues*

Simulating the motion of the gerotor gears was perhaps the most difficult part of performing these simulations. Many simulations that use FLUENT have fixed geometry through which a fluid flows. Some simulations involve moving geometry where the moving parts can be described by simply defining the appropriate walls as rotating walls. This method cannot be used with gerotor pumps because the displacement of the pump changes with time, unlike, for example, an axial fan. Instead, more advanced methods are required.

These simulations use the dynamic mesh capabilities of FLUENT. With this capability, a mesh can be deformed and re-meshed if necessary due to the motion of moving boundaries. Two methods of creating a mesh for the gerotor fluid volume were used and are described below.

2.5.1 Wedge Mesh

The first method of creating a dynamic mesh for the gerotor fluid volume used wedge elements. A typical view of the top face of the gerotor fluid volume is shown in Figure 2-5.

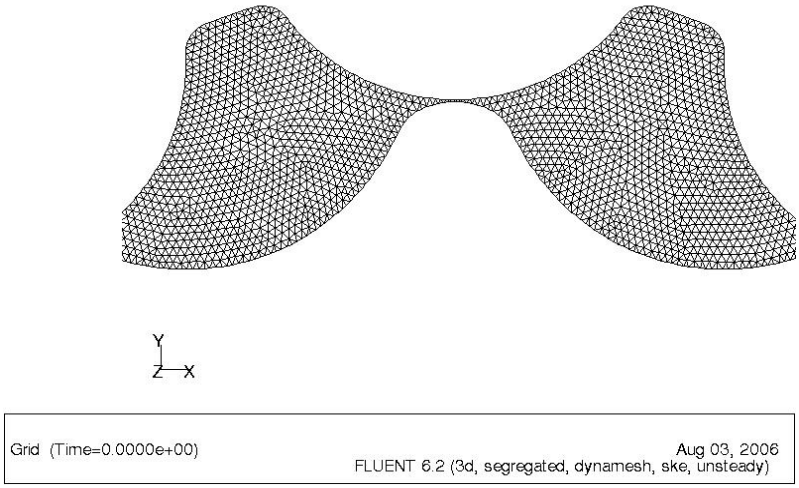

Figure 2-5: Wedge Mesh on the Top Face of Gerotor Fluid Volume

In order to create a wedge mesh, the top (or bottom) face of the gerotor fluid volume must be meshed using triangular elements within GAMBIT. While this is easily done in areas of large volume, the mesh regularly became highly skewed in areas of very small volume. In order to achieve a successful mesh of the face, the gap between the

inner and outer gerotor gears needed to be enlarged. This necessary, through undesirable practice introduced additional error into the simulation. To reduce the occurrence of skewed elements, the number of nodes along the edges of the face was increased. Advanced meshing schemes, such as two-sided size functions, were used to slowly enlarge the size of the elements as the distance from the edges increased, thus reducing the total size of the mesh.

Once the top face of the gerotor fluid volume was meshed, the vertical sides of the volume (corresponding to the inner and outer gerotor gear faces) were meshed using a mapped hex mesh. This mesh typically had 20-30 elements in the direction perpendicular to the top face. The volume was then meshed using the Cooper scheme, which creates finite volumes that are extrusions of the triangular face elements on the top face of the volume, thereby creating wedge elements.

After the mesh was exported and opened within FLUENT, the dynamic mesh functionality was enabled. The gerotor fluid volume and the top and bottom faces of the volume were defined as deforming areas of the mesh, while the inner and outer gear faces were defined as boundaries with rigid-body motion. The motion was described by a user-generated profile, which specified the rotational speed in radians/second about the appropriate center of rotation. When all the parameters and options were specified, the mesh motion would be simulated without solving for the flow variables to ensure the dynamic mesh would work as planned. Unfortunately, the dynamic mesh would fail frequently, necessitating a rebuild of the gerotor fluid volume. This resulted in a very time-consuming process.

2.5.2 Hexahedral Mesh

Because of the undesirable large gap between the gerotor teeth when using a wedge mesh, a new method of meshing the gerotor fluid volume was developed. With the assistance of FLUENT and EMP engineers, a process for creating the hexahedral mesh shown in Figure 2-6 was developed.

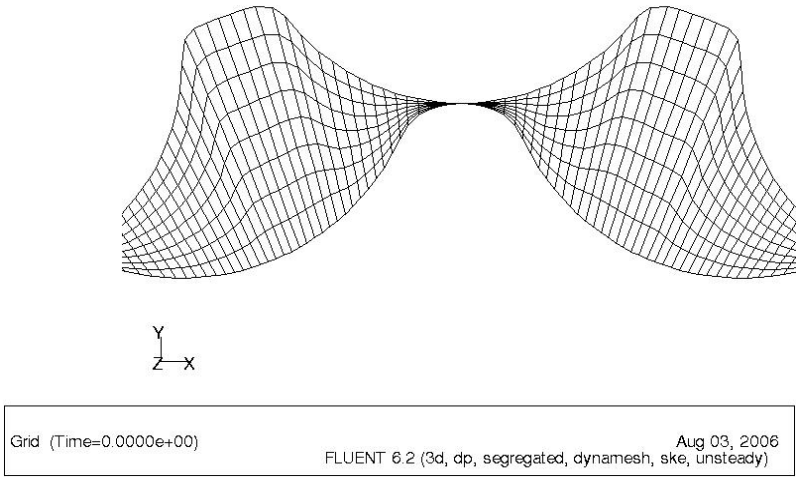

Figure 2-6: Hexahedral Mesh on the Top Face of the Gerotor Fluid Volume

The hexahedral meshing method was difficult and time-consuming to create. Meshing the top face of the gerotor fluid volume was not as simple as the wedge mesh. In this case, the top face had to be split into 180 small faces at intervals of 2 degrees about the center of the inner gerotor gear. These small faces were easily meshed using a mapped hexahedral mesh, with eight elements along the radial edges and two elements along the short edges. These meshed faces were then extruded into volumes by using the "Sweep Faces" volume function within GAMBIT. Each volume was then meshed using the same 20-30 elements in the perpendicular direction as in the wedge mesh. With this method, the gap between the inner and outer gerotor gears was reduced to about 0.0005 inches, a dramatic reduction from the wedge mesh.

After the mesh was exported, opened in FLUENT, and the dynamic mesh feature enabled, only the gerotor fluid volume was defined as a deforming boundary. The motion of the gears was defined by a user-defined function (UDF), supplied by the support engineers at FLUENT. This UDF uses a simple text file to define the parameters of the simulation, requiring only the rotational speed of the inner gear in RPM, the *(x,y)* location of the center of rotation for the outer gear, and the top, inner gear, and outer gear face ID numbers. After successfully compiling the UDF, solving the mesh motion was almost always an assured success. Comparisons between the wedge and hexahedral meshes show that the hexahedral mesh yields superior outlet mass flow rate and torque values when compared to the available experimental data.

2.6 *Result Corrections*

2.6.1 Outlet Mass Flow Rate

The outlet mass flow raw results supplied by FLUENT needed to be corrected so that they were closer to the experimental results. Figure 2-6 demonstrates the reasoning behind the correction.

Figure 2-7 shows the experimental outlet mass flow rate curves for the C14 pump at 20 and 80 PSI. Notice that the raw (uncorrected) lines are always lower than the experimental curves by a constant distance for each pressure. It was postulated that this difference was caused mainly by the large gap between the gerotor teeth needed for the wedge mesh to be successful (see Section 2.5). In order to correct for this offset, an Excel spreadsheet was used to perform a number of calculations.

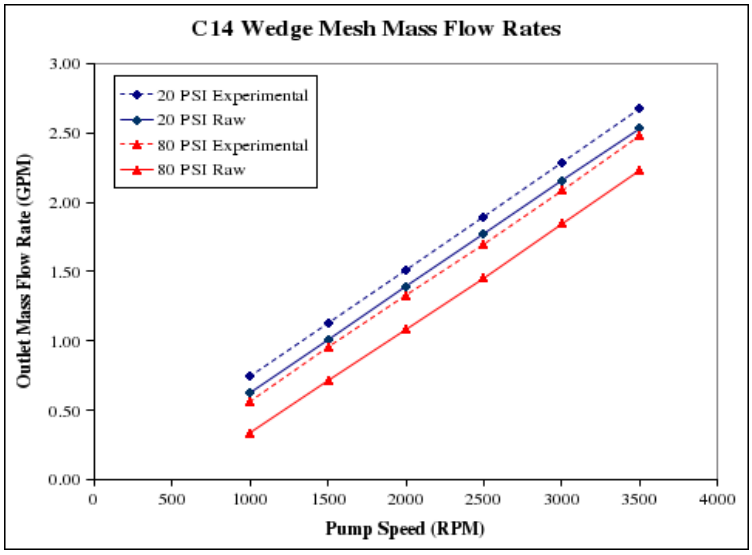

Figure 2-7: Outlet Mass Flow Rates for the C14 Pump with Wedge Mesh

First, the linear best fit line was calculated using the raw computational results. This line was then shifted upwards so that the line intersected the origin (zero flow at zero RPM), and the mass flow rate at each pump speed was calculated using this shifted line and was called the "Corrected Total Flow". Next, the total of the mass flow rates through the top, bottom, side, and pressure tap gaps was calculated. Finally, this total of gap mass flow rates was subtracted from the "Corrected Total Flow" to obtain the "Corrected Output Flow". More details and an example spreadsheet are shown in Appendix C.

This correction process produced computational results much closer to the experimental results. However, when the hexahedral mesh was used, the raw results were much closer to the experimental results than were the wedge mesh results. In order to show the differences between the raw and corrected outlet flow numbers, both will be shown in the following graphs and tables.

2.6.2 Viscous Torque Additions

Before the hexahedral mesh was developed, the wedge mesh technique was not able to accurately approximate the torque required to drive the pump. In an attempt to bring the torque numbers closer to the experimental values, viscous torque approximations were made for the side gap and the top surfaces of the inner and outer gerotor gears. These approximations were calculated by simulating simplified models of the top and side gaps. The viscous torque on the bottom surfaces of the inner and outer gears was assumed to be equal to the torque calculated for the top faces.

	Pump Speed	Top Gap Dimension			
		0.0005 inch	0.0013 inch (Baseline)	0.002 Inch	0.003 Inch
Inner Gear Torque (oz-in)	1000	0.497497	0.201507	0.134182	0.091810
	1500	0.752389	0.306728	0.205048	0.141017
	2000	1.010203	0.414098	0.277752	0.191898
	2500	1.270591	0.523367	0.352104	0.244277
	3000	1.533296	0.634360	0.427912	0.298052
	3500	1.798162	0.747040	0.505118	0.353199
Outer Gear Torque (oz-in)	1000	1.220570	0.481243	0.320211	0.220660
	1500	1.852682	0.737222	0.493181	0.342179
	2000	2.494865	1.000568	0.672377	0.469336
	2500	3.145798	1.270327	0.857095	0.601470
	3000	3.804654	1.545977	1.046715	0.738210
	3500	4.470888	1.826757	1.240926	0.879484

	Pump Speed	Side Gap Dimension			
		0.001 inch	0.002 inch	0.00325 Inch (Baseline)	0.004 Inch
Side Gap Torque (oz-in)	1000	4.569499	2.305459	1.479336	1.193763
	1500	6.900791	3.535050	2.309504	1.861845
	2000	9.301108	4.817106	3.190773	2.563779
	2500	11.762257	6.153571	4.114064	3.310512
	3000	14.276198	7.535726	5.085938	4.102432
	3500	16.847409	8.960563	5.971949	4.938934

Table 2-1: Viscous Torque Additions for the C14 Wedge Mesh

Table 2-1 summarizes the viscous torques added to the torque calculated by FLUENT after each simulation was completed. These torque values were placed into an Excel spreadsheet, where the torque would be added based on the top / bottom gap and side gap dimension for the current simulation. In this way, the torque values were brought closer to the experimental values. Note that this procedure was not necessary when using the hexahedral mesh, as all torque values were calculated directly in each simulation.

3. C14 Pump Results

The simulations of the C14 pump had two goals: first, to establish a method of creating the pump geometry, mesh, and simulation such that the results were similar to experimental results; and secondly to perform numerical experiments with modified geometry to determine the optimum combination of gap dimensions, inlet and outlet dimensions, and inlet and outlet angles.

All simulations with the C14 pump used 15W-40 motor oil as the pumped fluid. The simulations used a time step of 1×10^{-5} seconds, and 1000 time steps were calculated.

3.1 C14 Wedge Mesh Baseline

The first simulations completed were of the C14 pump using the wedge mesh. Experimental data were available for this pump as the models were being developed, and helped to ensure that the models were accurate.

Several parameters were recorded at the end of each time step, then averages were calculated using MATLAB (see Appendix C). These parameters include the following:

- Outlet mass flow rate
- Top, bottom, side, and pressure tap mass flow rates
- Torque on inner and outer gear faces and any other rotating surfaces

Table 3-1 shows the outlet mass flow rates (both the raw and corrected values) and compares them to experimentally determined values.

Pump Pressure	Pump Speed	Experimental Mass Flow Rate	Raw Computational Mass Flow Rate	Raw Percent Difference	Corrected Computational Mass Flow Rate	Corrected Percent Difference
PSI	RPM	GPM	GPM	%	GPM	%
20	1000	0.743	0.6242	-15.98%	0.7465	0.46%
	1500	1.126	1.0059	-10.66%	1.1225	-0.31%
	2000	1.510	1.3932	-7.73%	1.4929	-1.13%
	2500	1.896	1.7731	-6.48%	1.8727	-1.23%
	3000	2.285	2.1566	-5.62%	2.2582	-1.17%
	3500	2.676	2.5308	-5.43%	2.6342	-1.56%
40	1000	0.690	0.5227	-24.25%	0.7314	6.00%
	1500	1.072	0.9044	-15.64%	1.1075	3.31%
	2000	1.447	1.2842	-11.25%	1.4797	2.26%
	2500	1.831	1.6602	-9.33%	1.8577	1.46%
	3000	2.220	2.0457	-7.85%	2.2431	1.04%
	3500	2.617	2.4255	-7.32%	2.6060	-0.42%
60	1000	0.636	0.4287	-32.60%	0.7182	12.93%
	1500	1.012	0.8085	-20.11%	1.0924	7.95%
	2000	1.388	1.1789	-15.06%	1.4647	5.53%
	2500	1.765	1.5493	-12.22%	1.8407	4.29%
	3000	2.151	1.9442	-9.62%	2.2243	3.41%
	3500	2.550	2.3258	-8.79%	2.5872	1.46%
80	1000	0.562	0.3366	-40.11%	0.7032	25.13%
	1500	0.954	0.7126	-25.30%	1.0793	13.13%
	2000	1.329	1.0811	-18.65%	1.4515	9.22%
	2500	1.697	1.4515	-14.46%	1.8276	7.69%
	3000	2.082	1.8426	-11.50%	2.2055	5.93%
	3500	2.481	2.2300	-10.12%	2.5684	3.52%

Table 3-1: C14 Wedge Mesh Outlet Mass Flow Rates

The percent difference columns show that the raw computational mass flow rate numbers are not very close to the experimental numbers. The corrected numbers are very close to the experimental values for most of the simulations, except where pump pressures are high and speeds are low (1000 RPM at 80 PSI, for example).

Pump Pressure	Pump Speed	Experimental Total Torque	Experimental Losses	Experimental Torque	Raw Computational Torque	Percent Difference with Experimental	Corrected Computational Torque	Percent Difference with Experimental
PSI	RPM	oz-in	oz-in	oz-in	oz-in	%	oz-in	%
20	1000	17	5.93	11.07	11.512	3.99%	14.356	29.68%
	1500	18	6.15	11.85	12.569	6.07%	16.966	43.17%
	2000	20	6.75	13.25	13.865	4.64%	19.885	50.08%
	2500	22	6.50	15.50	15.288	-1.37%	22.989	48.32%
	3000	25	6.60	18.40	18.188	-1.15%	27.635	50.19%
	3500	28	6.70	21.30	22.050	3.52%	33.170	55.73%
40	1000	29	5.93	23.07	17.717	-23.20%	20.562	-10.87%
	1500	30	6.15	23.85	18.880	-20.84%	23.278	-2.40%
	2000	32	6.75	25.25	20.644	-18.24%	26.664	5.60%
	2500	34	6.50	27.50	21.967	-20.12%	29.668	7.88%
	3000	37	6.60	30.40	25.047	-17.61%	34.494	13.47%
	3500	40	6.70	33.30	29.162	-12.43%	40.282	20.97%
60	1000	38	5.93	32.07	24.084	-24.90%	26.929	-16.03%
	1500	41	6.15	34.85	25.315	-27.36%	29.713	-14.74%
	2000	41	6.75	34.25	27.354	-20.13%	33.374	-2.56%
	2500	45	6.50	38.50	28.692	-25.48%	36.394	-5.47%
	3000	48	6.60	41.40	31.956	-22.81%	41.402	0.00%
	3500	51	6.70	44.30	36.285	-18.09%	47.405	7.01%
80	1000	48	5.93	42.07	30.435	-27.66%	33.280	-20.89%
	1500	51	6.15	44.85	31.706	-29.31%	36.103	-19.50%
	2000	52	6.75	45.25	34.141	-24.55%	40.161	-11.25%
	2500	55	6.50	48.50	35.448	-26.91%	43.150	-11.03%
	3000	58	6.60	51.40	38.977	-24.17%	48.423	-5.79%
	3500	60	6.70	53.30	43.474	-18.44%	54.593	2.43%

Table 3-2: C14 Wedge Mesh Torque Values

Table 3-2 shows the torque values for the pump. The raw computational torque values are significantly lower than the experimental values, except for pump pressures of 20 PSI. The corrected torque values (see Section 2.6.2) are closer to the experimental values for all pump pressures except 20 PSI, where the torque is over-predicted by as much as 50%. These torques improved with the addition of the hexahedral mesh (see Section 3.6).

The outlet mass flow rate and torque values summarized in the tables above were used to calculate several efficiency curves, as described in Appendix A [12]. Figure 3-1 shows the volumetric efficiency curves for the experimental data and the raw computational data. The computational volumetric efficiencies are lower than the experimental results, due to the lower outlet mass flow rate. The curves show the same behavior as the experimental curves, where the volumetric efficiency is increased as the pump speed increases for all pump pressures.

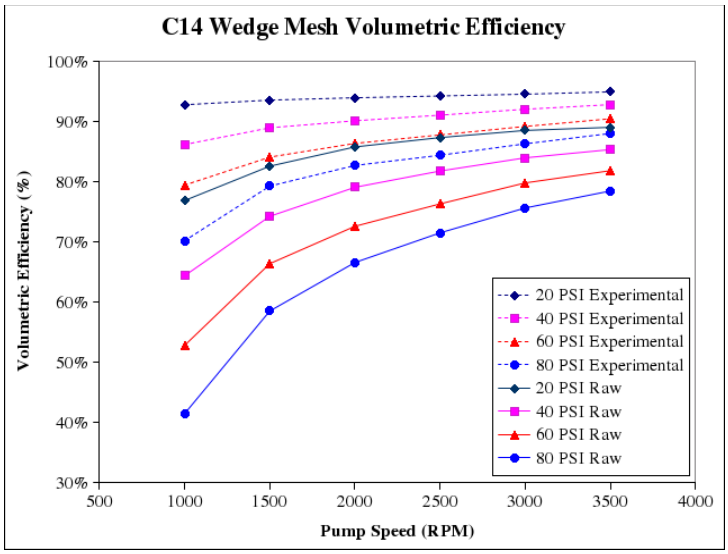

Figure 3-1: Volumetric Efficiency Curves (Raw vs. Experimental)

Figure 3-2 compares the raw computational volumetric efficiency curves with the corrected curves. The corrected curves are similar to the raw curves but are shifted upwards at every point. The 20 PSI curve is adjusted only slightly, while the 80 PSI curve is highly adjusted, especially at low pump speeds.

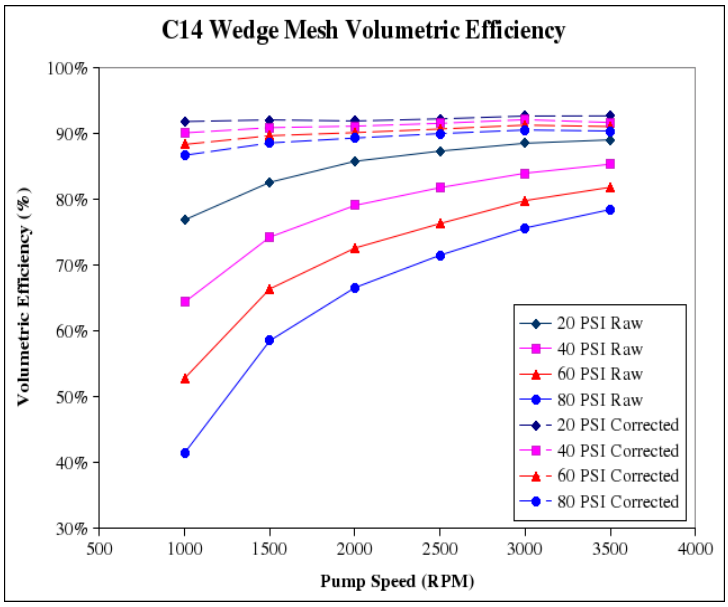

Figure 3-2: Volumetric Efficiency Curves (Raw vs. Corrected)

Figure 3-3 compares the overall efficiency curves for both the experimental and raw computational cases. Note that the raw curves show a much greater efficiency than the experimental curves. This occurs because of the higher outlet mass flow rate and low torque prediction supplied by FLUENT (see Appendix A).

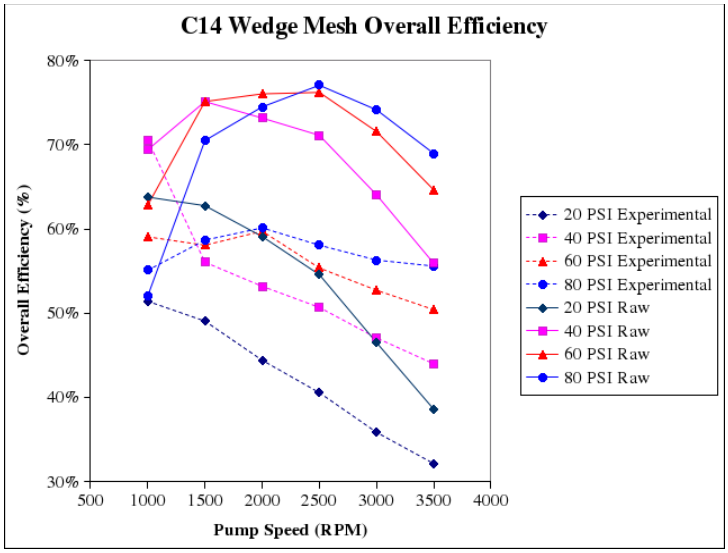

Figure 3-3: Overall Efficiency Curves (Raw vs. Experimental)

Figure 3-4 compares the raw and corrected computational overall efficiency curves. The corrected curves are adjusted upwards when the pump speeds are low, but are adjusted down at high pump speeds. This occurs because the outlet mass flow rates have been increased more than the torque has been increased for low pump speeds, and vice versa for high pump speeds.

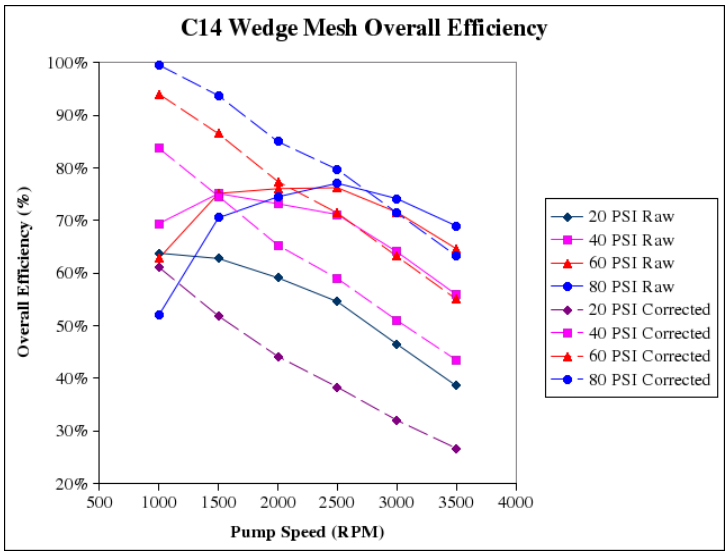

Figure 3-4: Overall Efficiency Curves (Raw vs. Corrected)

One final efficiency curve can be calculated from the overall and volumetric efficiency curves: the hydraulic efficiency curve (see Appendix A for derivation). Figure 3-5 shows the hydraulic efficiency curve for the experimental data (calculated from the overall and volumetric efficiencies) and the raw computational results. The computational curves are higher than the experimental curves for the same reasons as the overall efficiencies.

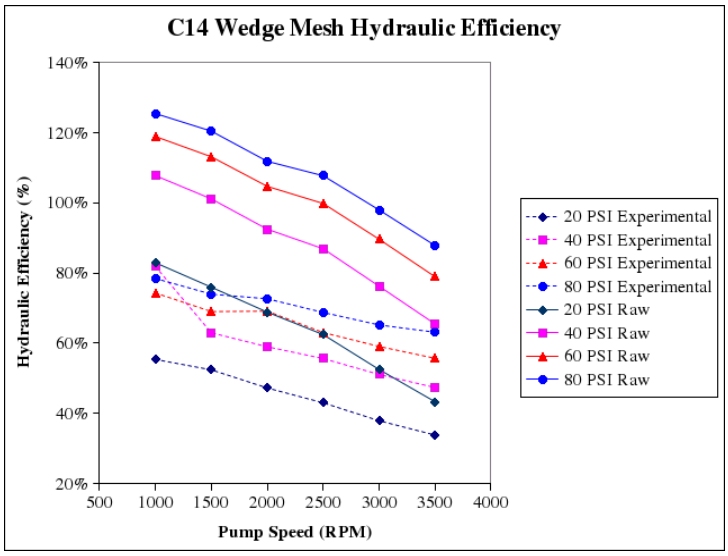

Figure 3-5: Hydraulic Efficiency Curves (Raw vs. Experimental)

Figure 3-6 compares the raw and corrected computational hydraulic efficiency curves. Here, the corrected efficiencies are lower than the raw efficiencies at each data point.

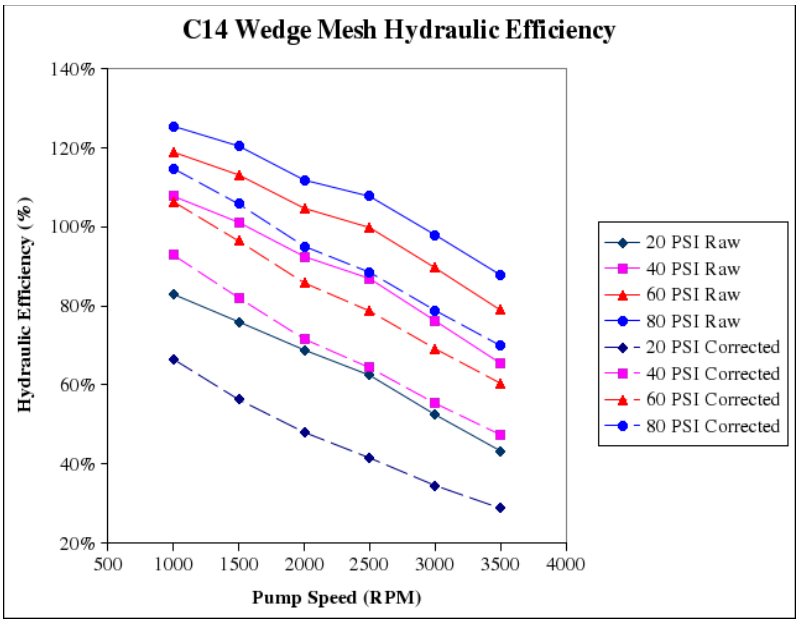

Figure 3-6: Hydraulic Efficiency Curves (Raw vs. Corrected)

Although the baseline results of the C14 pump using the wedge mesh were not as accurate as desired, it was determined that the computational results could serve to provide a relative comparison between the baseline design of the pump and various design changes. Thus, the mass flow rates, torque values, and efficiency curves described above will be used in Sections 3.2 through 3.6 to determine whether the design change was beneficial to the operation and efficiency of the pump.

3.2 C14 Top / Bottom Gap Optimization

The first geometry changes made to the C14 pump were differences in the top and bottom gap dimensions. The baseline pump had top and bottom gaps of 0.0013 inches. This dimension was changed to be 0.0005 inches, 0.002 inches, and 0.003 inches. In this way, the changes in pump output and efficiency could be seen from both increased and decreased gap dimensions. In these simulations the pressure rise across the pump was kept at 80 PSI, the maximum pressure used in the baseline calculations.

Top and Bottom Gap Size	Pump Speed	Experimental Mass Flow Rate	Raw Computational Mass Flow Rate	Raw Percent Difference	Corrected Computational Mass Flow Rate	Corrected Percent Difference	Corrected vs. Baseline Percent Difference
Inches	RPM	GPM	GPM	%	GPM	%	%
0.0005	1000	0.562	0.4026	-28.36%	0.7792	38.65%	10.68%
	1500	0.954	0.7852	-17.69%	1.1706	22.70%	8.51%
	2000	1.329	1.1762	-11.50%	1.5602	17.40%	7.56%
	2500	1.697	1.5740	-7.25%	1.9523	15.04%	6.86%
	3000	2.082	1.9780	-5.00%	2.3435	12.56%	6.25%
	3500	2.481	2.3587	-4.93%	2.7307	10.06%	6.29%
0.0013 (Baseline)	1000	0.562	0.3366	-40.11%	0.7040	25.27%	NA
	1500	0.954	0.7126	-25.30%	1.0788	13.08%	NA
	2000	1.329	1.0811	-18.65%	1.4506	9.15%	NA
	2500	1.697	1.4515	-14.47%	1.8270	7.66%	NA
	3000	2.082	1.8426	-11.50%	2.2057	5.94%	NA
	3500	2.481	2.2300	-10.12%	2.5690	3.55%	NA
0.002	1000	0.562	0.2433	-56.71%	0.6327	12.59%	-10.12%
	1500	0.954	0.6197	-35.04%	1.0089	5.75%	-6.48%
	2000	1.329	0.9992	-24.82%	1.3879	4.43%	-4.33%
	2500	1.697	1.3791	-18.73%	1.7646	3.98%	-3.41%
	3000	2.082	1.7820	-14.41%	2.1424	2.90%	-2.87%
	3500	2.481	2.1623	-12.85%	2.5194	1.55%	-1.93%
0.003	1000	0.562	0.1841	-67.24%	0.4318	-23.16%	-38.66%
	1500	0.954	0.3341	-64.98%	0.7958	-16.59%	-26.24%
	2000	1.329	0.7182	-45.96%	1.1615	-12.61%	-19.93%
	2500	1.697	1.1033	-34.99%	1.5218	-10.32%	-16.70%
	3000	2.082	1.4952	-28.18%	1.8926	-9.10%	-14.20%
	3500	2.481	1.8673	-24.74%	2.2648	-8.72%	-11.84%

Table 3-3: Top / Bottom Gap Outlet Mass Flow Rates

Table 3-3 shows the corrected outlet mass flow rate for the four cases simulated. It shows that the mass flow rate at the outlet is increased by about 6% over the baseline values when the top and bottom gaps are reduced to 0.0005 in. When the gap size is increased, the mass flow rate drops by approximately 5% for the 0.002 inch gap and over 15% for the 0.003 inch gap.

Top and Bottom Gap Size	Pump Speed	Experimental Torque	Raw Computational Torque	Percent Difference with Experimental	Corrected Computational Torque	Percent Difference with Experimental	Percent Difference with Baseline
Inches	RPM	oz-in	oz-in	%	oz-in	%	%
0.0005	1000	42.07	30.148	-28.34%	35.063	-16.66%	6.34%
	1500	44.85	31.535	-29.69%	39.055	-12.92%	8.73%
	2000	45.25	33.964	-24.94%	44.165	-2.40%	10.41%
	2500	48.50	35.018	-27.80%	47.965	-1.10%	12.27%
	3000	51.40	37.469	-27.10%	53.231	3.56%	13.45%
	3500	53.30	40.550	-23.92%	59.060	10.81%	14.23%
0.0013 (Baseline)	1000	42.07	30.126	-28.39%	32.971	-21.63%	NA
	1500	44.85	31.521	-29.72%	35.918	-19.92%	NA
	2000	45.25	33.981	-24.90%	40.001	-11.60%	NA
	2500	48.50	35.019	-27.80%	42.721	-11.92%	NA
	3000	51.40	37.472	-27.10%	46.919	-8.72%	NA
	3500	53.30	40.584	-23.86%	51.704	-2.99%	NA
0.0020	1000	42.07	30.117	-28.41%	32.505	-22.74%	-1.41%
	1500	44.85	31.483	-29.80%	35.189	-21.54%	-2.03%
	2000	45.25	33.969	-24.93%	39.060	-13.68%	-2.35%
	2500	48.50	35.016	-27.80%	41.549	-14.33%	-2.74%
	3000	51.40	37.435	-27.17%	45.470	-11.54%	-3.09%
	3500	53.30	40.520	-23.98%	49.984	-6.22%	-3.33%
0.0030	1000	42.07	30.075	-28.51%	32.179	-23.51%	-2.40%
	1500	44.85	31.473	-29.83%	34.749	-22.52%	-3.25%
	2000	45.25	33.930	-25.02%	38.443	-15.04%	-3.89%
	2500	48.50	34.980	-27.88%	40.785	-15.91%	-4.53%
	3000	51.40	37.454	-27.13%	44.612	-13.21%	-4.92%
	3500	53.30	40.560	-23.90%	48.997	-8.07%	-5.24%

Table 3-4: Top / Bottom Gap Torque Comparison

Table 3-4 compares the torque values with both the experimental and baseline results. The torque requirement is increased when the gap size is decreased, and decreased when the gap size is increased. This was the expected result. When looking at Tables 3-3 and 3-4, it is not readily apparent whether decreasing the top and bottom gaps would actually increase the efficiency of the pump, as both the mass flow rate and torque requirements increase. By looking at the efficiency curves for the different gap sizes, a determination can be made.

Figure 3-7 shows the corrected volumetric efficiency curves for the four cases simulated. As expected, the 0.0005 inch gap shows the highest volumetric efficiency, since the amount of flow leaking through the top and bottom gaps has been reduced. Note that the efficiencies drop off quickly as the gap size increases, especially at low pump speeds, where leakage related mass flow rates are high.

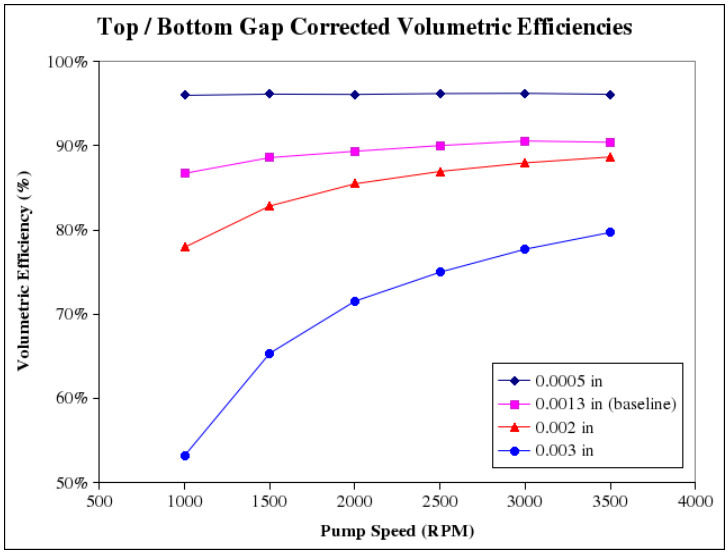

Figure 3-7: Top / Bottom Gap Volumetric Efficiency Curves

Figure 3-8 shows the hydraulic efficiencies. Here, the opposite trends to the volumetric efficiency curves are seen. The 0.003 inch gap has the greatest hydraulic efficiency, and higher efficiencies are seen at low pump speeds.

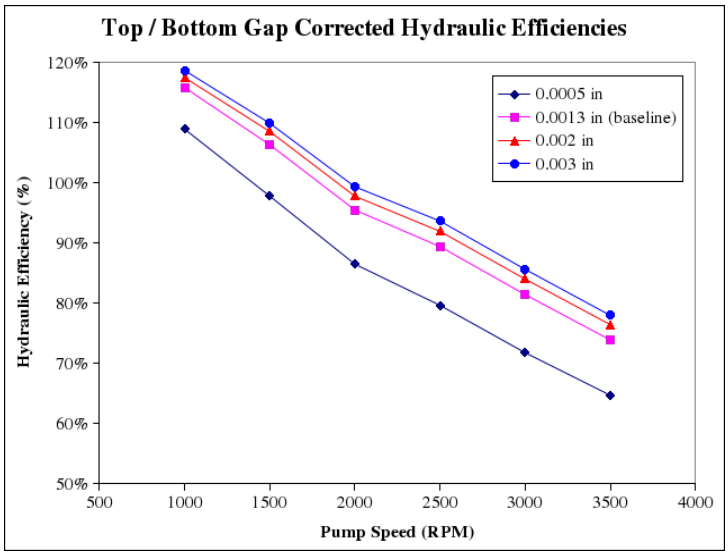

Figure 3-8: Top / Bottom Gap Hydraulic Efficiency Curves

Figure 3-9 allows for the most general comparison between the four gap sizes. This graph shows that the baseline dimension of 0.0013 inch is the best choice throughout the range of pump speeds. The 0.002 inch gap size shows nearly identical efficiencies at high pump speeds, but decreased efficiency at low pump speeds. The 0.0005 inch gap shows the opposite trend, with higher efficiency at low pump speeds and lower efficiency at high pump speeds.

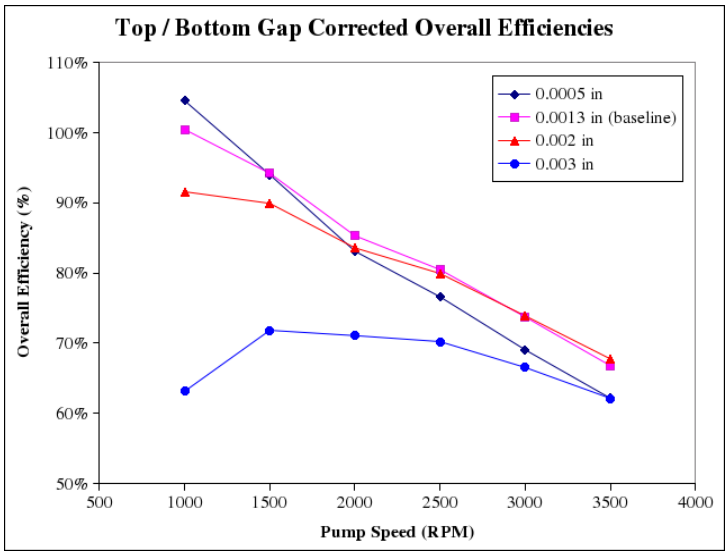

Figure 3-9: Top / Bottom Gap Overall Efficiency Curves

The top and bottom gap optimization procedure demonstrates that the baseline gap of 0.0013 inch is optimal for this pump.

3.3 C14 Side Gap Optimization

The second parameter to be optimized was the size of the side gap. This gap is a cylinder around the outer gerotor gear. The baseline pump had a side gap of 0.00325 in. This dimension was changed to be 0.001 in, 0.002 in, and 0.004 in. Again, pump pressures were kept at 80 PSI.

Side Gap Size	Pump Speed	Experimental Mass Flow Rate	Raw Computational Mass Flow Rate	Raw Percent Difference	Corrected Computational Mass Flow Rate	Corrected Percent Difference	Corrected vs. Baseline Percent Difference
Inches	RPM	GPM	GPM	%	GPM	%	%
0.001	1000	0.562	0.3422	-39.11%	0.7556	34.44%	1.19%
	1500	0.954	0.7397	-22.46%	1.1469	20.22%	0.84%
	2000	1.329	1.1321	-14.82%	1.5374	15.68%	0.73%
	2500	1.697	1.5212	-10.36%	1.9274	13.58%	0.57%
	3000	2.082	1.9218	-7.69%	2.3095	10.93%	0.40%
	3500	2.481	2.3078	-6.98%	2.6969	8.70%	0.45%
0.002	1000	0.562	0.3352	-40.36%	0.7467	32.86%	NA
	1500	0.954	0.7315	-23.32%	1.1374	19.23%	NA
	2000	1.329	1.1236	-15.46%	1.5263	14.84%	NA
	2500	1.697	1.5131	-10.84%	1.9165	12.93%	NA
	3000	2.082	1.9133	-8.10%	2.3004	10.49%	NA
	3500	2.481	2.2982	-7.37%	2.6847	8.21%	NA
0.00325 (Baseline)	1000	0.562	0.3301	-41.26%	0.7340	30.61%	-1.69%
	1500	0.954	0.7272	-23.77%	1.1238	17.80%	-1.19%
	2000	1.329	1.1182	-15.86%	1.5107	13.67%	-1.02%
	2500	1.697	1.5072	-11.18%	1.9020	12.08%	-0.75%
	3000	2.082	1.9097	-8.28%	2.2958	10.27%	-0.20%
	3500	2.481	2.2933	-7.57%	2.6741	7.78%	-0.40%
0.004	1000	0.562	0.3173	-43.54%	0.7262	29.21%	-2.75%
	1500	0.954	0.7127	-25.29%	1.1155	16.93%	-1.92%
	2000	1.329	1.1041	-16.92%	1.5035	13.13%	-1.49%
	2500	1.697	1.4929	-12.03%	1.8919	11.48%	-1.28%
	3000	2.082	1.8934	-9.06%	2.2735	9.20%	-1.17%
	3500	2.481	2.2764	-8.25%	2.6608	7.25%	-0.89%

Table 3-5: Side Gap Outlet Mass Flow Rates

Table 3-5 shows the outlet mass flow rates for all cases and compares them to the experimental and baseline cases. For a side gap of 0.001 in, the outlet mass flow rate is increased by only a fraction of a percent. When the side gap is increased, the outlet mass flow rate is decreased by a maximum of 2.75%. Thus, changing the side gap dimension has only a small effect on the outlet mass flow rate.

Side Gap Size	Pump Speed	Experimental Torque	Raw Computational Torque	Percent Difference with Experimental	Corrected Computational Torque	Percent Difference with Experimental	Percent Difference with Baseline
Inches	RPM	oz-in	oz-in	%	oz-in	%	%
0.001	1000	42.07	30.148	-28.34%	35.063	-16.66%	6.34%
	1500	44.85	31.535	-29.69%	39.055	-12.92%	8.73%
	2000	45.25	33.964	-24.94%	44.165	-2.40%	10.41%
	2500	48.50	35.018	-27.80%	47.965	-1.10%	12.27%
	3000	51.40	37.469	-27.10%	53.231	3.56%	13.45%
	3500	53.30	40.550	-23.92%	59.060	10.81%	14.23%
0.002	1000	42.07	30.126	-28.39%	32.971	-21.63%	NA
	1500	44.85	31.521	-29.72%	35.918	-19.92%	NA
	2000	45.25	33.981	-24.90%	40.001	-11.60%	NA
	2500	48.50	35.019	-27.80%	42.721	-11.92%	NA
	3000	51.40	37.472	-27.10%	46.919	-8.72%	NA
	3500	53.30	40.584	-23.86%	51.704	-2.99%	NA
0.00325 (Baseline)	1000	42.07	30.117	-28.41%	32.505	-22.74%	-1.41%
	1500	44.85	31.483	-29.80%	35.189	-21.54%	-2.03%
	2000	45.25	33.969	-24.93%	39.060	-13.68%	-2.35%
	2500	48.50	35.016	-27.80%	41.549	-14.33%	-2.74%
	3000	51.40	37.435	-27.17%	45.470	-11.54%	-3.09%
	3500	53.30	40.520	-23.98%	49.984	-6.22%	-3.33%
0.004	1000	42.07	30.075	-28.51%	32.179	-23.51%	-2.40%
	1500	44.85	31.473	-29.83%	34.749	-22.52%	-3.25%
	2000	45.25	33.930	-25.02%	38.443	-15.04%	-3.89%
	2500	48.50	34.980	-27.88%	40.785	-15.91%	-4.53%
	3000	51.40	37.454	-27.13%	44.612	-13.21%	-4.92%
	3500	53.30	40.560	-23.90%	48.997	-8.07%	-5.24%

Table 3-6: Side Gap Torque Comparison

Table 3-6 compares the torque values for the four cases simulated. The torque required to drive the pump increases when the side gap decreases by 6-14%. As is expected, the torque then decreases as the side gap increases. The torque differences are much greater than the mass flow rate differences, and as such will dominate in the efficiency calculations.

Figure 3-10 shows the corrected volumetric efficiencies. This shows that the 0.001 inch gap has the greatest volumetric efficiency, as is expected, as the leakage mass flow rate is reduced.

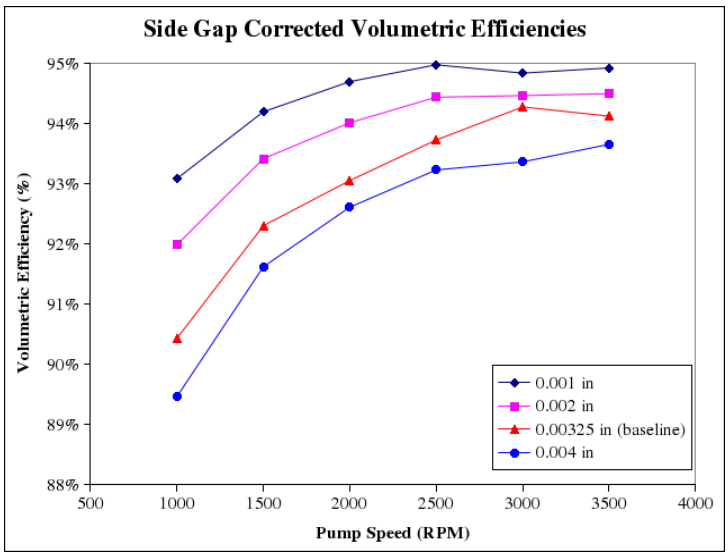

Figure 3-10: Side Gap Volumetric Efficiency Curves

Figure 3-11 shows the corrected hydraulic efficiency curves for the four cases simulated. Here, the largest gap has the greatest hydraulic efficiency, as was seen in the top and bottom gap optimization.

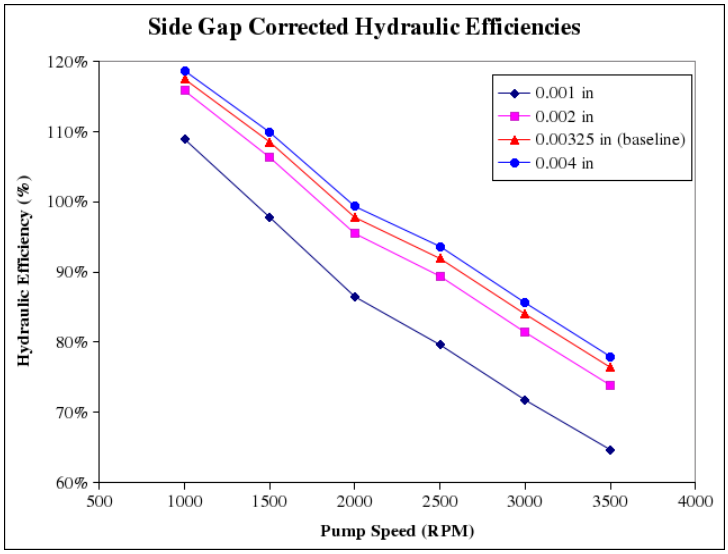

Figure 3-11: Side Gap Hydraulic Efficiency Curves

Figure 3-12 shows the overall efficiency curves, and provides a cumulative comparison of the four designs. Here, the largest gap size of 0.004 inches has the greatest overall efficiency. This occurs because the torque required to drive the pump is reduced to a greater extent than the outlet mass flow rate is reduced. Thus, it is recommended that the side gap be increased to 0.004 in.

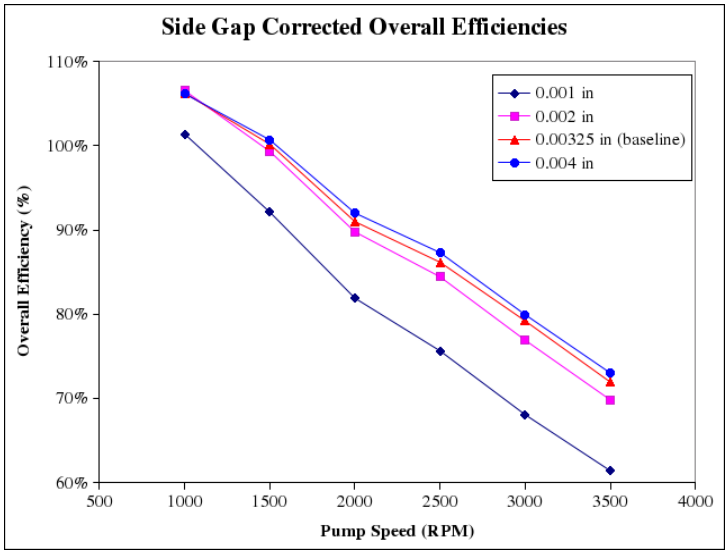

Figure 3-12: Side Gap Overall Efficiency Curves

3.4 C14 Inlet / Outlet Size Optimization

The inlet and outlet ports of the C14 pump use standard o-ring face seal (ORFS) connections to attach the inlet and outlet hoses to the pump. The baseline design of the pump uses a #8 ORFS for the inlet hose and a #6 ORFS for the outlet hose. In order to determine the differences in pump efficiency caused by changes in connection sizes, the following combinations were simulated (at a constant 80 PSI):

Inlet Size	Outlet Size
#6	#6
#8	#6
#8	#8
#10	#8
#10	#10

Table 3-7: Inlet / Outlet Size Combinations for Simulation

Inlet / Outlet Sizes	Pump Speed	Experimental Mass Flow Rate	Raw Computational Mass Flow Rate	Raw Percent Difference	Corrected Computational Mass Flow Rate	Corrected Percent Difference	Corrected vs. Baseline Percent Difference
	RPM	GPM	GPM	%	GPM	%	%
6 Inlet / 6 Outlet	1000	0.562	0.3311	-41.09%	0.7234	28.72%	2.71%
	1500	0.954	0.7133	-25.23%	1.1005	15.35%	1.96%
	2000	1.329	1.1073	-16.68%	1.4760	11.06%	1.71%
	2500	1.697	1.4837	-12.57%	1.8507	9.06%	1.26%
	3000	2.082	1.9026	-8.62%	2.2254	6.89%	0.85%
	3500	2.481	2.3010	-7.26%	2.5985	4.73%	1.10%
8 Inlet / 6 Outlet (Baseline)	1000	0.562	0.3361	-40.20%	0.7043	25.32%	NA
	1500	0.954	0.7118	-25.39%	1.0793	13.13%	NA
	2000	1.329	1.0805	-18.70%	1.4512	9.20%	NA
	2500	1.697	1.4513	-14.48%	1.8277	7.70%	NA
	3000	2.082	1.8427	-11.49%	2.2067	5.99%	NA
	3500	2.481	2.2300	-10.12%	2.5701	3.59%	NA
8 Inlet / 8 Outlet	1000	0.562	0.3416	-39.22%	0.7122	26.73%	1.12%
	1500	0.954	0.7207	-24.45%	1.0832	13.54%	0.36%
	2000	1.329	1.1073	-16.68%	1.4520	9.25%	0.05%
	2500	1.697	1.4983	-11.71%	1.8182	7.14%	-0.52%
	3000	2.082	1.8870	-9.37%	2.1842	4.91%	-1.02%
	3500	2.481	2.2818	-8.03%	2.5429	2.50%	-1.06%
10 Inlet / 8 Outlet	1000	0.562	0.3425	-39.06%	0.7187	27.87%	2.03%
	1500	0.954	0.7224	-24.28%	1.0927	14.53%	1.24%
	2000	1.329	1.1096	-16.51%	1.4650	10.23%	0.95%
	2500	1.697	1.5033	-11.41%	1.8353	8.15%	0.41%
	3000	2.082	1.8881	-9.31%	2.2008	5.70%	-0.27%
	3500	2.481	2.3050	-7.09%	2.5662	3.44%	-0.15%
10 Inlet / 10 Outlet	1000	0.562	0.3387	-39.73%	0.7209	28.27%	1.22%
	1500	0.954	0.7223	-24.29%	1.0963	14.92%	1.21%
	2000	1.329	1.1110	-16.40%	1.4679	10.45%	1.09%
	2500	1.697	1.5041	-11.37%	1.8359	8.19%	0.97%
	3000	2.082	1.8936	-9.05%	2.2066	5.98%	1.02%
	3500	2.481	2.3065	-7.03%	2.5685	3.53%	1.01%

Table 3-8: Inlet / Outlet Size Mass Flow Rates

Table 3-8 compares the outlet mass flow rates for the five cases simulated. This shows that the mass flow rate is increased slightly when the inlet connection is increased in size, but only by about one percent.

Inlet / Outlet Sizes	Pump Speed	Experimental Torque	Raw Computational Torque	Percent Difference with Experimental	Corrected Computational Torque	Percent Difference with Experimental	Percent Difference with Baseline
	RPM	oz-in	oz-in	%	oz-in	%	%
6 Inlet / 6 Outlet	1000	42.07	30.749	-26.91%	33.593	-20.15%	0.94%
	1500	44.85	31.831	-29.03%	36.228	-19.22%	0.35%
	2000	45.25	34.289	-24.22%	40.309	-10.92%	0.37%
	2500	48.50	36.454	-24.84%	44.156	-8.96%	2.33%
	3000	51.40	39.396	-23.35%	48.843	-4.97%	0.87%
	3500	53.30	42.549	-20.17%	53.669	0.69%	-1.69%
8 Inlet / 6 Outlet (Baseline)	1000	42.07	30.434	-27.66%	33.279	-20.90%	NA
	1500	44.85	31.706	-29.31%	36.103	-19.50%	NA
	2000	45.25	34.141	-24.55%	40.161	-11.25%	NA
	2500	48.50	35.448	-26.91%	43.149	-11.03%	NA
	3000	51.40	38.976	-24.17%	48.423	-5.79%	NA
	3500	53.30	43.474	-18.44%	54.594	2.43%	NA
8 Inlet / 8 Outlet	1000	42.07	30.384	-27.78%	33.229	-21.01%	-0.15%
	1500	44.85	31.662	-29.40%	36.059	-19.60%	-0.12%
	2000	45.25	34.241	-24.33%	40.262	-11.02%	0.25%
	2500	48.50	36.206	-25.35%	43.907	-9.47%	1.76%
	3000	51.40	39.660	-22.84%	49.107	-4.46%	1.41%
	3500	53.30	43.032	-19.26%	54.151	1.60%	-0.81%
10 Inlet / 8 Outlet	1000	42.07	30.276	-28.03%	33.120	-21.27%	-0.48%
	1500	44.85	31.568	-29.61%	35.966	-19.81%	-0.38%
	2000	45.25	34.110	-24.62%	40.131	-11.31%	-0.07%
	2500	48.50	36.015	-25.74%	43.717	-9.86%	1.32%
	3000	51.40	39.559	-23.04%	49.006	-4.66%	1.20%
	3500	53.30	42.397	-20.46%	53.517	0.41%	-1.97%
10 Inlet / 10 Outlet	1000	42.07	30.426	-27.68%	33.270	-20.92%	0.12%
	1500	44.85	31.543	-29.67%	35.940	-19.87%	-0.33%
	2000	45.25	34.023	-24.81%	40.043	-11.51%	-0.54%
	2500	48.50	35.937	-25.90%	43.639	-10.02%	-0.61%
	3000	51.40	39.193	-23.75%	48.640	-5.37%	-0.95%
	3500	53.30	42.244	-20.74%	53.363	0.12%	-1.46%

Table 3-9: Inlet / Outlet Size Torque Comparison

Table 3-9 compares each case with the experimental torque values and the baseline design. The torque required to drive the pump increases slightly with a restricted inlet connection, and decreases slightly with larger connections. These changes are the same order as the mass flow rate changes. The efficiency equations below help to distinguish what these differences mean.

Figure 3-13 shows the volumetric efficiency curves for the inlet and outlet sizing optimization. The design using a #6 ORFS for the inlet and a #6 ORFS for the outlet shows the best volumetric efficiency, mostly due to slightly smaller leakage mass flow rates than the other designs.

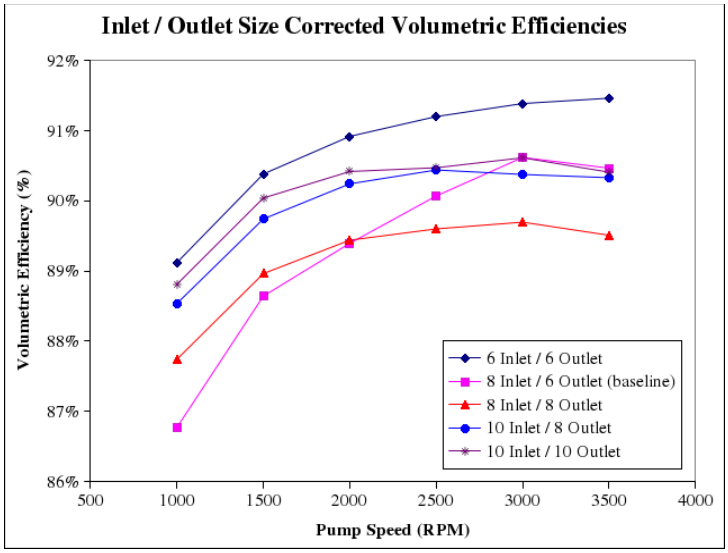

Figure 3-13: Inlet / Outlet Size Volumetric Efficiency Curves

Figure 3-14 shows the hydraulic efficiency curves for the five designs simulated. As with the other optimizations, this graph shows the opposite trends as the volumetric efficiency graph. In this case, the design using #10 ORFS for both the inlet and outlet has the highest efficiency, followed closely by the #10 inlet / #8 outlet design.

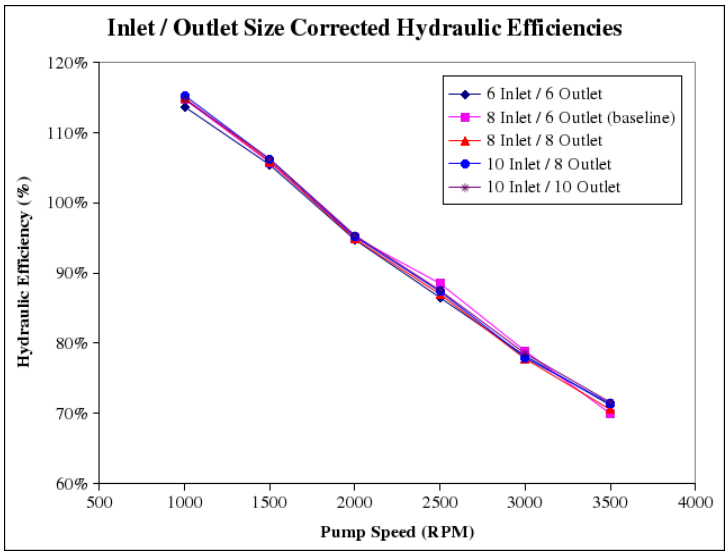

Figure 3-14: Inlet / Outlet Size Hydraulic Efficiency Curves

Figure 3-15 shows the overall efficiencies for the inlet and outlet size optimization. This graph shows that the design using a #10 ORFS for the inlet and a #8 ORFS for the outlet has the highest efficiency, followed by the design using #10 ORFS connections for both the inlet and outlet. The efficiency gain, however, is very minimal (one or two percent). While it is advisable to change the connections to larger fittings, the efficiency of the pump will not suffer significantly if the connections remain the same as the baseline pump.

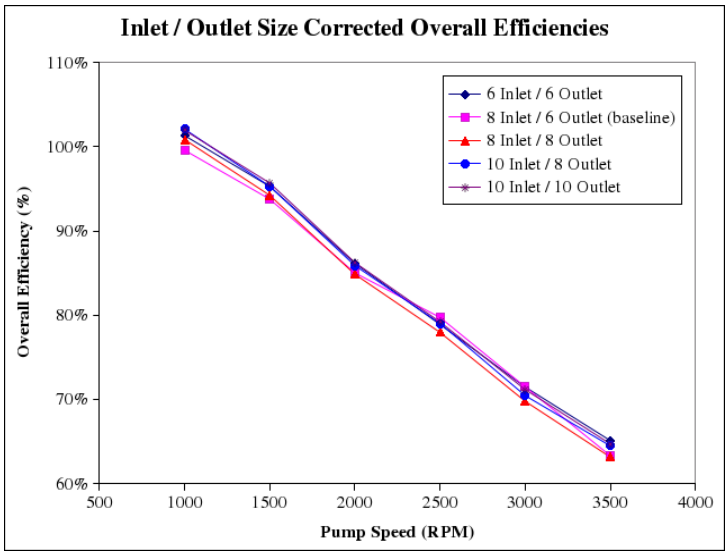

Figure 3-15: Inlet / Outlet Size Overall Efficiency Curves

3.5 C14 Inlet / Outlet Angle Optimization

The inlet and outlet ports for the baseline C14 pump exit the pump horizontally if the axis of the gerotor is positioned vertically. Simulations were performed to discover the differences in pump efficiency if these ports were positioned at different angles other than horizontal (or zero degrees). The ports were angled at 30, 45, 60, and 90 degrees from the horizontal. Figure 4-16 shows the C14 pump with the ports at zero degrees and at 45 degrees.

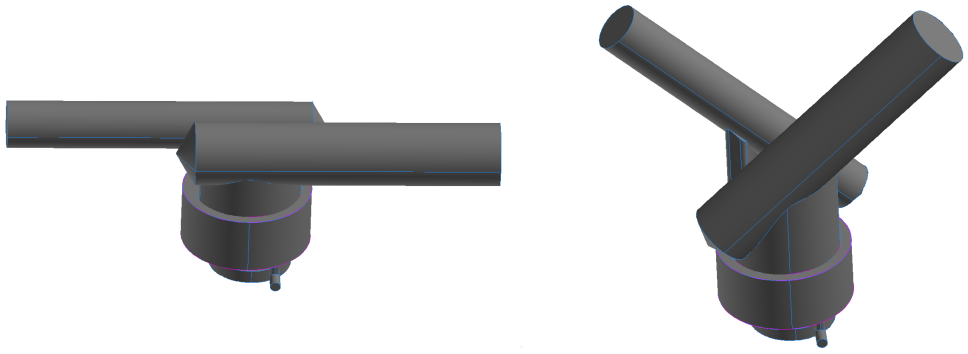

Zero Degrees **45 Degrees**

Figure 3-16: Inlet / Outlet Tube Angles

Inlet / Outlet Angle	Pump Speed	Experimental Mass Flow Rate	Raw Computational Mass Flow Rate	Raw Percent Difference	Corrected Computational Mass Flow Rate	Corrected Percent Difference	Corrected vs. Baseline Percent Difference
Degrees	RPM	GPM	GPM	%	GPM	%	%
0 (Baseline)	1000	0.562	0.33	-41.26%	0.72	28.45%	NA
	1500	0.954	0.73	-23.77%	1.1	15.07%	NA
	2000	1.329	1.12	-15.86%	1.47	10.54%	NA
	2500	1.697	1.51	-11.18%	1.84	8.69%	NA
	3000	2.082	1.91	-8.28%	2.22	6.74%	NA
	3500	2.481	2.29	-7.57%	2.59	4.20%	NA
30	1000	0.562	0.335	-40.48%	0.715	27.20%	-0.97%
	1500	0.954	0.710	-25.53%	1.088	14.00%	-0.93%
	2000	1.329	1.094	-17.68%	1.458	9.70%	-0.76%
	2500	1.697	1.485	-12.48%	1.825	7.56%	-1.04%
	3000	2.082	1.867	-10.32%	2.190	5.16%	-1.48%
	3500	2.481	2.292	-7.63%	2.561	3.23%	-0.93%
45	1000	0.562	0.333	-40.69%	0.715	27.22%	-0.95%
	1500	0.954	0.710	-25.59%	1.088	14.02%	-0.91%
	2000	1.329	1.093	-17.74%	1.458	9.72%	-0.74%
	2500	1.697	1.485	-12.50%	1.828	7.72%	-0.89%
	3000	2.082	1.867	-10.31%	2.193	5.35%	-1.30%
	3500	2.481	2.290	-7.69%	2.563	3.28%	-0.88%
60	1000	0.562	0.337	-40.02%	0.717	27.58%	-0.68%
	1500	0.954	0.715	-25.09%	1.091	14.32%	-0.65%
	2000	1.329	1.099	-17.32%	1.463	10.09%	-0.41%
	2500	1.697	1.490	-12.17%	1.834	8.10%	-0.55%
	3000	2.082	1.878	-9.81%	2.206	5.98%	-0.72%
	3500	2.481	2.297	-7.41%	2.578	3.90%	-0.29%
90	1000	0.562	0.336	-40.28%	0.713	26.85%	-1.25%
	1500	0.954	0.714	-25.18%	1.085	13.69%	-1.20%
	2000	1.329	1.098	-17.40%	1.455	9.48%	-0.96%
	2500	1.697	1.488	-12.33%	1.825	7.53%	-1.07%
	3000	2.082	1.865	-10.42%	2.194	5.38%	-1.28%
	3500	2.481	2.289	-7.73%	2.564	3.36%	-0.81%

Table 3-10: Inlet / Outlet Angles Mass Flow Rates

Table 3-10 compares the outlet mass flow rate each of the five cases and compares them to both the experimental results and the baseline result. The mass flow rate decreases slightly with any change in angle, but only by about one percent or less. This is a negligible change in flow rate.

Inlet / Outlet Angle	Pump Speed	Experimental Torque	Raw Computational Torque	Percent Difference with Experimental	Corrected Computational Torque	Percent Difference with Experimental	Percent Difference with Baseline
Degrees	RPM	oz-in	oz-in	%	oz-in	%	%
0 (Baseline)	1000	42.07	30.434	-27.66%	33.279	-20.90%	NA
	1500	44.85	31.705	-29.31%	36.103	-19.50%	NA
	2000	45.25	34.141	-24.55%	40.161	-11.25%	NA
	2500	48.50	35.448	-26.91%	43.150	-11.03%	NA
	3000	51.40	38.976	-24.17%	48.422	-5.79%	NA
	3500	53.30	43.475	-18.43%	54.594	2.43%	NA
30	1000	42.07	30.856	-26.66%	33.701	-19.89%	1.27%
	1500	44.85	32.163	-28.29%	36.560	-18.48%	1.27%
	2000	45.25	34.800	-23.09%	40.820	-9.79%	1.64%
	2500	48.50	36.811	-24.10%	44.512	-8.22%	3.16%
	3000	51.40	40.658	-20.90%	50.104	-2.52%	3.47%
	3500	53.30	43.361	-18.65%	54.480	2.21%	-0.21%
45	1000	42.07	30.890	-26.57%	33.735	-19.81%	1.37%
	1500	44.85	32.149	-28.32%	36.546	-18.52%	1.23%
	2000	45.25	34.771	-23.16%	40.791	-9.85%	1.57%
	2500	48.50	36.754	-24.22%	44.456	-8.34%	3.03%
	3000	51.40	40.611	-20.99%	50.057	-2.61%	3.38%
	3500	53.30	43.337	-18.69%	54.456	2.17%	-0.25%
60	1000	42.07	30.670	-27.10%	33.515	-20.34%	0.71%
	1500	44.85	31.961	-28.74%	36.359	-18.93%	0.71%
	2000	45.25	34.517	-23.72%	40.537	-10.42%	0.94%
	2500	48.50	36.495	-24.75%	44.197	-8.87%	2.43%
	3000	51.40	40.260	-21.67%	49.707	-3.29%	2.65%
	3500	53.30	43.045	-19.24%	54.165	1.62%	-0.79%
90	1000	42.07	30.706	-27.01%	33.551	-20.25%	0.82%
	1500	44.85	32.033	-28.58%	36.430	-18.77%	0.91%
	2000	45.25	34.753	-23.20%	40.773	-9.89%	1.52%
	2500	48.50	36.870	-23.98%	44.572	-8.10%	3.30%
	3000	51.40	41.093	-20.05%	50.540	-1.67%	4.37%
	3500	53.30	43.658	-18.09%	54.778	2.77%	0.34%

Table 3-11: Inlet / Outlet Angles Torque Comparison

Table 3-11 compares the torque requirements for the five cases. Here, the torques are increased slightly, from about one to three percent. With the decrease in mass flow rate and the increase in torque, it is expected that the baseline result will provide the most efficient design.

Figure 3-17 show the corrected volumetric efficiency curves. All of the simulations are very similar, with a slight edge given to the 60 degree case. However, the efficiency gain is only a small fraction of a percent.

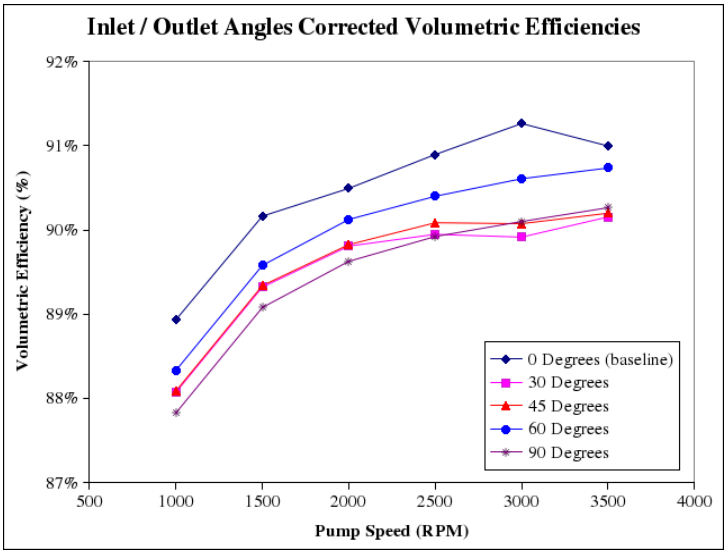

Figure 3-17: Inlet / Outlet Angles Volumetric Efficiency Curves

Figure 3-18 compares the corrected hydraulic efficiency curves. Here, the baseline design of zero degrees has the greatest efficiency, with the other designs following close behind.

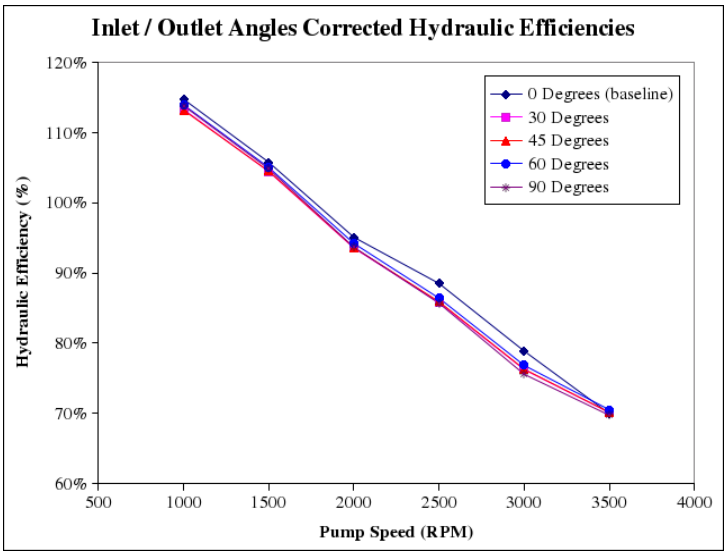

Figure 3-18: Inlet / Outlet Angles Hydraulic Efficiency Curves

Figure 3-19 compares the corrected overall efficiency curves for the inlet and outlet angle optimization. As expected, the baseline design is the most efficient. Thus it is recommended that the design of the inlet and outlet ports remain unchanged.

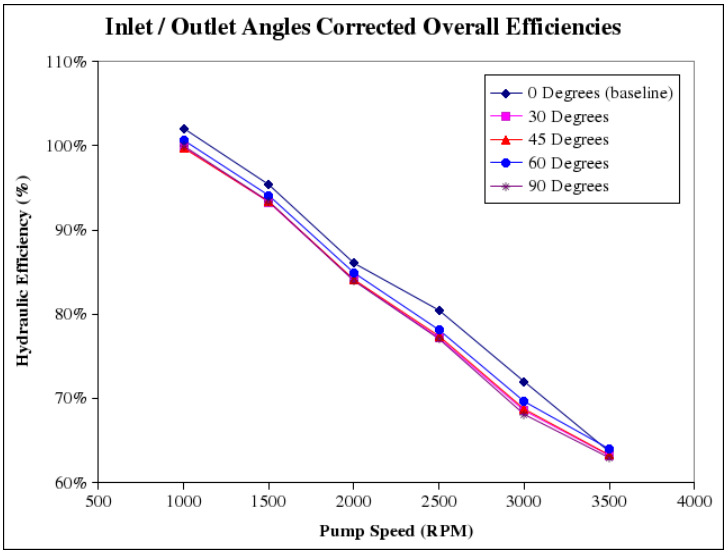

Figure 3-19: Inlet / Outlet Angles Overall Efficiency Curves

3.6 C14 Hexahedral Mesh Baseline

After the optimizations were complete for the C14 pump, a new method of meshing the gerotor fluid volume was developed with the assistance of EMP and FLUENT engineers. This hexahedral meshing scheme is summarized in Section 3.5.2. This method proved to be much more accurate in predicting both the outlet mass flow rate and the torque required to drive the pump.

Pump Pressure	Pump Speed	Experimental Mass Flow Rate	Raw Computational Mass Flow Rate	Raw Percent Difference	Corrected Computational Mass Flow Rate	Corrected Percent Difference
PSI	RPM	GPM	GPM	%	GPM	%
20	1000	0.743	0.7977	7.36%	0.7677	3.32%
	1500	1.126	1.2065	7.15%	1.1533	2.42%
	2000	1.510	1.6156	6.99%	1.5385	1.89%
	2500	1.896	2.0273	6.93%	1.9225	1.40%
	3000	2.285	2.4349	6.56%	2.3066	0.95%
	3500	2.676	2.8412	6.17%	2.6902	0.53%
40	1000	0.690	0.7770	12.61%	0.7635	10.65%
	1500	1.072	1.1857	10.61%	1.1497	7.25%
	2000	1.447	1.5946	10.20%	1.5359	6.14%
	2500	1.831	2.0066	9.59%	1.9208	4.90%
	3000	2.220	2.4144	8.76%	2.3068	3.91%
	3500	2.617	2.8211	7.80%	2.6922	2.87%
60	1000	0.636	0.7565	18.95%	0.7575	19.10%
	1500	1.012	1.1650	15.12%	1.1453	13.17%
	2000	1.388	1.5737	13.38%	1.5321	10.38%
	2500	1.765	1.9859	12.52%	1.9174	8.63%
	3000	2.151	2.3941	11.30%	2.3042	7.12%
	3500	2.550	2.8010	9.84%	2.6908	5.52%
80	1000	0.562	0.7385	31.41%	0.7493	33.33%
	1500	0.954	1.1462	20.15%	1.1386	19.35%
	2000	1.329	1.5540	16.93%	1.5252	14.76%
	2500	1.697	1.9658	15.84%	1.9100	12.55%
	3000	2.082	2.3736	14.01%	2.2967	10.31%
	3500	2.481	2.7809	12.09%	2.6831	8.15%

Table 3-12: C14 Hexahedral Mesh Outlet Mass Flow Rates

Table 3-12 compares the outlet mass flow rates for the hexahedral mesh computational pump with the experimental results. The raw results are already close to the experimental values, with a difference of about 15%. The corrected numbers are very close to the experimental values, particularly at 20 PSI. These results are far superior to the results obtained by using the wedge mesh (see Section 4.1).

Pump Pressure	Pump Speed	Experimental Torque	Computational Torque	Percent Difference with Experimental
PSI	RPM	oz-in	oz-in	%
20	1000	11.07	12.837	15.96%
	1500	11.85	14.718	24.20%
	2000	13.25	16.778	26.63%
	2500	15.50	19.075	23.06%
	3000	18.40	21.514	16.92%
	3500	21.30	24.204	13.63%
40	1000	23.07	22.664	-1.76%
	1500	23.85	24.533	2.86%
	2000	25.25	26.595	5.33%
	2500	27.50	28.923	5.17%
	3000	30.40	31.324	3.04%
	3500	33.30	33.988	2.07%
60	1000	32.07	32.469	1.24%
	1500	34.85	34.362	-1.40%
	2000	34.25	36.408	6.30%
	2500	38.50	38.785	0.74%
	3000	41.40	41.151	-0.60%
	3500	44.30	43.792	-1.15%
80	1000	42.07	42.893	1.96%
	1500	44.85	45.007	0.35%
	2000	45.25	47.495	4.96%
	2500	48.50	50.162	3.43%
	3000	51.40	52.364	1.88%
	3500	53.30	55.074	3.33%

Table 3-13: C14 Hexahedral Mesh Torque Comparison

Table 3-13 compares the computational torque with the experimentally determined values. Note that the torque does not require a correction when using the hexahedral mesh. The torque values are exceptionally close to the experimental values, with the exception of the 20 PSI cases. With these accurate mass flow and torque predictions, the efficiency curves should be more accurate than with the wedge mesh.

Figure 3-20 compares the raw volumetric efficiency curves to the experimental values. The raw results are higher than the experimental results by 7-20%. All of the raw results are very similar to each other, with a similar trend to lower efficiencies with higher pump pressures.

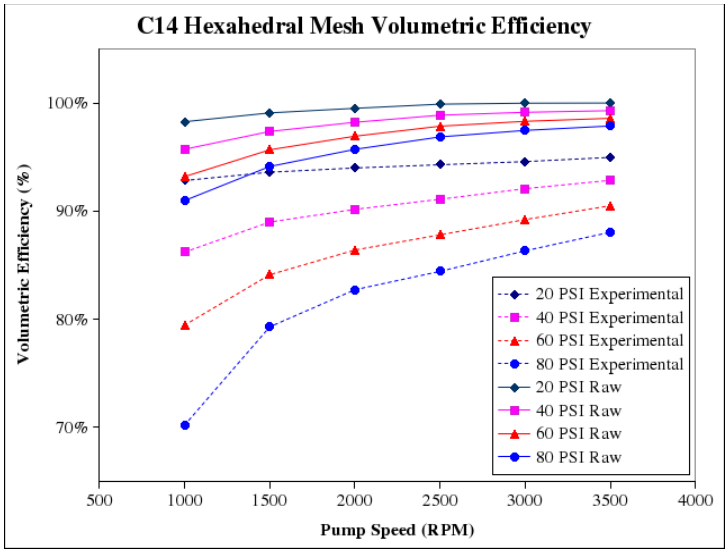

Figure 3-20: C14 Hexahedral Mesh Volumetric Efficiencies (Raw vs. Experimental)

Figure 3-21 compares the raw and corrected volumetric efficiency curves. The corrections reduce the efficiency by 5-6%.

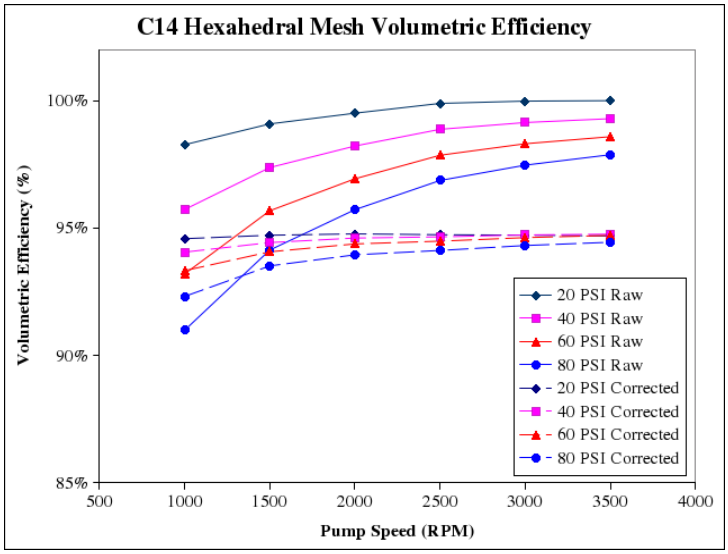

Figure 3-21: C14 Hexahedral Mesh Volumetric Efficiencies (Raw vs. Corrected)

Figure 3-22 shows the raw and experimental hydraulic efficiency curves. The raw curves are higher than the experimental curves, as was seen with the wedge mesh.

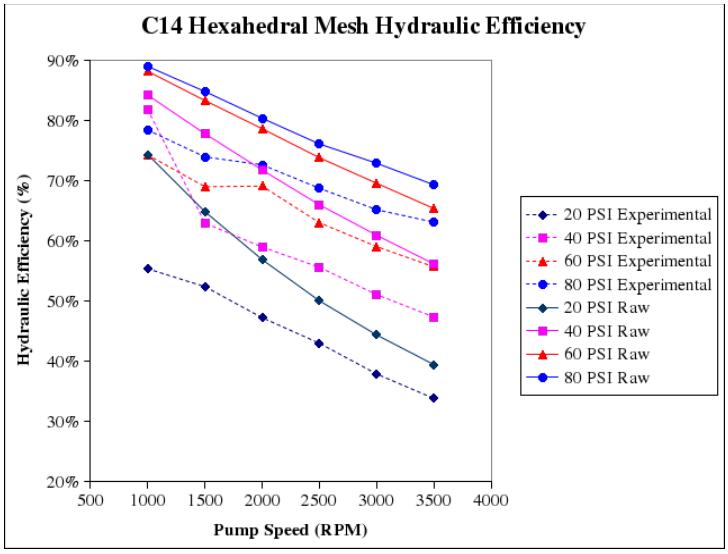

Figure 3-22: C14 Hexahedral Mesh Hydraulic Efficiencies (Raw vs. Experimental)

Figure 3-23 compares the raw and corrected hydraulic efficiency curves. The corrected values are nearly identical to the raw efficiencies.

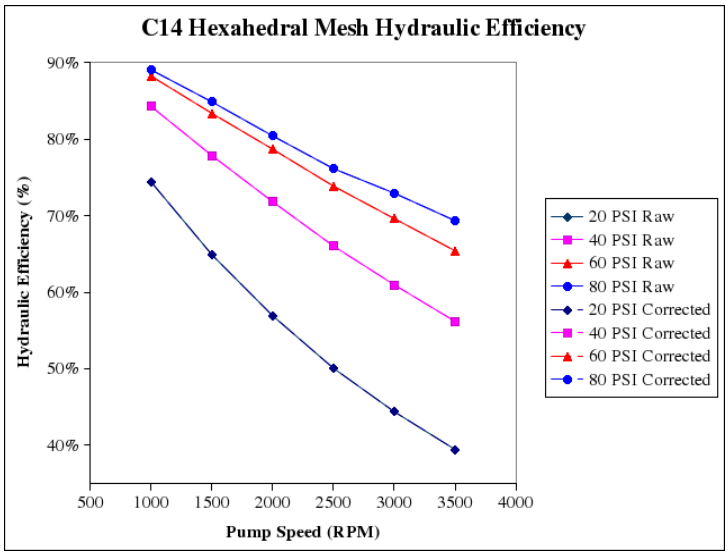

Figure 3-23: C14 Hexahedral Mesh Hydraulic Efficiencies (Raw vs. Corrected)

Figure 3-24 compares the overall efficiencies for the raw and experimental results. While the raw results are higher than the experimental results, the same trends are reflected. The 80 PSI case exhibits the greatest efficiency for both cases (at least at high pump speeds), and the 20 PSI case is the least efficient.

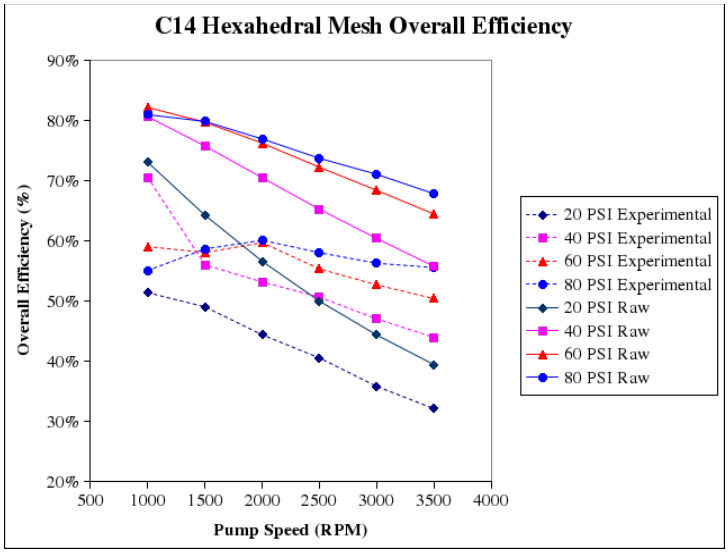

Figure 3-24: C14 Hexahedral Mesh Overall Efficiencies

(Raw vs. Experimental)

Finally, Figure 3-25 compares the raw and corrected overall efficiencies for the hexahedral mesh. As with the volumetric and hydraulic efficiencies, the overall efficiency has been decreased by approximately 3%.

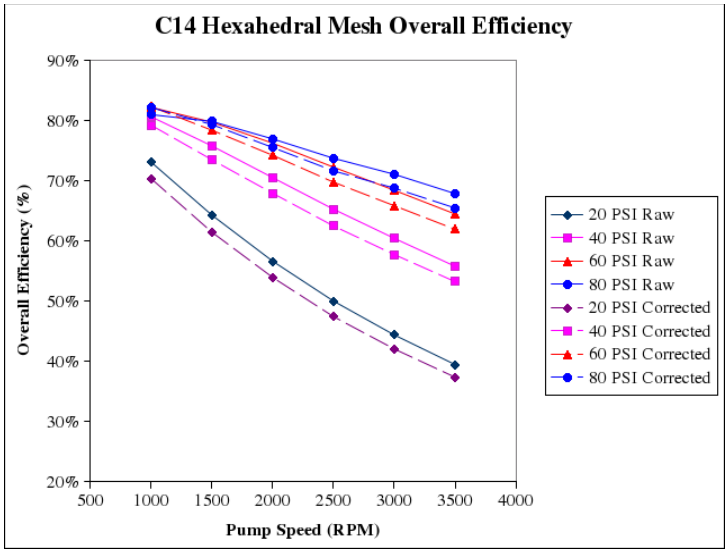

Figure 3-25: C14 Hexahedral Mesh Overall Efficiencies

(Raw vs. Corrected)

By using the hexahedral meshing scheme, the mass flow rate and torque predictions have come much closer to the experimentally determined values. Since this method is much better than the wedge mesh, it was used for the C15, GN1, and Mock pumps.

4. C15 Pump Results

The main purpose for simulating the C15 pump was to determine whether the method developed for simulating the C14 pump would work on a pump with a different gerotor, which has six teeth on the inner gear. This pump was modeled using the same 15W-40 oil as was used in the C14 pump at 100°C, but at pump speeds ranging from 1000 to 6000 RPM at 20-80 PSI. The simulations used a time step of 1 x 10^{-5} seconds, and 1000 time steps were calculated.

Pump Pressure	Pump Speed	Experimental Mass Flow Rate	Raw Computational Mass Flow Rate	Raw Percent Difference	Corrected Computational Mass Flow Rate	Corrected Percent Difference
PSI	RPM	GPM	GPM	%	GPM	%
20	1000	0.18	0.1706	-5.22%	0.1609	-10.61%
	2000	0.38	0.3453	-9.13%	0.3218	-15.32%
	3000	0.54	0.5204	-3.63%	0.4827	-10.61%
	4000	0.72	0.6937	-3.65%	0.6438	-10.58%
	5000	0.90	0.8674	-3.62%	0.8050	-10.56%
	6000	NA	1.0423	NA	0.9658	NA
40	1000	0.18	0.1674	-7.00%	0.1607	-10.72%
	2000	0.36	0.3421	-4.97%	0.3217	-10.64%
	3000	0.53	0.5171	-2.43%	0.4826	-8.94%
	4000	0.70	0.6905	-1.36%	0.6437	-8.04%
	5000	0.88	0.8643	-1.78%	0.8048	-8.55%
	6000	NA	1.0391	NA	0.9658	NA
60	1000	0.17	0.1643	-3.35%	0.1605	-5.59%
	2000	0.34	0.3388	-0.35%	0.3215	-5.44%
	3000	0.52	0.5139	-1.17%	0.4824	-7.23%
	4000	0.70	0.6874	-1.80%	0.6435	-8.07%
	5000	0.86	0.8612	0.14%	0.8047	-6.43%
	6000	NA	1.0360	NA	0.9656	NA
80	1000	0.16	0.1613	0.81%	0.1602	0.13%
	2000	0.32	0.3357	4.91%	0.3213	0.41%
	3000	0.51	0.5107	0.14%	0.4823	-5.43%
	4000	0.67	0.6843	2.13%	0.6463	-3.54%
	5000	0.86	0.8582	-0.21%	0.8046	-6.44%
	6000	NA	1.0330	NA	0.9655	NA

Table 4-1: C15 Pump Mass Flow Rates

Table 4-1 shows the outlet mass flow rates for the simulations and compares them to the experimental results. The corrected computational numbers are within 11% of the experimental values (except for one point). This time, however, the raw numbers are even closer.

Pump Pressure	Pump Speed	Experimental Total Torque	Experimental Losses	Experimental Torque	Computational Torque	Percent Difference with Experimental
PSI	RPM	oz-in	oz-in	oz-in	oz-in	%
20	1000	5.3	3.73	1.57	3.37	114.71%
	2000	9	3.06	5.94	5.44	-8.50%
	3000	11	2.85	8.15	7.78	-4.60%
	4000	12	2.81	9.19	10.25	11.58%
	5000	12	3.02	8.98	12.8	42.49%
	6000	13	3.35	9.65	15.35	59.08%
40	1000	7	3.73	3.27	4.58	40.00%
	2000	10	3.06	6.94	6.43	-7.31%
	3000	12.5	2.85	9.65	8.7	-9.82%
	4000	13	2.81	10.19	11.25	10.39%
	5000	13.5	3.02	10.48	13.83	31.98%
	6000	14.5	3.35	11.15	16.34	46.57%
60	1000	10	3.73	6.27	5.79	-7.74%
	2000	12.5	3.06	9.44	7.43	-21.28%
	3000	14.5	2.85	11.65	9.63	-17.35%
	4000	16	2.81	13.19	12.24	-7.17%
	5000	17	3.02	13.98	14.87	6.34%
	6000	18.5	3.35	15.15	17.34	14.44%
80	1000	12	3.73	8.27	6.99	-15.44%
	2000	15.5	3.06	12.44	8.44	-32.19%
	3000	17.5	2.85	14.65	10.56	-27.89%
	4000	18.5	2.81	15.69	13.26	-15.52%
	5000	19.75	3.02	16.73	15.93	-4.78%
	6000	20.5	3.35	17.15	18.37	7.10%

Table 4-2: C15 Torque Comparison

Table 4-2 compares the experimental and computational torque values. These torque values are not as consistent as with the C14 pump. The computational numbers differ by similar magnitudes as the C14 pump, but the low overall torque numbers increases the percent difference.

Figure 4-1 plots the experimental and raw computational curves for the C15 pump. Note that experimental results were not available for pump speeds of 6000 RPM. Some experimental results are greater than 100%, which may be due to the low resolution of the experimental data.

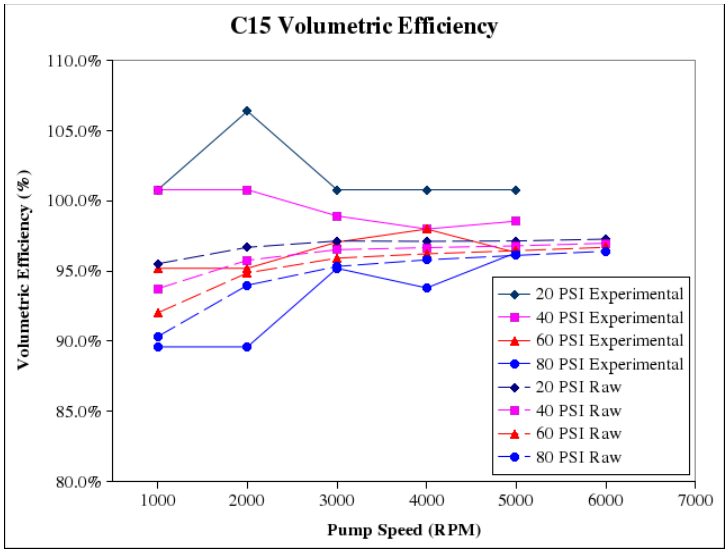

Figure 4-1: C15 Volumetric Efficiency Curves (Raw vs. Experimental)

Figure 4-2 shows the raw and corrected volumetric efficiency curves. As expected, the 20 PSI case shows the best volumetric efficiency. The corrected curves are lower than the raw curves because of the reduction in outlet mass flow rate. The difference between the raw and corrected curves is between 1 and 7%.

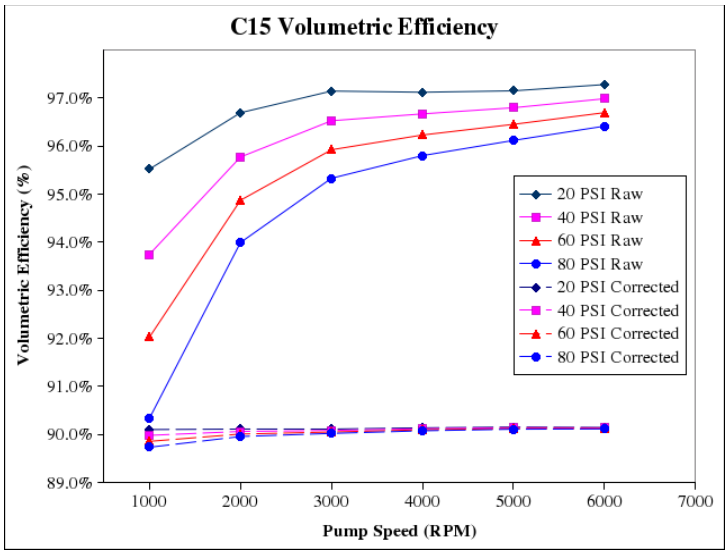

Figure 4-2: C15 Volumetric Efficiency Curves (Raw vs. Corrected)

Figure 4-3 shows the experimental and raw hydraulic efficiency curves. The raw curves are greater than the experimental curves, but show the same trends.

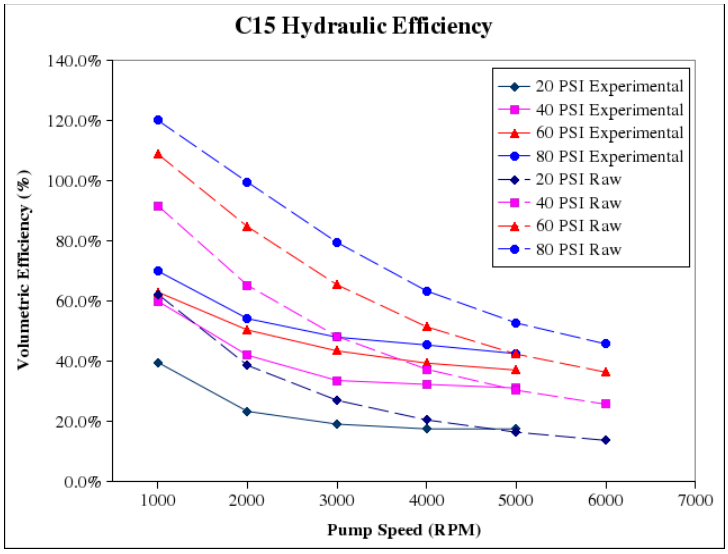

Figure 4-3: C15 Hydraulic Efficiency Curves (Raw vs. Experimental)

Figure 4-4 shows the raw and corrected hydraulic efficiency curves. Here, the 80 PSI case has the greatest efficiency. Some of the curves show efficiencies greater than 100%, which occurs because of the low torque predictions reported by FLUENT. Again, the raw and corrected curves are nearly identical.

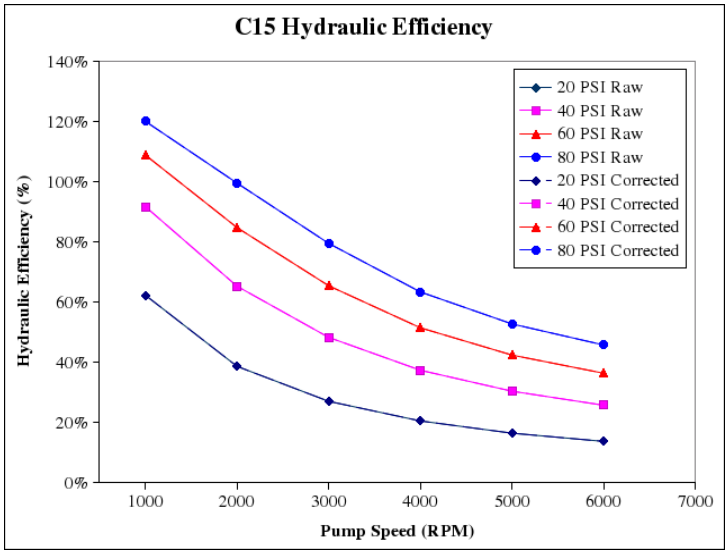

Figure 4-4: C15 Hydraulic Efficiency Curves (Raw vs. Corrected)

Figure 4-5 plots the experimental and raw computational overall efficiency curves for the C15 pump. The highest pressure of 80 PSI has the greatest efficiency, as was seen with the C14 pump. Again, the efficiencies over 100% are due to low torque predictions.

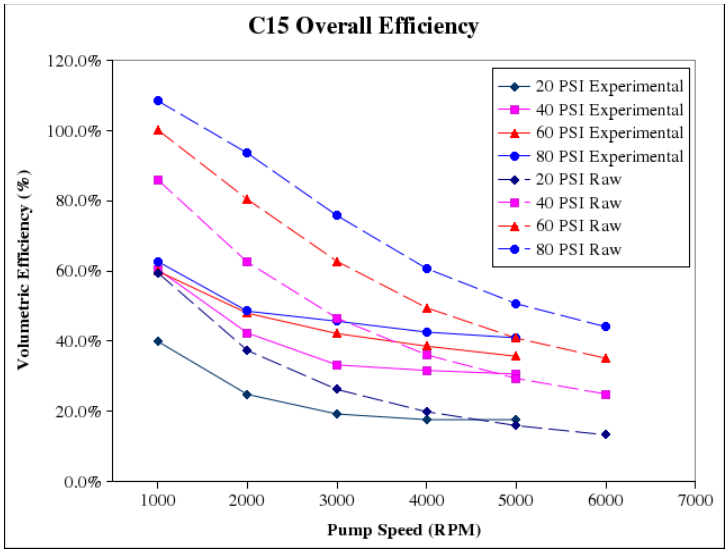

Figure 4-5: C15 Overall Efficiency Curves (Raw vs. Experimental)

Figure 4-6 compares the raw and corrected overall efficiency curves. The corrected curves are lowered by approximately 3%.

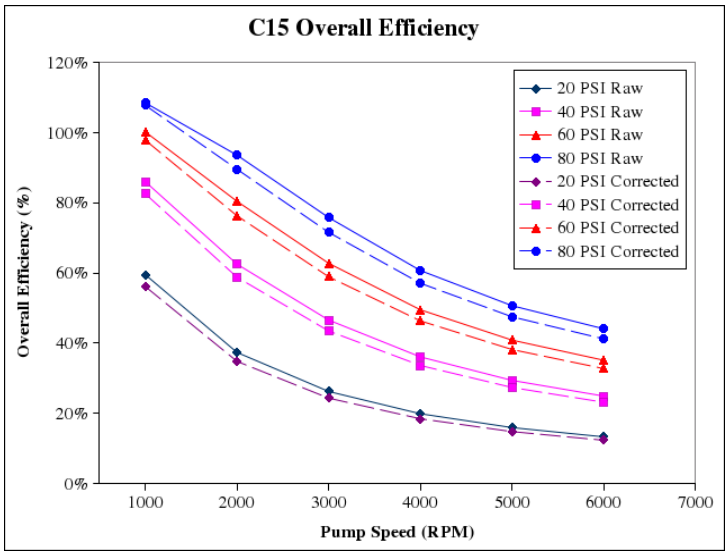

Figure 4-6: C15 Overall Efficiency Curves (Raw vs. Corrected)

5. GN1 Pump Results

The GN1 pump is a diesel fuel pump operating at high pressure compared to the C14 and C15 pumps. This pump uses the same gerotor as the C14 pump, but is simulated with the VISCOR diesel calibration fluid at a pressure of 300 PSI at speeds ranging from 1000 to 3500 RPM.

Pump Pressure	Pump Speed	Experimental Mass Flow Rate	Raw Computational Mass Flow Rate	Raw Percent Difference	Corrected Computational Mass Flow Rate	Corrected Percent Difference
PSI	RPM	GPM	GPM	%	GPM	%
300	1000	0.058	–0.1121	-100.00%	0.0450	-22.41%
	1500	0.087	–0.0256	-100.00%	0.1025	17.82%
	2000	0.116	0.0145	-87.50%	0.1598	37.76%
	2500	0.146	0.0852	-41.64%	0.2170	48.63%
	3000	0.175	0.1421	-18.80%	0.2745	56.86%
	3500	0.200	0.1773	-11.35%	0.3319	65.95%

Table 5-1: GN1 Outlet Mass Flow Rates

Table 5-1 compares the raw and corrected outlet mass flow rates with the experimentally determined values. The raw results show that the majority of the flow was reversed in the simulations, due to the high pressure rise of the pump. Thus, a major correction was needed to achieve positive mass flow rates. Note, however, that the raw value is much closer than the corrected value at high pump speeds.

Pump Pressure	Pump Speed	Experimental Total Torque	Experimental Losses	Experimental Torque	Computational Torque	Percent Difference with Experimental
PSI	RPM	oz-in	oz-in	oz-in	oz-in	%
300	1000	NA	4.33	NA	48.25	NA
	1500	NA	5.55	NA	28.35	NA
	2000	NA	6.15	NA	49.66	NA
	2500	NA	6.6	NA	48.25	NA
	3000	NA	6.8	NA	50.9	NA
	3500	57	6.93	50.07	53.71	7.27%

Table 5-2: GN1 Torque Comparison

Table 5-2 compares the computational torque calculations to the only experimental data point available. This shows a difference of 7.27%, which is comparable to the results seen with the C14 and C15 pumps.

Figure 5-1 shows the volumetric, hydraulic, and overall efficiencies for the GN1 pump. The corrected overall and volumetric efficiencies are greater than the raw curves by 15 to 60%. These curves compare with an experimental value of 17.69% for the overall efficiency at 3500 RPM. The raw and corrected hydraulic efficiencies are again nearly identical.

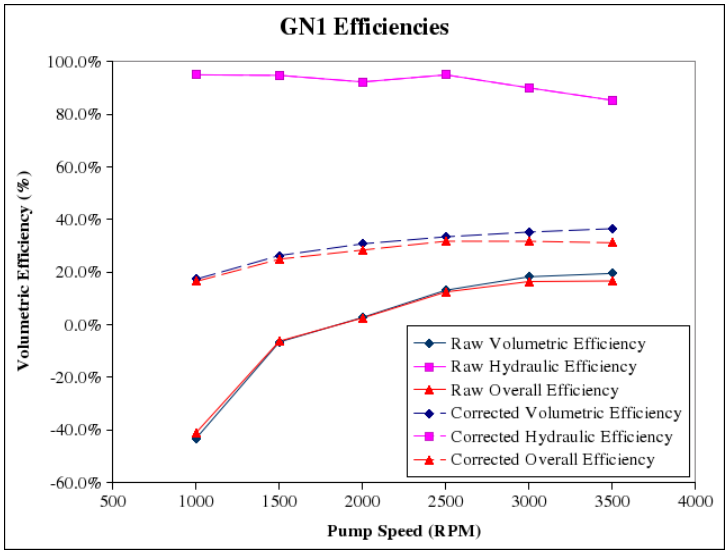

Figure 5-1: GN1 Efficiency Curves

The numbers calculated by FLUENT do not inspire confidence in the simulations for this type of pump. The high pressures on the boundary conditions of the simulated pump force the fluid backwards through the pump, leading to a qualitatively incorrect solution. While the method developed works well for the C14 and C15 pumps, it needs to be modified significantly in order to produce correct results when high pressures are involved.

6. Mock Pump Results

The main purpose for simulating the Mock pump was to determine whether the method developed for simulating the other pumps would work on a much larger pump. This pump was modeled using the same SAE 30 engine oil at 200°F, at pump speeds ranging from 1207 to 3793 RPM at 40-120 PSI. The simulations used a time step of 1 x 10^{-5} seconds, and 1000 time steps were calculated.

6.1 Mock Pump – Revision A

The outlet mass flow rates for the first design of the Mock pump are shown in Table 6-1. The table shows that the computational values have very good agreement with the experimental data for low pump speeds. At high pump speeds, however, the mass flow rates are high by as much as 67%. Figure 6-1 gives an indication as to why the flow rates differ so greatly.

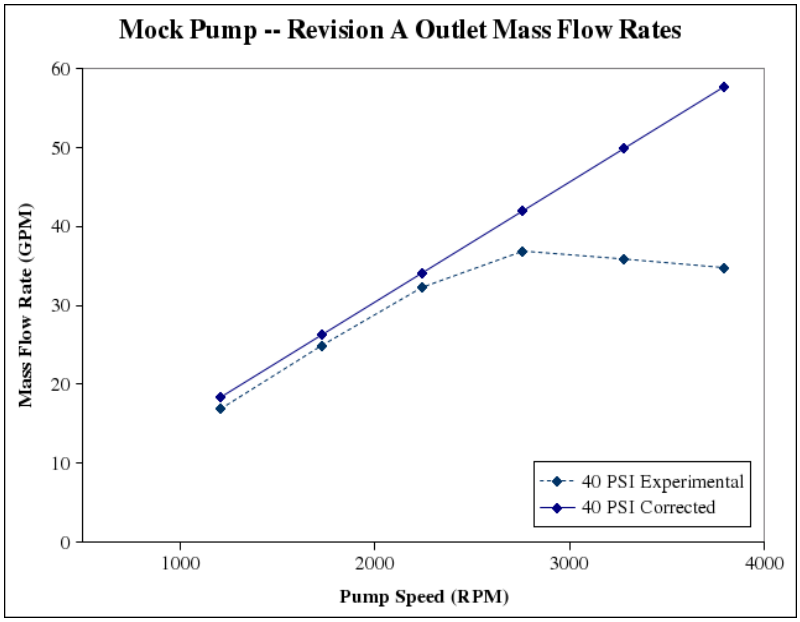

Figure 6-1: Mock Pump – Revision A Outlet Mass Flow Rates

The computational mass flow rates form a very straight line, as was seen in the other pumps modeled and as expected from a positive displacement pump. The experimental values, however, begin very linear, but drop as pump speed increases. This is an indication that significant cavitation is occurring within the pump. As the computational models do not account for cavitation, they continue to predict a linear trend to the outlet mass flow rates.

Pump Pressure	Pump Speed	Experimental Mass Flow Rate	Raw Computational Mass Flow Rate	Raw Percent Difference	Corrected Computational Mass Flow Rate	Corrected Percent Difference
PSI	RPM	GPM	GPM	%	GPM	%
40	1207	16.9	18.7945	11.21%	18.3751	8.73%
	1724	24.9	26.7748	7.53%	26.2472	5.41%
	2241	32.3	35.1144	8.71%	34.1167	5.62%
	2759	36.9	43.0912	16.78%	42.0028	13.83%
	3276	35.9	51.1960	42.61%	49.8725	38.92%
	3793	34.8	59.2350	70.22%	57.7428	65.93%
60	1207	16.7	18.7251	12.13%	18.3702	10.00%
	1724	24.6	26.7072	8.57%	26.2415	6.67%
	2241	31.9	35.0379	9.84%	34.1107	6.93%
	2759	36.9	43.0182	16.58%	41.9960	13.81%
	3276	36.1	51.2476	41.96%	49.8639	38.13%
	3793	34.7	59.1265	70.39%	57.7348	66.38%
80	1207	16.4	18.6575	13.77%	18.3766	12.05%
	1724	24.3	26.6414	9.64%	26.2522	8.03%
	2241	31.7	34.9650	10.30%	34.1261	7.65%
	2759	36.8	42.9489	16.71%	42.0156	14.17%
	3276	36.0	51.1729	42.15%	49.8880	38.58%
	3793	34.6	59.0554	70.68%	57.7631	66.95%
100	1207	16.1	18.5899	15.47%	18.3701	14.10%
	1724	24.1	26.5755	10.27%	26.2444	8.90%
	2241	31.6	34.8903	10.41%	34.1176	7.97%
	2759	36.8	42.8742	16.51%	42.0058	14.15%
	3276	36.1	51.0964	41.54%	49.8773	38.16%
	3793	34.7	58.9860	69.99%	57.7510	66.43%
120	1207	15.8	18.5241	17.24%	18.3619	16.21%
	1724	23.8	26.5115	11.39%	26.2341	10.23%
	2241	31.3	34.8156	11.23%	34.1059	8.96%
	2759	36.8	42.8012	16.31%	41.9920	14.11%
	3276	36.1	51.0217	41.33%	49.8619	38.12%
	3793	34.5	58.9130	70.76%	57.7335	67.34%

Table 6-1: Mock Pump – Revision A Outlet Mass Flow Rates

Table 6-2 compares the torque computed by FLUENT with the experimentally determined values. The torque values are greatly over-predicted, as more fluid is being pumped in the computational simulation than in the experimental case.

Pump Pressure	Pump Speed	Experimental Total Torque	Computational Torque	Percent Difference with Experimental
PSI	RPM	in-lb	in-lb	%
40	1207	34	41.16	21.07%
	1724	40	60.59	51.48%
	2241	46	97.89	112.80%
	2759	51	129.09	153.11%
	3276	56	165.17	194.95%
	3793	62	206.44	232.97%
60	1207	46	51.6	12.18%
	1724	52	75.04	44.30%
	2241	58	101.26	74.59%
	2759	63	133.32	111.62%
	3276	67	170.98	155.19%
	3793	73	210.99	189.03%
80	1207	57	50.01	-12.26%
	1724	64	71.72	12.06%
	2241	70	104.9	49.86%
	2759	76	137.92	81.48%
	3276	78	174.43	123.63%
	3793	83	215.62	159.78%
100	1207	70	60.47	-13.62%
	1724	75	86.17	14.90%
	2241	82	108.41	32.21%
	2759	87	142.34	63.61%
	3276	89	178.02	100.02%
	3793	93	220.26	136.84%
120	1207	82	58.82	-28.26%
	1724	87	82.89	-4.72%
	2241	94	111.93	19.07%
	2759	99	146.8	48.28%
	3276	101	181.55	79.75%
	3793	110	224.87	104.43%

Table 6-2: Mock Pump – Revision A Torque Comparison

Because the outlet mass flow rates and torques are significantly different from the experimental values, it is expected that the efficiency curves will also be incorrect. However, they are included here for completeness.

Figure 6-2 shows the experimental and raw volumetric efficiency curves. The experimental curves quickly drop off due to the cavitation. The computational curves are all very close to each other compared to the experimental curves.

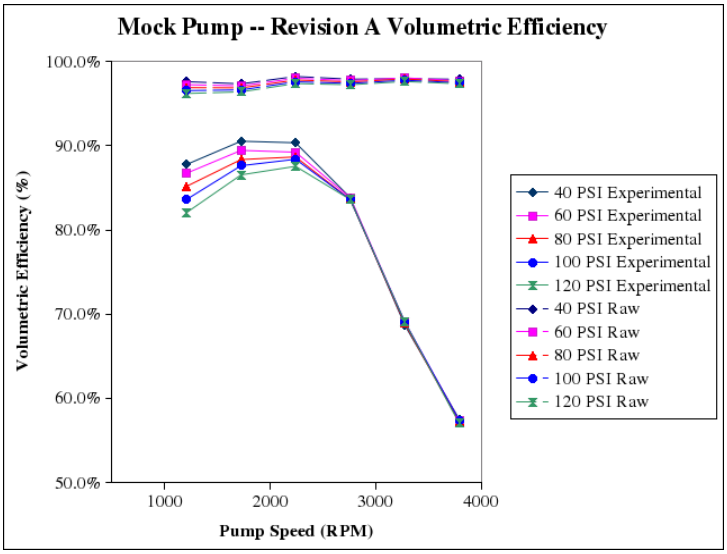

Figure 6-2: Mock Pump – Revision A Volumetric Efficiency Curves (Raw vs. Experimental)

Figure 6-3 shows the raw and corrected volumetric efficiency curves. The corrected curves are extremely close to one another. This occurs because the outlet mass flow rate is much greater than the total mass flow rates through the clearance volumes. As expected, the 40 PSI case shows the best volumetric efficiency.

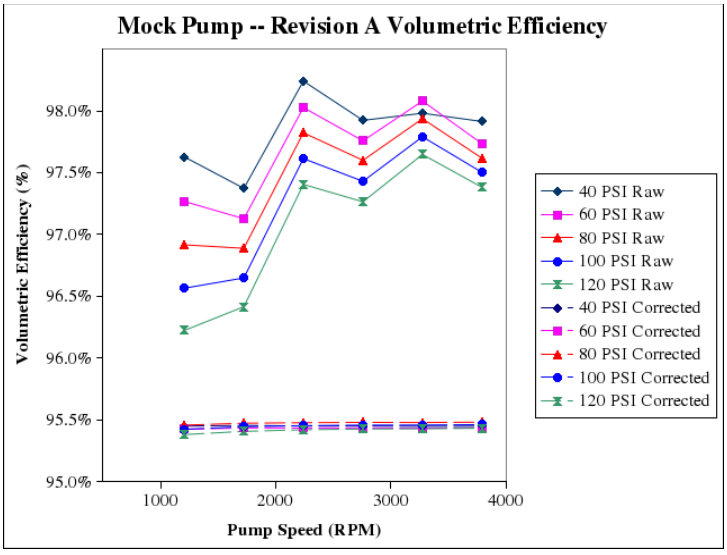

Figure 6-3: Mock Pump – Revision A Volumetric Efficiency Curves (Raw vs. Corrected)

Figure 6-4 shows the experimental and raw computational hydraulic efficiency curves. The experimental curves show greater efficiencies than the raw curves for most pump speeds. As expected, the 120 PSI case has the greatest efficiency.

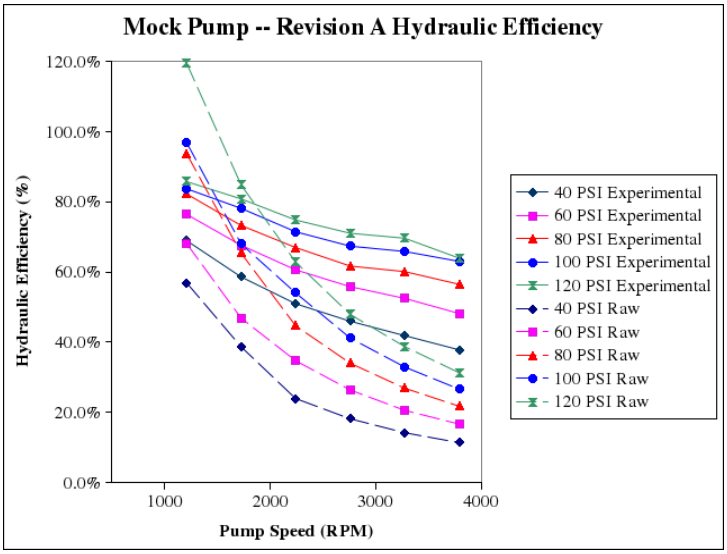

Figure 6-4: Mock Pump – Revision A Hydraulic Efficiency Curves (Raw vs. Experimental)

Figure 6-5 compares the raw and corrected hydraulic efficiencies. These curves are very similar to the hydraulic efficiency curves, where the 120 PSI case has the greatest overall efficiency. As in the other pumps, the raw and corrected curves are nearly identical.

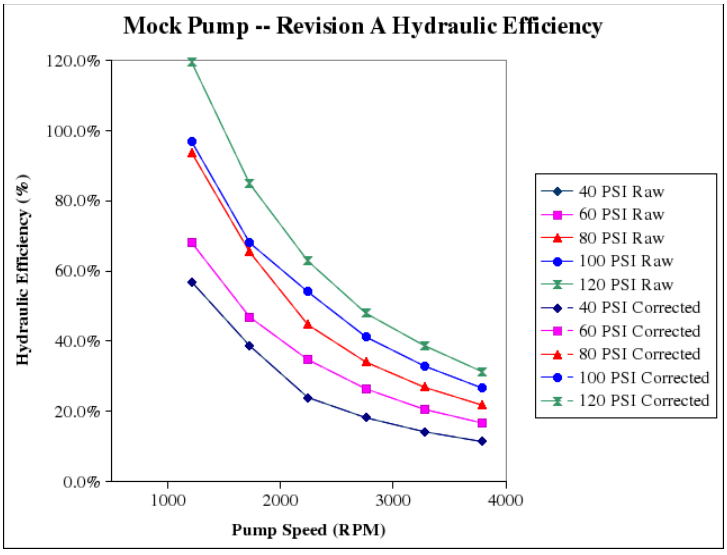

Figure 6-5: Mock Pump – Revision A Hydraulic Efficiency Curves (Raw vs. Corrected)

Figure 6-6 shows the experimental and raw computational overall efficiency curves. The curves have similar magnitudes, with the experimental efficiencies decreasing as pump speed increases due to cavitation.

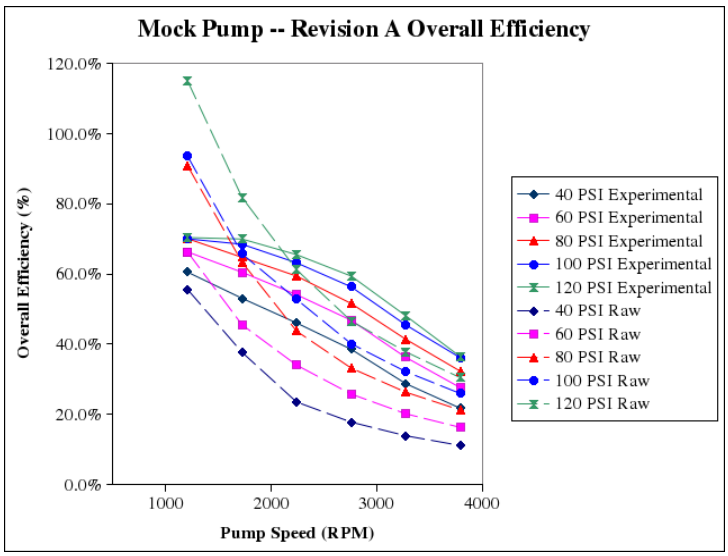

Figure 6-6: Mock Pump – Revision A Overall Efficiency Curves (Raw vs. Experimental)

Figure 6-7 compares the raw and corrected overall efficiency curves. The correction is a very slight decrease of approximately one percent.

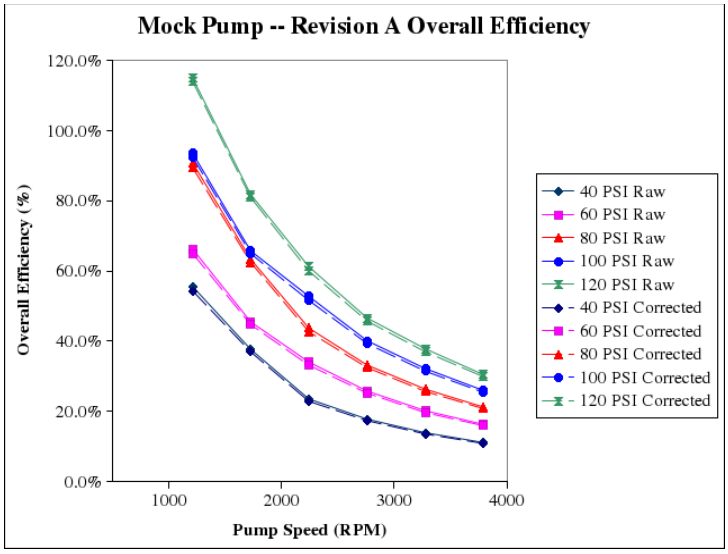

Figure 6-7: Mock Pump – Revision A Overall Efficiency Curves (Raw vs. Corrected)

The computational results of Revision A of the Mock pump are very different from the experimental values. The simulations to not account for cavitation, as cavitation was beyond the scope of this project. Future simulations would benefit from predicting cavitation, as cavitation is an undesirable phenomenon.

6.2 Mock Pump – Revision B

The geometry of the Mock pump was altered in an attempt to reduce or eliminate the cavitation experienced in experimental testing of the pump. This new geometry is called Revision B.

Table 6-3 shows the outlet mass flow rates of the computational and experimental pumps. The corrected numbers are much closer to the experimental value, but still differs by more than 15% at high pump speeds. Figure 6-8 compares the outlet mass flow rates for the corrected computational and experimental cases at 40 PSI. The graph shows that the experimental mass flow rate drops from the straight line, indicating that the cavitation has been reduced, but not eliminated.

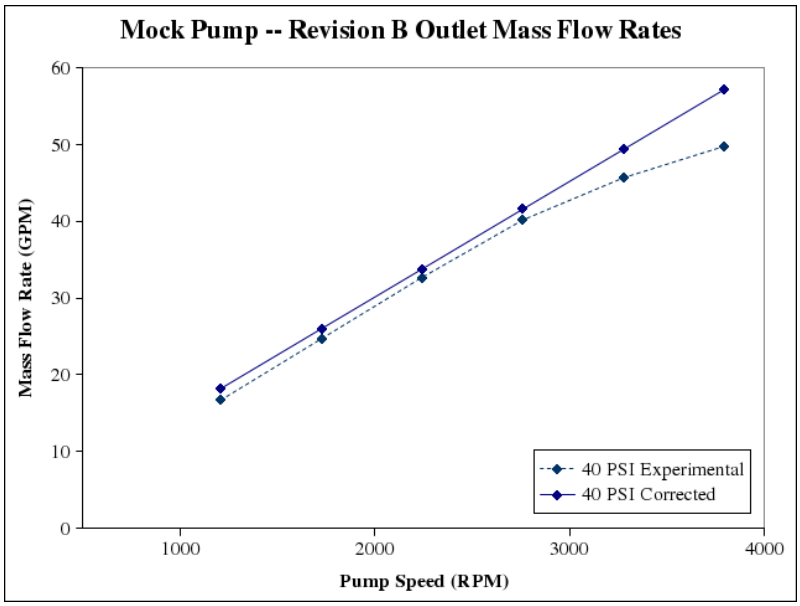

Figure 6-8: Mock Pump – Revision B Outlet Mass Flow Rates

Pump Pressure	Pump Speed	Experimental Mass Flow Rate	Raw Computational Mass Flow Rate	Raw Percent Difference	Corrected Computational Mass Flow Rate	Corrected Percent Difference
PSI	RPM	GPM	GPM	%	GPM	%
40	1207	16.7	18.6895	11.91%	18.2021	8.99%
	1724	24.7	26.6538	7.91%	26.0058	5.29%
	2241	32.7	34.9686	6.94%	33.7910	3.34%
	2759	40.2	42.9275	6.78%	41.6070	3.50%
	3276	45.7	51.1320	11.89%	49.3935	8.08%
	3793	49.8	58.9842	18.44%	57.1968	14.85%
60	1207	16.1	18.5810	15.41%	18.1945	13.01%
	1724	24.3	26.5489	9.25%	25.9969	6.98%
	2241	32.2	34.8529	8.24%	33.7812	4.91%
	2759	39.9	42.8154	7.31%	41.5958	4.25%
	3276	45.3	51.0163	12.62%	49.3811	9.01%
	3793	49.5	58.8721	18.93%	57.1826	15.52%
80	1207	15.6	18.4725	18.41%	18.1873	16.59%
	1724	23.7	26.4439	11.58%	25.9247	9.39%
	2241	31.8	34.7391	9.24%	33.7728	6.20%
	2759	39.5	42.7034	8.11%	41.5863	5.28%
	3276	45.1	50.9025	12.87%	49.3708	9.47%
	3793	49.4	58.7618	18.95%	57.1709	15.73%
100	1207	15.1	18.3675	21.64%	18.1779	20.38%
	1724	23.2	26.3407	13.54%	25.9780	11.97%
	2241	31.3	34.6252	10.62%	33.7606	7.86%
	2759	39.0	42.5913	9.21%	41.5723	6.60%
	3276	44.7	50.7869	13.62%	49.3551	10.41%
	3793	49.0	58.6515	19.70%	57.1532	16.64%
120	1207	14.7	18.2626	24.24%	18.1695	23.60%
	1724	22.8	26.2358	15.07%	25.9689	13.90%
	2241	30.8	34.5114	12.05%	33.7509	9.58%
	2759	38.4	42.4810	10.63%	41.5614	8.23%
	3276	44.4	50.6730	14.13%	49.3433	11.13%
	3793	49.1	58.5430	19.23%	57.1397	16.37%

Table 6-3: Mock Pump – Revision B Outlet Mass Flow Rates

Table 6-4 shows the computational and experimental torque values. The torque is fairly well predicted only at high pump pressures and low speeds. The torque is highly over-predicted elsewhere. Future work with these simulations should attempt to predict the torque more closely.

Pump Pressure	Pump Speed	Experimental Total Torque	Computational Torque	Percent Difference with Experimental
PSI	RPM	in-lb	in-lb	%
40	1207	33	48.08	45.69%
	1724	39	69.07	77.10%
	2241	45	95.85	112.99%
	2759	53	126.1	137.92%
	3276	59	161.89	174.39%
	3793	65	199.94	207.60%
60	1207	45	52.61	16.92%
	1724	50	74.78	49.56%
	2241	57	99.48	74.53%
	2759	64	130.62	104.09%
	3276	71	165.53	133.14%
	3793	77	204.64	165.76%
80	1207	58	57.14	-1.49%
	1724	62	80.49	29.82%
	2241	69	103.12	49.45%
	2759	75	135.17	80.22%
	3276	82	169.16	106.30%
	3793	89	209.35	135.22%
100	1207	69	61.66	-10.64%
	1724	74	86.2	16.48%
	2241	81	106.76	31.80%
	2759	87	139.72	60.60%
	3276	94	172.82	83.85%
	3793	100	214.06	114.06%
120	1207	81	66.17	-18.30%
	1724	86	91.91	6.87%
	2241	93	110.4	18.70%
	2759	100	144.27	44.27%
	3276	107	176.49	64.95%
	3793	112	218.77	95.33%

Table 6-4: Mock Pump – Revision B Torque Comparison

Figure 6-9 shows the experimental and raw volumetric efficiencies. As with Revision A, the raw volumetric efficiencies curves are very close together for both pump speeds and pump pressures.

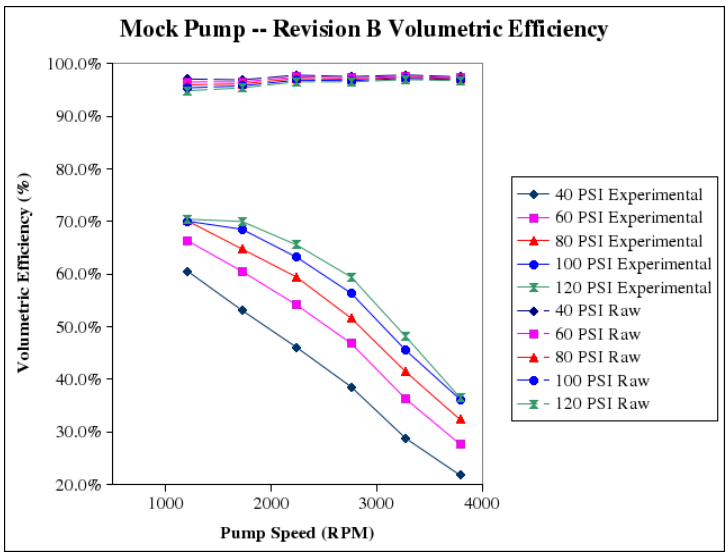

Figure 6-9: Mock Pump – Revision B Volumetric Efficiency Curves (Raw vs. Experimental)

Figure 6-10 shows the raw and corrected volumetric efficiencies. These curves are within approximately four percentage points of each other. As with Revision A, the corrected curves are very close together.

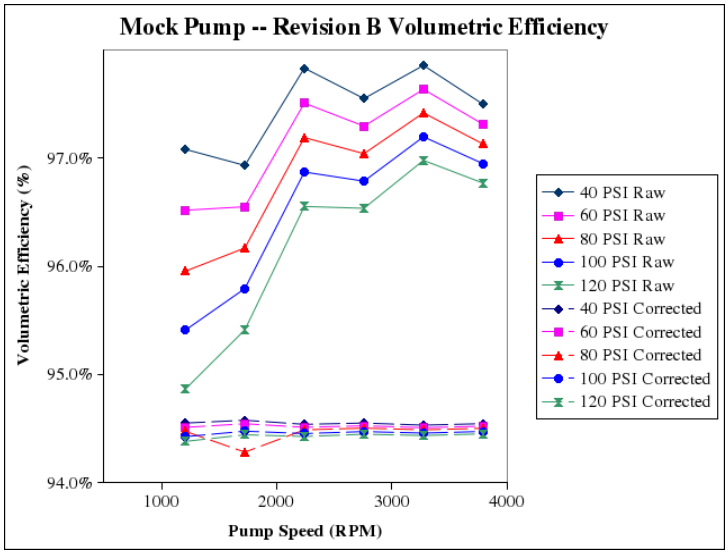

Figure 6-10: Mock Pump – Revision B Volumetric Efficiency Curves (Raw vs. Corrected)

Figure 6-11 compares the experimental and raw computational hydraulic efficiencies. The curves remain very similar to the Revision A results, with the 120 PSI case showing the greatest efficiency.

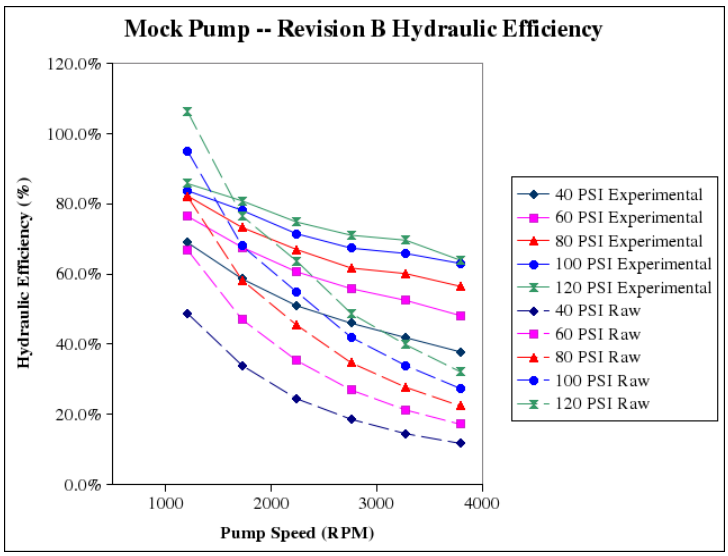

Figure 6-11: Mock Pump – Revision B Hydraulic Efficiency Curves (Raw vs. Experimental)

Figure 6-12 compares the raw and corrected hydraulic efficiencies of the Revision B pump. As with Revision A, the raw and corrected curves are nearly identical.

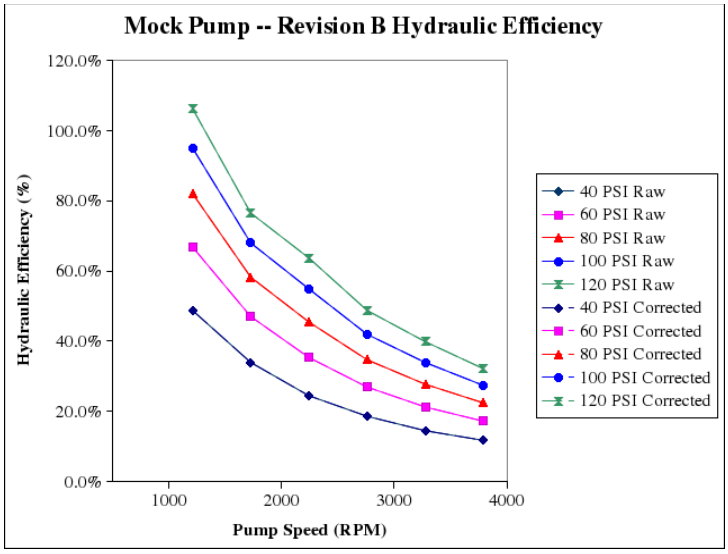

Figure 6-12: Mock Pump – Revision B Hyrdaulic Efficiency Curves (Raw vs. Corrected)

Figure 6-13 plots the experimental and raw computational overall efficiency curves for Revision B of the Mock Pump. These curves are very similar to the Revision A curves, with the highest efficiency at 120 PSI.

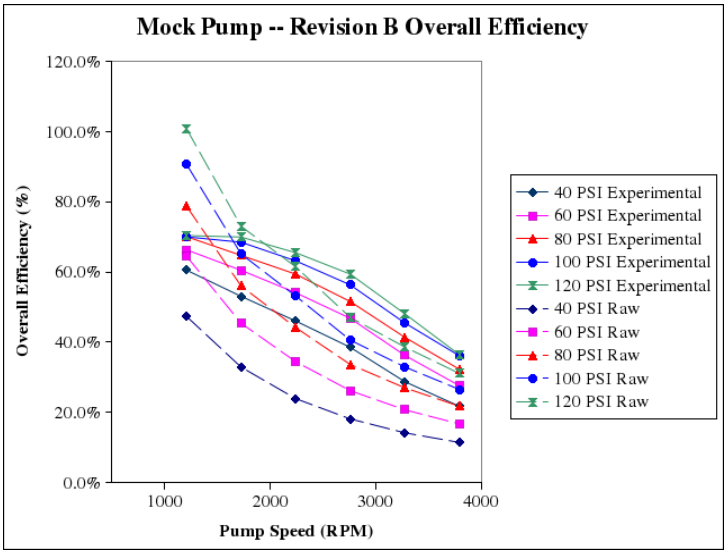

Figure 6-13: Mock Pump – Revision B Overall Efficiency Curves (Raw vs. Experimental)

Figure 6-14 plots the raw and corrected overall efficiency curves. The corrected curves are shifted downwards from the raw curves by about one percent.

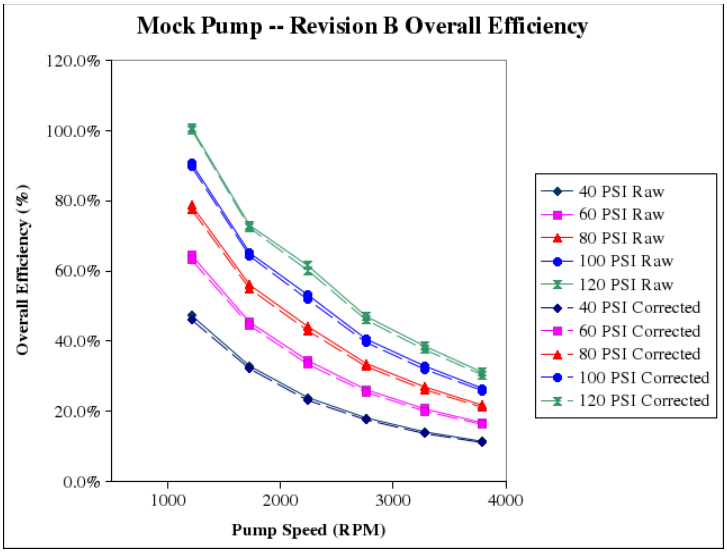

Figure 6-14: Mock Pump – Revision B Overall Efficiency Curves (Raw vs. Corrected)

7. Conclusions and Discussions

- The wedge mesh approach for resolving the gerotor fluid volume was not as accurate as the hexahedral meshing scheme, but was able to provide a relative baseline for geometrical optimization.
- The geometries that give the greatest overall efficiency for the C14 pump are to use the baseline of 0.0013 inches for the top and bottom gaps; increase the side gap to 0.004 inches; increase the inlet and outlet connections to a #10 and #8, respectively; and keep the baseline angle of zero degrees for the inlet and outlet tube angles.
- The hexagonal mesh technique is superior to the wedge mesh, as both torque and outlet mass flow rates are closer to experimental values.
- The corrected outlet mass flow rate for the C14 pump (with superior hexahedral mesh) show poorer agreement with experimental data at high pressures and low pump speeds. The torque prediction is poorer at low pressures and high pump speeds.
- The corrected outlet mass flow rate for the C15 pump is poorer at low pump pressures, with little change with respect to pump speed. The torque values are poorer at low pump pressures and high pump speeds
- The mass flow rates for the GN1 pump are poor at high RPM when compared with the experimental data. The computational torque is fairly accurate at the single experimental data point.
- The corrected outlet mass flow rates for the Mock pumps are poor at high RPM, as are the computed torque values.
- It is well known that cavitation will effect torque at low pressures and high speeds. However, the mass flow rate and torque trends do not scale with cavitation alone. We believe these trends arise from a combination of cavitation, a transition from laminar to turbulent flow, and, in the case of the GN1 pump, high pump pressure.
- The assumption for using the standard k-ϵ turbulence model may not be accurate at each design point simulated or for every part of the pump itself. Some parts of the model are undoubtedly experiencing laminar flow, while other parts are fully turbulent. Low pump speed simulations will experience more laminar flow than high pump speed simulations. This transition from laminar to turbulent flow may explain some of the discrepancies from the experimental data, such as in the C14 wedge mesh baseline results, where outlet mass flow rates are over-predicted at low pump speeds. This may also explain why the computational torque values are under-predicted at high pump pressures.

- The high pressure of the GN1 pump resulted in reversed flow through the pump. The current method does not accurately predict pumps at high pressures.
- Constraints on the project did not allow for the inclusion of cavitation and partial laminar / turbulent flow simulations. It is recommended that further simulations include these aspects of the flow in gerotor pumps either within FLUENT or through user-defined functions. The models also need to be adjusted so that high pump pressures (such as in the GN1 pump) can be simulated accurately.

References

1. Fabiani, M., Mancò, S., Nervegna, N., Rundo, M., Armenio, G., Pachetti, C., Trichilo, R., "Modeling and Simulation of Gerotor Gearing in Lubricating Oil Pumps," SAE Transactions, vol. 108, pp. 989-1003, 1999.
2. Mancò, S, Nervegna, N., Rundo, N., Armenio, G., Pachetti, C., Trichilo, R., "Gerotor Lubricating Oil Pump for IC Engines," SAE Paper 982689, 1998.
3. Kluger, Michael A., Fussner, Douglas R., Roethler, B., "A Performance Comparison of Various Automatic Transmission Pumping Systems," SAE Paper 960424, 1996.
4. Jiang, Y., Perng, C., "Efficient 3D Transient Computational Model for Vane Oil Pump and Gerotor Oil Pump Simulators," SAE Paper 970841, 1997.
5. Haworth, D.C., Maguire, J.M., Matthes, W.R., Rhein, R., El Tahry, S.H., "Dynamic Fluid Flow Analysis of Oil Pumps," SAE Paper 960422, 1996.
6. Goulet, Mark G. Fundamentals of Selection and Design: Oil Pumps for Internal Combustion Engines and Gearboxes.
7. Fluent, Inc. GAMBIT Version 2.2 User's Guide. GAMBIT Manual. 2005.
8. Anderson, John D. Jr. Computational Fluid Dynamics. New York: McGraw-Hill, 1995.
9. Fluent, Inc. FLUENT Version 6.2 User's Guide. FLUENT Manual. 2005.
10. White, Frank M. Fluid Mechanics. Fourth Ed. Boston: McGraw-Hill, 1999.
11. White, Frank M. Viscous Fluid Flow. Third Ed. Boston: McGraw-Hill, 2006.
12. Nichols-Portland, Inc. Gerotor Selection and Pump Design.

Appendix A – Efficiency Equations

Mechanical efficiency can be defined as follows [12]:

$$\eta_m = \frac{T_a' N}{T_a N} = \frac{T_a'}{T_a} \rightarrow Assumed = 1 \qquad \textit{Eq. A.1}$$

where T_a is the actual driving torque on the gerotor shaft (experimental value) and T'_a is the torque supplied to the gerotor (T_a – "mechanical friction torque"). Mechanical efficiency will be assumed to equal one. Therefore, in what follows,

$$T_a' \approx T_a \qquad \textit{Eq. A.2}$$

From "Gerotor Selection and Pump Design" by Nichols-Portland, overall pump efficiency is defined as:

$$\eta_{overall\ experimental} = \frac{\Delta p * Q_{out}}{T_a * 2\pi * N} \qquad \textit{Eq. A.3}$$

where Δp is the pressure rise across the pump, Q_{out} is the volumetric flow rate at the outlet, and N is the pump speed. The overall efficiency can also be defined using the torque calculated by FLUENT:

$$\eta_{overall\ computed} = \frac{\Delta p * Q_{out}}{T_c * 2\pi * N} \qquad \textit{Eq. A.4}$$

where T_c is the computed torque value.

The above definitions for the overall efficiency (*Equations A.3* and *A.4*) do not directly address the losses resulting from leakage mass flow through the gaps. Thus the overall efficiency is separated into volumetric and hydraulic efficiencies.

The volumetric efficiency is defined as:

$$\eta_v = \frac{Q_{out}}{Q_{out\ \ theoretical}} \qquad \textit{Eq. A.5}$$

where $Q_{out\ theoretical}$ is the theoretical output of the pump. This is calculated using the displacement of the gerotor D in inches^3/rev/inch, the thickness of the gerotor t, and the speed of the pump N:

$$Q_{out\ \ theoretical} = D * t * N \qquad \textit{Eq. A.6}$$

If the overall efficiency is defined as:

$$\eta_{overall} = \eta_m * \eta_v * \eta_h \qquad \textit{Eq. A.7}$$

where η_h is the hydraulic efficiency, and the assumption of *Equation A.1* is used, *Equation A.6* can be rearranged to find the hydraulic efficiency:

$$\eta_h = \frac{\eta_{overall\ \ computed}}{\eta_v} \qquad \textit{Eq. A.8}$$

Appendix B – Material Properties

15W-40 Engine Oil at 100°C

Density:	843 kg/m^3
Viscosity:	0.0123921 kg/m-s

SAE 30 Engine Oil at 100°C

Density:	891 kg/m^3
Viscosity:	0.0107811 kg/m-s

VISCOR Diesel Calibration Fluid at 24°C

Density:	822.2 kg/m^3
Viscosity:	0.002063722 kg/m-s

Appendix C – MATLAB Program

A MATLAB program was written to facilitate the post-processing needed after the simulations were complete. This program performs several calculations quickly and easily, requiring only a few parameters from the user before running. These tasks are summarized below:

1. Queries user for the name of the transcript file
2. Calls a Perl program to scan the transcript file for torque data as a function of time
3. Reads the .out files created by FLUENT, which track mass flow rates, pressures, and other parameters as a function of time
4. Plot time dependent data and save as jpeg files
5. Calculate average mass flow rates, pressures, torques, and other data, and writes them to a text file

```
%%%%%%%%%%%%%%%%%%%%%%%%%%%%%%%%%%%%%
% Gerotor efficiency calculations   %
%                                   %
% Michigan Technological University %
% Engineered Machined Products      %
%                                   %
% Dr. Amitabh Narain                %
% Jordan Bilyeu                     %
%%%%%%%%%%%%%%%%%%%%%%%%%%%%%%%%%%%%%

clear
clc

%%%%%%%%%%%%%%%%%%%%%%%%%%%%%%%%%%%%%%
% Get Transcript Name From From User %
%%%%%%%%%%%%%%%%%%%%%%%%%%%%%%%%%%%%%%

transcript = input('Enter transcript file name: ','s');

% Use Perl to get torque data from transcript file and display Perl output
perlout = perl('gettorquedata_mock_revb_newmesh.cgi',transcript);
disp(' ')
disp(perlout)

%%%%%%%%%%%%%%%%%%%%
% Open Output File %
%%%%%%%%%%%%%%%%%%%%

output = fopen('command_window_output.out','wt');

%%%%%%%%%%%%%%%%%%%%%%%%%%
% Load FLUENT .out files %
%%%%%%%%%%%%%%%%%%%%%%%%%%

[mf_outlet_boundary_header, mf_outlet_boundary_time, mf_outlet_boundary_data] =
matlab_readColData('mf_outlet_boundary.out',2,2);

[mf_top_gap_header, mf_top_gap_time, mf_top_gap_data] = matlab_readColData('mf_top_gap.out',2,2);
[mf_bottom_gap_header, mf_bottom_gap_time, mf_bottom_gap_data] = matlab_readColData('mf_bottom_gap.out',2,2);
[mf_side_gap_header, mf_side_gap_time, mf_side_gap_data] = matlab_readColData('mf_side_gap.out',2,2);
[mf_gerotor_teeth_bottom_header, mf_gerotor_teeth_bottom_time, mf_gerotor_teeth_bottom_data] =
matlab_readColData('mf_gerotor_teeth_bottom.out',2,2);
[mf_gerotor_teeth_top_header, mf_gerotor_teeth_top_time, mf_gerotor_teeth_top_data] =
matlab_readColData('mf_gerotor_teeth_top.out',2,2);
[mf_press_tap_upper_header, mf_press_tap_upper_time, mf_press_tap_upper_data] =
matlab_readColData('mf_press_tap_upper.out',2,2);
[mf_press_tap_lower_header, mf_press_tap_lower_time, mf_press_tap_lower_data] =
matlab_readColData('mf_press_tap_lower.out',2,2);
[max_pressure_header, max_pressure_time, max_pressure_data] = matlab_readColData('max_pressure.out',2,2);
[min_pressure_header, min_pressure_time, min_pressure_data] = matlab_readColData('min_pressure.out',2,2);
```

```
% Load torque data from transcript file (generated by Perl script)
% Innergear
[innergear_pressure_moment_header, innergear_pressure_moment_data, innergear_pressure_moment_time] =
matlab_readColData('innergear_pressure_moment.out',2,0);
[innergear_viscous_moment_header, innergear_viscous_moment_data, innergear_viscous_moment_time] =
matlab_readColData('innergear_viscous_moment.out',2,0);
[innergear_total_moment_header, innergear_total_moment_data, innergear_total_moment_time] =
matlab_readColData('innergear_total_moment.out',2,0);

% Outergear
[outergear_pressure_moment_header, outergear_pressure_moment_data, outergear_pressure_moment_time] =
matlab_readColData('outergear_pressure_moment.out',2,0);
[outergear_viscous_moment_header, outergear_viscous_moment_data, outergear_viscous_moment_time] =
matlab_readColData('outergear_viscous_moment.out',2,0);
[outergear_total_moment_header, outergear_total_moment_data, outergear_total_moment_time] =
matlab_readColData('outergear_total_moment.out',2,0);

% Side Gap
[sidegap_pressure_moment_header, sidegap_pressure_moment_data, sidegap_pressure_moment_time] =
matlab_readColData('sidegap_pressure_moment.out',2,0);
[sidegap_viscous_moment_header, sidegap_viscous_moment_data, sidegap_viscous_moment_time] =
matlab_readColData('sidegap_viscous_moment.out',2,0);
[sidegap_total_moment_header, sidegap_total_moment_data, sidegap_total_moment_time] =
matlab_readColData('sidegap_total_moment.out',2,0);

% Top Gap
[topgap_pressure_moment_header, topgap_pressure_moment_data, topgap_pressure_moment_time] =
matlab_readColData('topgap_pressure_moment.out',2,0);
[topgap_viscous_moment_header, topgap_viscous_moment_data, topgap_viscous_moment_time] =
matlab_readColData('topgap_viscous_moment.out',2,0);
[topgap_total_moment_header, topgap_total_moment_data, topgap_total_moment_time] =
matlab_readColData('topgap_total_moment.out',2,0);

% Bottom Gap
[bottomgap_pressure_moment_header, bottomgap_pressure_moment_data, bottomgap_pressure_moment_time] =
matlab_readColData('bottomgap_pressure_moment.out',2,0);
[bottomgap_viscous_moment_header, bottomgap_viscous_moment_data, bottomgap_viscous_moment_time] =
matlab_readColData('bottomgap_viscous_moment.out',2,0);
[bottomgap_total_moment_header, bottomgap_total_moment_data, bottomgap_total_moment_time] =
matlab_readColData('bottomgap_total_moment.out',2,0);

% Shaft Side Upper
[shaftsideupper_pressure_moment_header, shaftsideupper_pressure_moment_data, shaftsideupper_pressure_moment_time]
= matlab_readColData('shaftsideupper_pressure_moment.out',2,0);
[shaftsideupper_viscous_moment_header, shaftsideupper_viscous_moment_data, shaftsideupper_viscous_moment_time] =
matlab_readColData('shaftsideupper_viscous_moment.out',2,0);
[shaftsideupper_total_moment_header, shaftsideupper_total_moment_data, shaftsideupper_total_moment_time] =
matlab_readColData('shaftsideupper_total_moment.out',2,0);

% Shaft Side Lower
[shaftsidelower_pressure_moment_header, shaftsidelower_pressure_moment_data, shaftsidelower_pressure_moment_time]
= matlab_readColData('shaftsidelower_pressure_moment.out',2,0);
[shaftsidelower_viscous_moment_header, shaftsidelower_viscous_moment_data, shaftsidelower_viscous_moment_time] =
matlab_readColData('shaftsidelower_viscous_moment.out',2,0);
[shaftsidelower_total_moment_header, shaftsidelower_total_moment_data, shaftsidelower_total_moment_time] =
matlab_readColData('shaftsidelower_total_moment.out',2,0);

%%%%%%%%%%%%%%%%%%%%%%%%%%%%%%%%%%%%%%%%%%%%%%%%%%%%
% Convert pressure data from Pascals to psi %
%%%%%%%%%%%%%%%%%%%%%%%%%%%%%%%%%%%%%%%%%%%%%%%%%%%%

max_pressure_data = max_pressure_data * (1/6894.757);
min_pressure_data = min_pressure_data * (1/6894.757);

%%%%%%%%%%%%%%%%%%%%%%%%%%%%
% Get absolute moment data %
%%%%%%%%%%%%%%%%%%%%%%%%%%%%

% Fluent simulation may have been defined such that the torque calculated
% is negative.  This will get positive torque values
mf_outlet_boundary_data = mf_outlet_boundary_data * -1;
% mf_y_2_data = mf_y_2_data * -1;

% Innergear
% innergear_pressure_moment_data = -1* innergear_pressure_moment_data;
innergear_viscous_moment_data = -1 * innergear_viscous_moment_data;
% innergear_total_moment_data = -1 * innergear_total_moment_data;

% Outergear
outergear_pressure_moment_data = -1* outergear_pressure_moment_data;
outergear_viscous_moment_data = -1 * outergear_viscous_moment_data;
outergear_total_moment_data = -1 * outergear_total_moment_data;

% Side Gap
sidegap_pressure_moment_data = -1* sidegap_pressure_moment_data;
%sidegap_viscous_moment_data = -1 * sidegap_viscous_moment_data;
%sidegap_total_moment_data = -1 * sidegap_total_moment_data;
```

```
% Bottom Gap1
%bottomgap1_pressure_moment_data = -1* bottomgap1_pressure_moment_data;
%bottomgap1_viscous_moment_data = -1 * bottomgap1_viscous_moment_data;
%bottomgap1_total_moment_data = -1 * bottomgap1_total_moment_data;

% Bottom Gap2
%bottomgap2_pressure_moment_data = -1* bottomgap2_pressure_moment_data;
%bottomgap2_viscous_moment_data = -1 * bottomgap2_viscous_moment_data;
%bottomgap2_total_moment_data = -1 * bottomgap2_total_moment_data;

% Top Gap1
%topgap1_pressure_moment_data = -1* topgap1_pressure_moment_data;
%topgap1_viscous_moment_data = -1 * topgap1_viscous_moment_data;
%topgap1_total_moment_data = -1 * topgap1_total_moment_data;

% Top Gap2
%topgap2_pressure_moment_data = -1* topgap2_pressure_moment_data;
%topgap2_viscous_moment_data = -1 * topgap2_viscous_moment_data;
%topgap2_total_moment_data = -1 * topgap2_total_moment_data;

% Shaft Side Upper
%shaftsideupper_pressure_moment_data = -1* shaftsideupper_pressure_moment_data;
%shaftsideupper_viscous_moment_data = -1 * shaftsideupper_viscous_moment_data;
%shaftsideupper_total_moment_data = -1 * shaftsideupper_total_moment_data;

% Shaft Side lower
%shaftsidelower_pressure_moment_data = -1* shaftsidelower_pressure_moment_data;
%shaftsidelower_viscous_moment_data = -1 * shaftsidelower_viscous_moment_data;
%shaftsidelower_total_moment_data = -1 * shaftsidelower_total_moment_data;

%%%%%%%%%
% Plots %
%%%%%%%%%

mf_outlet_boundary = figure;
plot(mf_outlet_boundary_time, mf_outlet_boundary_data)
xlabel('Flow Time (seconds)')
ylabel('Mass Flow Rate (kg/s)')
title('Mass Flow Rate at Outlet Boundary')
saveas(mf_outlet_boundary, 'matlab_mf_outlet_boundary.jpg')

mf_top_gap = figure;
plot(mf_top_gap_time, mf_top_gap_data)
xlabel('Flow Time (seconds)')
ylabel('Mass Flow Rate (kg/s)')
title('Mass Flow Rate Through Top Gap')
saveas(mf_top_gap, 'matlab_mf_top_gap.jpg')

mf_bottom_gap = figure;
plot(mf_bottom_gap_time, mf_bottom_gap_data)
xlabel('Flow Time (seconds)')
ylabel('Mass Flow Rate (kg/s)')
title('Mass Flow Rate Through Bottom Gap')
saveas(mf_bottom_gap, 'matlab_mf_bottom_gap.jpg')

mf_side_gap = figure;
plot(mf_side_gap_time, mf_side_gap_data)
xlabel('Flow Time (seconds)')
ylabel('Mass Flow Rate (kg/s)')
title('Mass Flow Rate Through Side Gap')
saveas(mf_side_gap, 'matlab_mf_side_gap.jpg')

mf_gerotor_teeth = figure;
plot(mf_gerotor_teeth_bottom_time,
mf_gerotor_teeth_bottom_data,mf_gerotor_teeth_top_time,mf_gerotor_teeth_top_data)
xlabel('Flow Time (seconds)')
ylabel('Mass Flow Rate (kg/s)')
title('Mass Flow Rate Through Gerotor Teeth')
legend('Bottom','Top')
saveas(mf_gerotor_teeth, 'matlab_mf_gerotor_teeth.jpg')

mf_press_tap_upper = figure;
plot(mf_press_tap_upper_time, mf_press_tap_upper_data)
xlabel('Flow Time (seconds)')
ylabel('Mass Flow Rate (kg/s)')
title('Mass Flow Rate Through Upper Pressure Tap')
saveas(mf_press_tap_upper, 'matlab_mf_press_tap_upper.jpg')

mf_press_tap_lower = figure;
plot(mf_press_tap_lower_time, mf_press_tap_lower_data)
xlabel('Flow Time (seconds)')
ylabel('Mass Flow Rate (kg/s)')
title('Mass Flow Rate Through Lower Pressure Tap')
saveas(mf_press_tap_lower, 'matlab_mf_press_tap_lower.jpg')

min_pressure = figure;
plot(min_pressure_time, min_pressure_data)
xlabel('Flow Time (seconds)')
ylabel('Pressure (psi)')
```

```
title('Minimum Overall Pressure')
saveas(min_pressure, 'matlab_min_pressure.jpg')

max_pressure = figure;
plot(max_pressure_time, max_pressure_data)
xlabel('Flow Time (seconds)')
ylabel('Pressure (psi)')
title('Maximum Overall Pressure')
saveas(max_pressure, 'matlab_max_pressure.jpg')

% Innergear
innergear_pressure_moment = figure;
plot(innergear_pressure_moment_time, innergear_pressure_moment_data)
xlabel('Flow Time (seconds)')
ylabel('Torque (Nm)')
title('Innergear Pressure Moment on Inner Gerotor')
saveas(innergear_pressure_moment, 'matlab_innergear_pressure_moment.jpg')

innergear_viscous_moment = figure;
plot(innergear_viscous_moment_time, innergear_viscous_moment_data)
xlabel('Flow Time (seconds)')
ylabel('Torque (Nm)')
title('Innergear Viscous Moment on Inner Gerotor')
saveas(innergear_viscous_moment, 'matlab_innergear_viscous_moment.jpg')

innergear_total_moment = figure;
plot(innergear_total_moment_time, innergear_total_moment_data)
xlabel('Flow Time (seconds)')
ylabel('Torque (Nm)')
title('Innergear Total Moment on Inner Gerotor')
saveas(innergear_total_moment, 'matlab_innergear_total_moment.jpg')

% Outergear
outergear_pressure_moment = figure;
plot(outergear_pressure_moment_time, outergear_pressure_moment_data)
xlabel('Flow Time (seconds)')
ylabel('Torque (Nm)')
title('Outergear Pressure Moment on Inner Gerotor')
saveas(outergear_pressure_moment, 'matlab_outergear_pressure_moment.jpg')

outergear_viscous_moment = figure;
plot(outergear_viscous_moment_time, outergear_viscous_moment_data)
xlabel('Flow Time (seconds)')
ylabel('Torque (Nm)')
title('Outergear Viscous Moment on Inner Gerotor')
saveas(outergear_viscous_moment, 'matlab_outergear_viscous_moment.jpg')

outergear_total_moment = figure;
plot(outergear_total_moment_time, outergear_total_moment_data)
xlabel('Flow Time (seconds)')
ylabel('Torque (Nm)')
title('Outergear Total Moment on Inner Gerotor')
saveas(outergear_total_moment, 'matlab_outergear_total_moment.jpg')

% Side Gap
sidegap_pressure_moment = figure;
plot(sidegap_pressure_moment_time, sidegap_pressure_moment_data)
xlabel('Flow Time (seconds)')
ylabel('Torque (Nm)')
title('Side Gap Pressure Moment on Inner Gerotor')
saveas(sidegap_pressure_moment, 'matlab_sidegap_pressure_moment.jpg')

sidegap_viscous_moment = figure;
plot(sidegap_viscous_moment_time, sidegap_viscous_moment_data)
xlabel('Flow Time (seconds)')
ylabel('Torque (Nm)')
title('Side Gap Viscous Moment on Inner Gerotor')
saveas(sidegap_viscous_moment, 'matlab_sidegap_viscous_moment.jpg')

sidegap_total_moment = figure;
plot(sidegap_total_moment_time, sidegap_total_moment_data)
xlabel('Flow Time (seconds)')
ylabel('Torque (Nm)')
title('Side Gap Total Moment on Inner Gerotor')
saveas(sidegap_total_moment, 'matlab_sidegap_total_moment.jpg')

% Top Gap
topgap_pressure_moment = figure;
plot(topgap_pressure_moment_time, topgap_pressure_moment_data)
xlabel('Flow Time (seconds)')
ylabel('Torque (Nm)')
title('Top Gap Pressure Moment on Inner Gerotor')
saveas(topgap_pressure_moment, 'matlab_topgap_pressure_moment.jpg')

topgap_viscous_moment = figure;
plot(topgap_viscous_moment_time, topgap_viscous_moment_data)
xlabel('Flow Time (seconds)')
ylabel('Torque (Nm)')
title('Top Gap Viscous Moment on Inner Gerotor')
```

```
saveas(topgap_viscous_moment, 'matlab_topgap_viscous_moment.jpg')

topgap_total_moment = figure;
plot(topgap_total_moment_time, topgap_total_moment_data)
xlabel('Flow Time (seconds)')
ylabel('Torque (Nm)')
title('Top Gap Total Moment on Inner Gerotor')
saveas(topgap_total_moment, 'matlab_topgap_total_moment.jpg')

% Bottom Gap
bottomgap_pressure_moment = figure;
plot(bottomgap_pressure_moment_time, bottomgap_pressure_moment_data)
xlabel('Flow Time (seconds)')
ylabel('Torque (Nm)')
title('Bottom Gap Pressure Moment on Inner Gerotor')
saveas(bottomgap_pressure_moment, 'matlab_bottomgap_pressure_moment.jpg')

bottomgap_viscous_moment = figure;
plot(bottomgap_viscous_moment_time, bottomgap_viscous_moment_data)
xlabel('Flow Time (seconds)')
ylabel('Torque (Nm)')
title('Bottom Gap Viscous Moment on Inner Gerotor')
saveas(bottomgap_viscous_moment, 'matlab_bottomgap_viscous_moment.jpg')

bottomgap_total_moment = figure;
plot(bottomgap_total_moment_time, bottomgap_total_moment_data)
xlabel('Flow Time (seconds)')
ylabel('Torque (Nm)')
title('Bottom Gap Total Moment on Inner Gerotor')
saveas(bottomgap_total_moment, 'matlab_bottomgap_total_moment.jpg')

% Shaft Side Upper
shaftsideupper_pressure_moment = figure;
plot(shaftsideupper_pressure_moment_time, shaftsideupper_pressure_moment_data)
xlabel('Flow Time (seconds)')
ylabel('Torque (Nm)')
title('Shaft Side Upper Pressure Moment on Inner Gerotor')
saveas(shaftsideupper_pressure_moment, 'matlab_shaftsideupper_pressure_moment.jpg')

shaftsideupper_viscous_moment = figure;
plot(shaftsideupper_viscous_moment_time, shaftsideupper_viscous_moment_data)
xlabel('Flow Time (seconds)')
ylabel('Torque (Nm)')
title('Shaft Side Upper Viscous Moment on Inner Gerotor')
saveas(shaftsideupper_viscous_moment, 'matlab_shaftsideupper_viscous_moment.jpg')

shaftsideupper_total_moment = figure;
plot(shaftsideupper_total_moment_time, shaftsideupper_total_moment_data)
xlabel('Flow Time (seconds)')
ylabel('Torque (Nm)')
title('Shaft Side Upper Total Moment on Inner Gerotor')
saveas(shaftsideupper_total_moment, 'matlab_shaftsideupper_total_moment.jpg')

% Shaft Side Lower
shaftsidelower_pressure_moment = figure;
plot(shaftsidelower_pressure_moment_time, shaftsidelower_pressure_moment_data)
xlabel('Flow Time (seconds)')
ylabel('Torque (Nm)')
title('Shaft Side Lower Pressure Moment on Inner Gerotor')
saveas(shaftsidelower_pressure_moment, 'matlab_shaftsidelower_pressure_moment.jpg')

shaftsidelower_viscous_moment = figure;
plot(shaftsidelower_viscous_moment_time, shaftsidelower_viscous_moment_data)
xlabel('Flow Time (seconds)')
ylabel('Torque (Nm)')
title('Shaft Side Lower Viscous Moment on Inner Gerotor')
saveas(shaftsidelower_viscous_moment, 'matlab_shaftsidelower_viscous_moment.jpg')

shaftsidelower_total_moment = figure;
plot(shaftsidelower_total_moment_time, shaftsidelower_total_moment_data)
xlabel('Flow Time (seconds)')
ylabel('Torque (Nm)')
title('Shaft Side Lower Total Moment on Inner Gerotor')
saveas(shaftsidelower_total_moment, 'matlab_shaftsidelower_total_moment.jpg')

total_gap_nogerotor_mf = mf_bottom_gap_data + mf_top_gap_data + mf_side_gap_data;% + mf_pressure_tap_data;

total_gap_nogerotor_mf_fig = figure;
plot(mf_outlet_boundary_time,total_gap_nogerotor_mf)
xlabel('Flow Time (seconds)')
ylabel('Mass Flow Rate (kg/s)')
title('Total Mass Flow Rate Through All Gaps (Neglecting Gap in Gerotor Teeth)')
saveas(total_gap_nogerotor_mf_fig, 'matlab_total_gap_nogerotor_mf.jpg')

%%%%%%%%%%%%%%%%%%%%%%%%%%%%%%%%%%%%%%%%%%%%%%%%%%%%%%%%%%%%%%%%%%%%%%%%%%%%
% Convert mass flow rates to volumetric flow rates (liter/min) %
%%%%%%%%%%%%%%%%%%%%%%%%%%%%%%%%%%%%%%%%%%%%%%%%%%%%%%%%%%%%%%%%%%%%%%%%%%%%

oil_density = 843;   %kg/m^3
```

```
q_outlet_boundary = 60000*(mf_outlet_boundary_data / oil_density); %liters/min
q_top_gap = 60000*(mf_top_gap_data / oil_density);
q_bottom_gap = 60000*(mf_bottom_gap_data / oil_density);
q_side_gap = 60000*(mf_side_gap_data / oil_density);
q_gerotor_teeth = 60000*(mf_gerotor_teeth_bottom_data / oil_density);
q_press_tap_upper = 60000*(mf_press_tap_upper_data / oil_density);
q_press_tap_lower = 60000*(mf_press_tap_lower_data / oil_density);

q_leakage = q_top_gap + q_bottom_gap + q_side_gap + q_gerotor_teeth + q_press_tap_upper + q_press_tap_lower;
q_leakage_nogerotor = q_top_gap + q_bottom_gap + q_side_gap + q_press_tap_upper + q_press_tap_lower;

%%%%%%%%%%%%%%%%%%%%%%%%%%%%%%
% Calculate Average Moments %
%%%%%%%%%%%%%%%%%%%%%%%%%%%%%%

% Innergear
[s_innergear_pressure_moment_1, s_innergear_pressure_moment_2] = size(innergear_pressure_moment_data);
start_innergear_pressure_moment = round(0.25*s_innergear_pressure_moment_1);
innergear_pressure_moment_small =
innergear_pressure_moment_data(start_innergear_pressure_moment:s_innergear_pressure_moment_1);
innergear_pressure_moment_average = mean(innergear_pressure_moment_small);

[s_innergear_viscous_moment_1, s_innergear_viscous_moment_2] = size(innergear_viscous_moment_data);
start_innergear_viscous_moment = round(0.25*s_innergear_viscous_moment_1);
innergear_viscous_moment_small =
innergear_viscous_moment_data(start_innergear_viscous_moment:s_innergear_viscous_moment_1);
innergear_viscous_moment_average = mean(innergear_viscous_moment_small);

[s_innergear_total_moment_1, s_innergear_total_moment_2] = size(innergear_total_moment_data);
start_innergear_total_moment = round(0.25*s_innergear_total_moment_1);
innergear_total_moment_small =
innergear_total_moment_data(start_innergear_total_moment:s_innergear_total_moment_1);
innergear_total_moment_average = mean(innergear_total_moment_small);

% Outergear
[s_outergear_pressure_moment_1, s_outergear_pressure_moment_2] = size(outergear_pressure_moment_data);
start_outergear_pressure_moment = round(0.25*s_outergear_pressure_moment_1);
outergear_pressure_moment_small =
outergear_pressure_moment_data(start_outergear_pressure_moment:s_outergear_pressure_moment_1);
outergear_pressure_moment_average = mean(outergear_pressure_moment_small);

[s_outergear_viscous_moment_1, s_outergear_viscous_moment_2] = size(outergear_viscous_moment_data);
start_outergear_viscous_moment = round(0.25*s_outergear_viscous_moment_1);
outergear_viscous_moment_small =
outergear_viscous_moment_data(start_outergear_viscous_moment:s_outergear_viscous_moment_1);
outergear_viscous_moment_average = mean(outergear_viscous_moment_small);

[s_outergear_total_moment_1, s_outergear_total_moment_2] = size(outergear_total_moment_data);
start_outergear_total_moment = round(0.25*s_outergear_total_moment_1);
outergear_total_moment_small =
outergear_total_moment_data(start_outergear_total_moment:s_outergear_total_moment_1);
outergear_total_moment_average = mean(outergear_total_moment_small);

% Side Gap
[s_sidegap_pressure_moment_1, s_sidegap_pressure_moment_2] = size(sidegap_pressure_moment_data);
start_sidegap_pressure_moment = round(0.25*s_sidegap_pressure_moment_1);
sidegap_pressure_moment_small =
sidegap_pressure_moment_data(start_sidegap_pressure_moment:s_sidegap_pressure_moment_1);
sidegap_pressure_moment_average = mean(sidegap_pressure_moment_small);

[s_sidegap_viscous_moment_1, s_sidegap_viscous_moment_2] = size(sidegap_viscous_moment_data);
start_sidegap_viscous_moment = round(0.25*s_sidegap_viscous_moment_1);
sidegap_viscous_moment_small =
sidegap_viscous_moment_data(start_sidegap_viscous_moment:s_sidegap_viscous_moment_1);
sidegap_viscous_moment_average = mean(sidegap_viscous_moment_small);

[s_sidegap_total_moment_1, s_sidegap_total_moment_2] = size(sidegap_total_moment_data);
start_sidegap_total_moment = round(0.25*s_sidegap_total_moment_1);
sidegap_total_moment_small = sidegap_total_moment_data(start_sidegap_total_moment:s_sidegap_total_moment_1);
sidegap_total_moment_average = mean(sidegap_total_moment_small);

% Top Gap
[s_topgap_pressure_moment_1, s_topgap_pressure_moment_2] = size(topgap_pressure_moment_data);
start_topgap_pressure_moment = round(0.25*s_topgap_pressure_moment_1);
topgap_pressure_moment_small =
topgap_pressure_moment_data(start_topgap_pressure_moment:s_topgap_pressure_moment_1);
topgap_pressure_moment_average = mean(topgap_pressure_moment_small);

[s_topgap_viscous_moment_1, s_topgap_viscous_moment_2] = size(topgap_viscous_moment_data);
start_topgap_viscous_moment = round(0.25*s_topgap_viscous_moment_1);
topgap_viscous_moment_small = topgap_viscous_moment_data(start_topgap_viscous_moment:s_topgap_viscous_moment_1);
topgap_viscous_moment_average = mean(topgap_viscous_moment_small);

[s_topgap_total_moment_1, s_topgap_total_moment_2] = size(topgap_total_moment_data);
start_topgap_total_moment = round(0.25*s_topgap_total_moment_1);
topgap_total_moment_small = topgap_total_moment_data(start_topgap_total_moment:s_topgap_total_moment_1);
topgap_total_moment_average = mean(topgap_total_moment_small);
```

```
% Bottom Gap
[s_bottomgap_pressure_moment_1, s_bottomgap_pressure_moment_2] = size(bottomgap_pressure_moment_data);
start_bottomgap_pressure_moment = round(0.25*s_bottomgap_pressure_moment_1);
bottomgap_pressure_moment_small =
bottomgap_pressure_moment_data(start_bottomgap_pressure_moment:s_bottomgap_pressure_moment_1);
bottomgap_pressure_moment_average = mean(bottomgap_pressure_moment_small);

[s_bottomgap_viscous_moment_1, s_bottomgap_viscous_moment_2] = size(bottomgap_viscous_moment_data);
start_bottomgap_viscous_moment = round(0.25*s_bottomgap_viscous_moment_1);
bottomgap_viscous_moment_small =
bottomgap_viscous_moment_data(start_bottomgap_viscous_moment:s_bottomgap_viscous_moment_1);
bottomgap_viscous_moment_average = mean(bottomgap_viscous_moment_small);

[s_bottomgap_total_moment_1, s_bottomgap_total_moment_2] = size(bottomgap_total_moment_data);
start_bottomgap_total_moment = round(0.25*s_bottomgap_total_moment_1);
bottomgap_total_moment_small =
bottomgap_total_moment_data(start_bottomgap_total_moment:s_bottomgap_total_moment_1);
bottomgap_total_moment_average = mean(bottomgap_total_moment_small);

% Shaft Side Upper
[s_shaftsideupper_pressure_moment_1, s_shaftsideupper_pressure_moment_2] =
size(shaftsideupper_pressure_moment_data);
start_shaftsideupper_pressure_moment = round(0.25*s_shaftsideupper_pressure_moment_1);
shaftsideupper_pressure_moment_small =
shaftsideupper_pressure_moment_data(start_shaftsideupper_pressure_moment:s_shaftsideupper_pressure_moment_1);
shaftsideupper_pressure_moment_average = mean(shaftsideupper_pressure_moment_small);

[s_shaftsideupper_viscous_moment_1, s_shaftsideupper_viscous_moment_2] = size(shaftsideupper_viscous_moment_data);
start_shaftsideupper_viscous_moment = round(0.25*s_shaftsideupper_viscous_moment_1);
shaftsideupper_viscous_moment_small =
shaftsideupper_viscous_moment_data(start_shaftsideupper_viscous_moment:s_shaftsideupper_viscous_moment_1);
shaftsideupper_viscous_moment_average = mean(shaftsideupper_viscous_moment_small);

[s_shaftsideupper_total_moment_1, s_shaftsideupper_total_moment_2] = size(shaftsideupper_total_moment_data);
start_shaftsideupper_total_moment = round(0.25*s_shaftsideupper_total_moment_1);
shaftsideupper_total_moment_small =
shaftsideupper_total_moment_data(start_shaftsideupper_total_moment:s_shaftsideupper_total_moment_1);
shaftsideupper_total_moment_average = mean(shaftsideupper_total_moment_small);

% Shaft Side Lower
[s_shaftsidelower_pressure_moment_1, s_shaftsidelower_pressure_moment_2] =
size(shaftsidelower_pressure_moment_data);
start_shaftsidelower_pressure_moment = round(0.25*s_shaftsidelower_pressure_moment_1);
shaftsidelower_pressure_moment_small =
shaftsidelower_pressure_moment_data(start_shaftsidelower_pressure_moment:s_shaftsidelower_pressure_moment_1);
shaftsidelower_pressure_moment_average = mean(shaftsidelower_pressure_moment_small);

[s_shaftsidelower_viscous_moment_1, s_shaftsidelower_viscous_moment_2] = size(shaftsidelower_viscous_moment_data);
start_shaftsidelower_viscous_moment = round(0.25*s_shaftsidelower_viscous_moment_1);
shaftsidelower_viscous_moment_small =
shaftsidelower_viscous_moment_data(start_shaftsidelower_viscous_moment:s_shaftsidelower_viscous_moment_1);
shaftsidelower_viscous_moment_average = mean(shaftsidelower_viscous_moment_small);

[s_shaftsidelower_total_moment_1, s_shaftsidelower_total_moment_2] = size(shaftsidelower_total_moment_data);
start_shaftsidelower_total_moment = round(0.25*s_shaftsidelower_total_moment_1);
shaftsidelower_total_moment_small =
shaftsidelower_total_moment_data(start_shaftsidelower_total_moment:s_shaftsidelower_total_moment_1);
shaftsidelower_total_moment_average = mean(shaftsidelower_total_moment_small);

% Complete Total Moment Average
complete_total_moment_average = innergear_total_moment_average + ...
    outergear_total_moment_average + sidegap_total_moment_average + ...
    topgap_total_moment_average + bottomgap_total_moment_average  + ...
    shaftsidelower_total_moment_average + shaftsideupper_total_moment_average;

% Write average torques to an output file
% Innergear
fprintf(output, 'Innergear pressure moment in N-m: ');
fprintf(output, '%f \n\n',innergear_pressure_moment_average);

fprintf(output, 'Innergear viscous moment in N-m: ');
fprintf(output, '%f \n\n',innergear_viscous_moment_average);

fprintf(output, 'Innergear total moment in N-m: ');
fprintf(output, '%f \n\n',innergear_total_moment_average);

% Outergear
fprintf(output, 'Outergear pressure moment in N-m: ');
fprintf(output, '%f \n\n',outergear_pressure_moment_average);

fprintf(output, 'Outergear viscous moment in N-m: ');
fprintf(output, '%f \n\n',outergear_viscous_moment_average);

fprintf(output, 'Outergear total moment in N-m: ');
fprintf(output, '%f \n\n',outergear_total_moment_average);

% Side Gap
fprintf(output, 'Side Gap pressure moment in N-m: ');
fprintf(output, '%f \n\n',sidegap_pressure_moment_average);
```

```
fprintf(output, 'Side Gap viscous moment in N-m: ');
fprintf(output, '%f \n\n',sidegap_viscous_moment_average);

fprintf(output, 'Side Gap total moment in N-m: ');
fprintf(output, '%f \n\n',sidegap_total_moment_average);

% Top Gap
fprintf(output, 'Top Gap pressure moment in N-m: ');
fprintf(output, '%f \n\n',topgap_pressure_moment_average);

fprintf(output, 'Top Gap viscous moment in N-m: ');
fprintf(output, '%f \n\n',topgap_viscous_moment_average);

fprintf(output, 'Top Gap total moment in N-m: ');
fprintf(output, '%f \n\n',topgap_total_moment_average);

% Bottom Gap
fprintf(output, 'Bottom Gap pressure moment in N-m: ');
fprintf(output, '%f \n\n',bottomgap_pressure_moment_average);

fprintf(output, 'Bottom Gap viscous moment in N-m: ');
fprintf(output, '%f \n\n',bottomgap_viscous_moment_average);

fprintf(output, 'Bottom Gap total moment in N-m: ');
fprintf(output, '%f \n\n',bottomgap_total_moment_average);

% Shaft Side Upper
fprintf(output, 'Shaft Side Upper pressure moment in N-m: ');
fprintf(output, '%f \n\n',shaftsideupper_pressure_moment_average);

fprintf(output, 'Shaft Side Upper viscous moment in N-m: ');
fprintf(output, '%f \n\n',shaftsideupper_viscous_moment_average);

fprintf(output, 'Shaft Side Upper total moment in N-m: ');
fprintf(output, '%f \n\n',shaftsideupper_total_moment_average);

% Shaft Side Lower
fprintf(output, 'Shaft Side Lower pressure moment in N-m: ');
fprintf(output, '%f \n\n',shaftsidelower_pressure_moment_average);

fprintf(output, 'Shaft Side Lower viscous moment in N-m: ');
fprintf(output, '%f \n\n',shaftsidelower_viscous_moment_average);

fprintf(output, 'Shaft Side Lower total moment in N-m: ');
fprintf(output, '%f \n\n',shaftsidelower_total_moment_average);


% Complete Total Moment
fprintf(output, '************************************');
fprintf(output, 'Complete Total moment in N-m: ');
fprintf(output, '%f \n\n',complete_total_moment_average);

%%%%%%%%%%%%%%%%%%%%%%%%%%%%%%%%%%%%%%%%
% Calculate Average Mass Flow Rates %
%%%%%%%%%%%%%%%%%%%%%%%%%%%%%%%%%%%%%%%%

[s_mf_outlet_boundary_data_1, s_mf_outlet_boundary_data_2] = size(mf_outlet_boundary_data);
start_mf_outlet_boundary_data = round(0.25*s_mf_outlet_boundary_data_1);
mf_outlet_boundary_data_small =
mf_outlet_boundary_data(start_mf_outlet_boundary_data:s_mf_outlet_boundary_data_1);
mf_outlet_boundary_data_average = mean(mf_outlet_boundary_data_small);

[s_mf_top_gap_data_1, s_mf_top_gap_data_2] = size(mf_top_gap_data);
start_mf_top_gap_data = round(0.25*s_mf_top_gap_data_1);
mf_top_gap_data_small = mf_top_gap_data(start_mf_top_gap_data:s_mf_top_gap_data_1);
mf_top_gap_data_average = mean(mf_top_gap_data_small);

[s_mf_bottom_gap_data_1, s_mf_bottom_gap_data_2] = size(mf_bottom_gap_data);
start_mf_bottom_gap_data = round(0.25*s_mf_bottom_gap_data_1);
mf_bottom_gap_data_small = mf_bottom_gap_data(start_mf_bottom_gap_data:s_mf_bottom_gap_data_1);
mf_bottom_gap_data_average = mean(mf_bottom_gap_data_small);

[s_mf_gerotor_teeth_bottom_data_1, s_mf_gerotor_teeth_bottom_data_2] = size(mf_gerotor_teeth_bottom_data);
start_mf_gerotor_teeth_bottom_data = round(0.25*s_mf_gerotor_teeth_bottom_data_1);
mf_gerotor_teeth_bottom_data_small =
mf_gerotor_teeth_bottom_data(start_mf_gerotor_teeth_bottom_data:s_mf_gerotor_teeth_bottom_data_1);
mf_gerotor_teeth_bottom_data_average = mean(mf_gerotor_teeth_bottom_data_small);

[s_mf_press_tap_upper_data_1, s_mf_press_tap_upper_data_2] = size(mf_press_tap_upper_data);
start_mf_press_tap_upper_data = round(0.25*s_mf_press_tap_upper_data_1);
mf_press_tap_upper_data_small =
mf_press_tap_upper_data(start_mf_press_tap_upper_data:s_mf_press_tap_upper_data_1);
mf_press_tap_upper_data_average = mean(mf_press_tap_upper_data_small);

[s_mf_press_tap_lower_data_1, s_mf_press_tap_lower_data_2] = size(mf_press_tap_lower_data);
start_mf_press_tap_lower_data = round(0.25*s_mf_press_tap_lower_data_1);
mf_press_tap_lower_data_small =
mf_press_tap_lower_data(start_mf_press_tap_lower_data:s_mf_press_tap_lower_data_1);
```

```
mf_press_tap_lower_data_average = mean(mf_press_tap_lower_data_small);

[s_mf_side_gap_data_1, s_mf_side_gap_data_2] = size(mf_side_gap_data);
start_mf_side_gap_data = round(0.25*s_mf_side_gap_data_1);
mf_side_gap_data_small = mf_side_gap_data(start_mf_side_gap_data:s_mf_side_gap_data_1);
mf_side_gap_data_average = mean(mf_side_gap_data_small);

%%%%%%%
% EOF %
%%%%%%%
```

Appendix D – Excel Spreadsheet

After the MATLAB program (Appendix C) has calculated the time-averaged mass flow rates, pressures, and torques, an Excel spreadsheet is used to calculate the correction factors (both for torque and mass flow rate) and the volumetric, hydraulic, and overall efficiencies of the pump.

User input is required in the light blue cells. The yellow cells indicate the calculated corrected efficiency values. This example is from the Mock Pump – Revision B spreadsheet. It shows some of the mass flow rate calculations, and the volumetric efficiency calculations. Other parts calculate the corrected torque and hydraulic and overall efficiencies. Other sheets automatically plot the outlet flow and pump efficiencies.

	Pump Speed (RPM)	Computational Mass Flow Rate (kg/s)	Linear Fit	Linear Fit Mass Flow Rate (kg/s)	Corrected Total Flow (kg/s)	Corrected Output Flow (kg/s)	Corrected Output Flow (gpm)	Original Volumetric Efficiency	Corrected Volumetric Efficiency
	1207	1.0506	y=c1*x + c2	1.0506	1.0601	1.0232	18.2	0.9661	0.9652
	1724	1.4983		1.5047	1.5142	1.4619	26.01	0.9663	0.9654
40	**2241**	1.9657	c1	1.9588	1.9683	1.8995	33.79	0.9662	0.9651
PSI	**2759**	2.4131	8.78E-04	2.4138	2.4233	2.3389	41.61	0.9662	0.9652
	3276	2.8743	c2	2.8679	2.8773	2.7766	49.39	0.9661	0.9650
	3793	3.3157	-9.49E-03	3.3219	3.3314	3.2152	57.2	0.9661	0.9651
	1207	1.0445	y=c1*x + c2	1.0445	1.0599	1.0228	18.19	0.9656	0.9649
	1724	1.4924		1.4986	1.5140	1.4614	26	0.9660	0.9653
60	**2241**	1.9592	c1	1.9526	1.9680	1.8990	33.78	0.9660	0.9649
PSI	**2759**	2.4068	8.78E-04	2.4075	2.4229	2.3382	41.6	0.9660	0.9651
	3276	2.8678	c2	2.8615	2.8769	2.7759	49.38	0.9660	0.9649
	3793	3.3094	-1.54E-02	3.3155	3.3309	3.2144	57.18	0.9660	0.9650
	1207	1.0384	y=c1*x + c2	1.0385	1.0598	1.0224	18.19	0.9652	0.9647
	1724	1.4865		1.4924	1.5138	1.4573	25.92	0.9634	0.9627
80	**2241**	1.9528	c1	1.9464	1.9677	1.8985	33.77	0.9658	0.9648
PSI	**2759**	2.4005	8.78E-04	2.4012	2.4226	2.3377	41.59	0.9659	0.9650
	3276	2.8614	c2	2.8552	2.8765	2.7753	49.37	0.9658	0.9648
	3793	3.3032	-2.14E-02	3.3091	3.3305	3.2138	57.17	0.9659	0.9650
	1207	1.0325	y=c1*x + c2	1.0325	1.0596	1.0218	18.18	0.9647	0.9644
	1724	1.4807		1.4864	1.5134	1.4603	25.98	0.9654	0.9649
100	**2241**	1.9464	c1	1.9402	1.9673	1.8978	33.76	0.9655	0.9647
PSI	**2759**	2.3942	8.78E-04	2.3950	2.4220	2.3369	41.57	0.9657	0.9649
	3276	2.8549	c2	2.8488	2.8759	2.7744	49.36	0.9657	0.9647
	3793	3.2970	-2.71E-02	3.3027	3.3297	3.2128	57.15	0.9657	0.9649
	1207	1.0266	y=c1*x + c2	1.0265	1.0594	1.0214	18.17	0.9642	0.9641
	1724	1.4748		1.4803	1.5132	1.4598	25.97	0.9650	0.9647
120	**2241**	1.9400	c1	1.9341	1.9670	1.8972	33.75	0.9653	0.9645
PSI	**2759**	2.3880	8.78E-04	2.3888	2.4217	2.3363	41.56	0.9655	0.9647
	3276	2.8485	c2	2.8426	2.8755	2.7738	49.34	0.9655	0.9646
	3793	3.2909	-3.29E-02	3.2964	3.3293	3.2120	57.14	0.9656	0.9648